ERRATA

Report No. DOT/FAA/TC-12/53

Principles and Practices of Microscale Combustion Calorimetry

April 2013

Prepared for

Department of Transportation
Federal Aviation Administration
William J. Hughes Technical Center
Atlantic City International Airport, NJ 08405

Title page was changed to reflect the new title and the revision date.

Technical Report Documentation Page was changed to reflect the new title and the revision date.

The title of Section 3.1 was changed to Oxygen Consumption Flow Calorimetry.

In addition to new text, one figure, one table, and 13 equations were added to Section 3.1. As a result, figures were renumbered starting at figure 8, tables were renumbered starting at table2, and equations were renumbered starting with equation 27.

Released December 2014
1 Attachment: TC-12-53-R1

DOT/FAA/TC-12/53, R1

Federal Aviation Administration
William J. Hughes Technical Center
Aviation Research Division
Atlantic City International Airport
New Jersey 08405

Principles and Practice of Microscale Combustion Calorimetry

April 2013

Final Report

Revised: December 2014

U.S. Department of Transportation
Federal Aviation Administration

NOTICE

This report is available at the Federal Aviation Administration William J. Hughes Technical Center's Full-Text Technical Reports page: actlibrary.tc.faa.gov in Adobe Acrobat portable document format (PDF).

Technical Report Documentation Page

1. Report No.	2. Government Accession No.	3. Recipient's Catalog No.
DOT/FAA/TC-12/53, R1		

4. Title and Subtitle	5. Report Date
PRINCIPLES AND PRACTICE OF MICROSCALE COMBUSTION CALORIMETRY	April 2013 Revised: December 2014
	6. Performing Organization Code

7. Author(s)	8. Performing Organization Report No.
Richard E. Lyon[1], Richard N. Walters[1], Stanislav I. Stoliarov[2], and Natallia Safronava[3]	

9. Performing Organization Name and Address	10. Work Unit No. (TRAIS)
[1]Airport and Aircraft R&D Division Federal Aviation Administration William J. Hughes Technical Center Atlantic City Airport, NJ 08405 [2]Department of Fire Protection Engineering University of Maryland College Park, MD 20742 [3]Technology & Management International 1433 Hooper Avenue, Suite 330, Toms River, NJ 08753	11. Contract or Grant No.

12. Sponsoring Agency Name and Address	13. Type of Report and Period Covered
U.S. Department of Transportation Federal Aviation Administration Northwest Mountain Region – Transport Airplane Directorate 1601 Lind Avenue, SW Renton, WA 98057	14. Sponsoring Agency Code ANM-115

15. Supplementary Notes

The Federal Aviation Administration William J. Hughes Technical Center Aviation Research Division COR was Richard E. Lyon.

16. Abstract

The principles and practice of pyrolysis combustion flow calorimetry as embodied in the Federal Aviation Administration microscale combustion calorimeter (MCC) are reviewed to produce a technical basis for a standard set of operating parameters and procedures that produce accurate, repeatable, and reproducible thermal combustion properties of materials as codified in the American Society for Testing and Materials (ASTM) D7309 Standard Test Method for Determining Flammability Characteristics of Plastics and Other Solid Materials Using Microscale Combustion Calorimetry. The relationship between MCC thermal combustion properties of materials and the results of fire and flammability tests are presented and discussed.

17. Key Words	18. Distribution Statement
Pyrolysis, Combustion, Microscale combustion calorimeter, Flammability, Polymers, Plastics	This document is available to the U.S. public through the National Technical Information Service (NTIS), Springfield, Virginia 22161. This document is also available from the Federal Aviation Administration William J. Hughes Technical Center at actlibrary.tc.faa.gov.

19. Security Classif. (of this report)	20. Security Classif. (of this page)	21. No. of Pages	22. Price
Unclassified	Unclassified	95	

TABLE OF CONTENTS

LIST OF FIGURES

LIST OF TABLES

LIST OF SYMBOLS AND ACRONYMS

A	Frequency factor (s^{-1})
c	Heat capacity (J/kg-K)
E_a	Activation energy (J/mole)
F	Combustion stream flow rate
$\bar{h}$	Average convective heat transfer coefficient (W/m^2)
h_c	Heat of combustion of gases (J/g)
m	Sample mass
M_w	Molecular Weight (g/mole)
q''	Heat flux or areal heat release rate (W/m^2)
Q_∞	Total Heat Release (J/g)
Q'	Specific Heat Release Rate (W/g)
$Q'_{\max}$	Maximum values (W/g)
R	Gas constant (J/mole-K)
T	Temperature (K)
X_{O_2}	Volume (or mole) fraction of oxygen in combustor
V_{eff}	Effective volume (m^3)
ε	Surface emissivity
σ	Boltzmann radiation constant (5.7 x 10^8 W m^{-2} K^{-4})
κ	Thermal conductivity (W/m-K)
ρ	Density (kg/m^3)
ABS	Acrylonitrile-butadiene-styrene
ASTM	American Society for Testing and Materials
CHF	Critical heat flux
CO/CO_x	Carbon Monoxide Fraction
DAC	Data acquisition and control
DT	Differential Temperature
DTGA	Derivative Thermogravimetric Analysis
EHOC	Effective heat of combustion
EPR	Ethylene-propylene rubber
FAA	Federal Aviation Administration
FEP	Fluorinated ethylene propylene
HB	Horizontal Burning
HDPE	High-density polyethylene
HIPS	High impact polystyrene
HRR	Specific heat release rate Q' as indicated on MCC software (W/g)
LOI	Limiting Oxygen Index (%)
MAX	Measurement & Automation Explorer
MCC	Microscale combustion calorimeter
PA66	Nylon 66
PB	Polybutadiene
PC	Polycarbonate
PCFC	Pyrolysis-combustion flow calorimetry

PEEK	Poly ether ether ketone
PEI	Poly etherimide
PET	Polyethyleneterephthalate
PID	Proportional Integral Derivative
PIS	Polyisoprene
PMMA	Polymethylmethacrylate
POM	Polyoxymethylene
PP	Polypropylene
PPS	Polyphenylene sulfide
PPSU	Polyphenyl sulfone
PS	Polystyrene
PT	Phenolic Triazine
PVC	Polyvinyl chloride
PVDF	Polyvinylidene fluoride
SEA	Specific Extinction Area of Smoke (m^2/kg)

EXECUTIVE SUMMARY

This report describes the theory, construction, and operation of a microscale combustion calorimeter (MCC) and explains how the results relate to other flammability tests. The MCC was developed by the Federal Aviation Administration (FAA) to screen research materials for a fireproof aircraft cabin. Standard flammability tests require kilograms of material, thus the milligram (10^{-6} kg) samples of MCC are microscale by comparison. The MCC uses principles of analytical pyrolysis, combustion gas analysis, and flow calorimetry (i.e., pyrolysis-combustion flow calorimetry [PCFC]) to simulate the flaming combustion of plastics in a convenient laboratory test. The MCC described in this report is a particular embodiment of PCFC in which the processes of flaming combustion are separated into fuel generation (condensed phase) and heat generation (gas phase) that can be individually controlled. This level of operating flexibility is useful for research, development, and quality control of fire-resistant plastics. The operating parameters and procedures described in this report were codified by the American Society for Testing and Materials (ASTM) in 2007 as ASTM D7309, "A Standard Test Method for Determining Flammability Characteristics of Plastics and Other Solid Materials Using Microscale Combustion Calorimetry." The MCC described in this report is a particular design used by the FAA that conforms to ASTM D7309, but may not represent all such devices.

FAA Microscale Combustion Calorimeter

1. INTRODUCTION.

This report describes the theory, construction, and operation of a microscale combustion calorimeter (MCC) and explains how the results relate to other flammability tests. The MCC was developed by the Federal Aviation Administration (FAA) to screen research materials for a fireproof aircraft cabin [1-5]. Standard flammability tests require kilograms of material, thus the milligram (10^{-6} kg) samples of MCC are microscale by comparison. The MCC uses principles of analytical pyrolysis, combustion gas analysis by oxygen depletion, and flow calorimetry (i.e., pyrolysis-combustion flow calorimetry [PCFC]) to simulate flaming combustion in a convenient laboratory test [5]. The MCC described in this report is a particular embodiment of PCFC in which the processes of flaming combustion are separated into fuel generation (condensed phase) and heat generation (gas phase) in individually controlled microscale reactors. This configuration allows the user to change the heating rate, sample size, and atmosphere (inert or reactive) in the condensed-phase micro-reactor (pyrolyzer) to examine the effect of these parameters on the fuel-generation process of the solid. The user can also change the temperature, residence time, and atmosphere of the fuel gases in the gas-phase microreactor (combustor) to examine the effect of these parameters on the rate or extent of chemical reactions in the flame. This level of operating flexibility is useful for research, development, and quality control of fire resistant plastics.

The goal of this report is to review the principles of PCFC, as practiced in the FAA MCC, to provide a technical basis for a set of operating parameters and procedures that will ensure accurate, repeatable, and reproducible MCC results. This standard practice ensures that the sample is thermally equilibrated during the test and that the processes of pyrolysis and combustion are forced to completion so that the results depend only on the chemical composition of the material being tested and not on the conditions of the test. This standard practice is codified as the Standard Test Method for Determining Flammability Characteristics of Plastics and Other Solid Materials Using Microscale Combustion Calorimetry. The MCC configuration, data acquisition and control features, analysis software, and user interfaces described in this report are a particular embodiment of PCFC used by the FAA that conforms to ASTM D7309-13 [6], but may not represent all such devices.

2. THEORY OF OPERATION.

2.1 FLAMING VS. NONFLAMING COMBUSTION.

Flaming combustion occurs when gaseous fuels mix with air (oxygen) at high temperatures to generate heat, light, and combustion products. In laboratory and industrial burners, gaseous hydrocarbon fuels are mixed with air prior to ignition to prevent soot formation. Heat production is a maximum in premixed hydrocarbon gas flames because no thermal energy is required to vaporize the fuel and combustion is relatively complete, producing carbon dioxide (CO_2) and water in near quantitative yield [7]. In contrast to the controlled process of premixed flaming combustion of gases and vapors in burners and engines, flaming combustion of solids involves coupling of the condensed-phase and gas-phase processes that can lead to auto-acceleration, hazardous conditions, and incomplete combustion [8 and 9].

The burning of condensed phases (liquids and solids) by flaming combustion involves pyrolysis/vaporization of the solid/liquid to gaseous fuel and combustion of the gaseous fuel [10]. The rates of these two chemical processes are determined by diffusion of heat and oxygen, respectively. Figure 1 is a schematic diagram of a burning bar of polymer. The pyrolysis zone is shown as a thin, speckled layer at the end of the specimen beneath the flame. The amount of heat entering the pyrolysis zone from the flame must be sufficient to break the chemical bonds in the polymer and reduce it to low molecular weight, volatile species to continue the fuel generation process. Since the flame consumes all of the oxygen in the air above the specimen, the pyrolysis process is anaerobic. Figure 1 shows the volatile pyrolysis products as the shaded, fuel-rich region above the solid and internal to the flame sheet (combustion zone). The combustion zone is the region of the flame where the fuel gases mix with air at a near-stoichiometric ratio and burn at temperatures ≈ 2000K. The combustion zone is a thin sheet at the outer surface of the flame, and is indicated as the white region at the flame periphery in the two-dimensional figure 1.

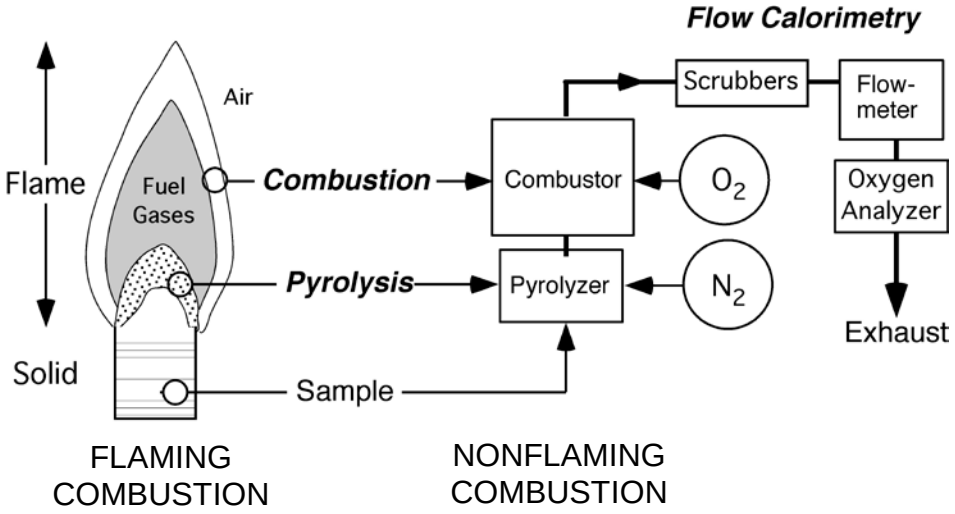

Figure 1. Flaming and Nonflaming Combustion

From an energy perspective, the burning of condensed phases is less efficient than premixed burning because a fraction of the heat of combustion is required to vaporize (liquids) or pyrolyze (solids) the condensed phase to generate gaseous fuel. If the fraction of the combustion heat is insufficient to completely pyrolyze the solid, the heat released by combustion is reduced and burning is incomplete. Flaming combustion of condensed phases is less efficient than premixed burning from a chemical perspective because the fuel and air mix only by diffusion, so that the dimensions, residence time, and temperature of the combustion zone may be insufficient for complete combustion because of chemical kinetic or oxygen limitations. Thus, flaming combustion of condensed phases is a coupled, potentially inefficient process that occurs at a rate controlled mainly by diffusion of heat into the solid and diffusion of air into the flame.

In contrast to the flaming combustion of solids, the nonflaming combustion of solids in PCFC or MCC is highly controlled and efficient under proper conditions [5]. In this regard, MCC more closely resembles the premixed burning of gases and vapors in batch mode than the flaming

combustion of solids because the processes of pyrolysis and combustion are separated and carried to completion in a controlled manner.

2.2 PYROLYSIS: THE FUEL GENERATION PROCESS.

Pyrolysis is the process by which the solid polymer thermally decomposes to gaseous fuel at a burning surface (flaming combustion) or in the MCC (nonflaming combustion). The fuel-generation process is anaerobic at the burning surface because the flame consumes all of the available oxygen. Figure 2 shows that the mass fraction of solid residue measured immediately after flaming combustion has ceased in a fire calorimeter is the same as that measured after anaerobic pyrolysis in a thermogravimetric analyzer [11] or MCC.

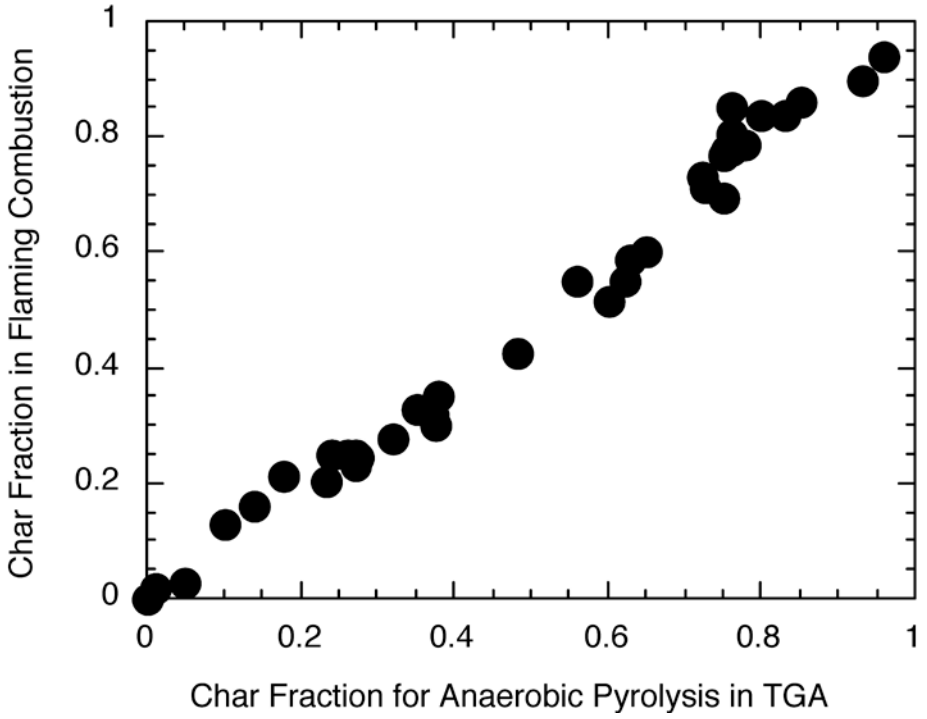

Figure 2. Char Fraction in Flaming Combustion vs. Anaerobic Pyrolysis

The fuel-generation process, as it occurs in the MCC, is idealized as a single-step pyrolysis reaction in which a polymer thermally decomposes to fuel gases and possibly a solid char with rate constant *k*:

$$\text{POLYMER} \rightarrow \text{GAS} (\uparrow) + \text{CHAR (s)}$$

The mass loss rate due to thermal cleavage of primary chemical bonds (thermolysis) to produce volatile fuel in terms of the instantaneous sample mass m and char or inert mass m_c is:

$$-\frac{dm}{dt} = k(m - m_c) \tag{1}$$

Typically, k has the Arrhenius form, $k(T) = k = A\exp[-E_a/RT]$ with frequency factor A, activation energy E_a, gas constant R, and temperature T. Equation 1 must be recast in terms of quantities that are measured in the MCC (i.e., the initial mass of the sample m_0 and the inert/char fraction after the test) $\mu = m_c/m_0$. This is accomplished by defining a specific mass, $x = m/m_0$, so that the specific mass loss rate is proportional to the pyrolyzable mass fraction $(x - \mu)$:

$$-\frac{dx}{dt} = k(x - \mu) \tag{2}$$

Specifying a constant heating rate, $\beta = dT/dt$ transforms the dependent variable in equation 2 from time to temperature. Separating variables and integrating

$$-\ln\left[\frac{x-\mu}{1-\mu}\right] = Y(T) \tag{3}$$

where

$$Y(T) = \frac{A}{\beta}\int_{T_0}^{T} \exp\left[-\frac{E_a}{R\theta}\right] d\theta \approx \frac{k(T)RT^2}{\beta\left(E_a + 2RT\right)} \tag{4}$$

Equation 4 is the Arrhenius temperature integral and the last term is a semi-exact solution for the usual case where $E_a >> RT$ and the starting temperature T_0 is room temperature [12]. According to equations 3 and 4, the specific mass x at temperature T for an experiment conducted at a constant heating rate is:

$$x(T) = \mu + (1-\mu)\exp\left[-Y(T)\right] \tag{5}$$

Differentiating equation 5 with respect to time gives the specific mass loss rate at temperature T in a constant heating rate experiment:

$$x'(T) = -\frac{dx}{dt} = -\beta\frac{dx}{dT} = (1-\mu)k(T)\exp\left[-Y(T)\right] \tag{6}$$

Setting the time derivative of equation 6 (second derivative of x with respect to time) equal to zero shows that the Arrhenius rate constant, k, has a particular value at the temperature of maximum pyrolysis rate, T_p [13].

$$k(T_p) = Ae^{-E_a/RT} = \frac{\beta E_a}{RT_p^2} \tag{7}$$

The temperature at maximum pyrolysis rate, T_p, is obtained from the root E_a/RT_p of equation 7, written in the form:

$$\ln\left[\frac{E_a}{RT}\right]^2 + \frac{E_a}{RT} - \ln\left[\frac{AE_a}{\beta R}\right] = 0 \tag{8}$$

Consequently, E_a and A are not independent and can assume any values that satisfy equation 8 for a particular (measured) β and T_p. This is known as kinetic compensation. In fire modeling, it is found that T_p, not the individual values of E_a and A, determines the burning rate [14].

Substituting $k(T_p)$ into equation 6 gives the maximum specific mass loss rate in a constant heating rate experiment with e being the natural number.

$$x'_{\max} = \frac{-1}{m_0}\frac{dm}{dt}\bigg|_{T=T_p} = (1-\mu)\frac{\beta E_a}{e^{\gamma} RT_p^2} \tag{9}$$

The exponent $\gamma = E_a/(E_a+2RT_p)$ in the denominator of equation 9 is near unity for typical polymer thermal-decomposition parameters, $E_a >> 2RT_p$.

The term RT_p^2/E_a, which appears in equations 7 and 9, is the characteristic temperature interval for pyrolysis ΔT. According to equation 6, the specific mass loss rate at temperature T and at some lower temperature, T-ΔT, are in the ratio:

$$r = \frac{x'(T-\Delta T)}{x'(T)} = \frac{k(T-\Delta T)}{k(T)} e^{-y(T-\Delta T)+y(T)} \tag{10}$$

For $T = T_p >> \Delta T$, the ratio of the pyrolysis rate constants becomes:

$$\frac{k(T_p-\Delta T)}{k(T_p)} = \frac{\exp\left[-\frac{E_a}{R}\left(\frac{1}{T_p}+\frac{\Delta T}{T_p^2}+\frac{(\Delta T)^2}{T_p^3}+\square\right)\right]}{\exp\left[-\frac{E_a}{RT_p}\right]} \approx \exp\left[-\frac{E_a\,\Delta T}{RT_p^2}\right] \tag{11}$$

Substituting equations 4 and 11 into equation 10:

$$\ln\left[\frac{x'(T_p - \Delta T)}{x'(T_p)}\right] = -\lambda = 1 - \frac{E_a}{R}\frac{\Delta T}{T_p^2} - \exp\left[-\frac{E_a \Delta T}{R T_p^2}\right] \tag{12a}$$

or

$$1 + \lambda = \frac{E_a \Delta T}{R T_p^2} + \exp\left[-\frac{E_a \Delta T}{R T_p^2}\right] \tag{12b}$$

When $\lambda = 1/e$ in equation 12b, $E_a \Delta T / R T_p^2 = 1$, and the characteristic temperature interval for pyrolysis is:

$$\Delta T = \frac{R T_p^2}{E_a} \tag{13}$$

According to equation 12a, the ratio of the mass loss rates at $\lambda = 1/e$ is $x'(T_p - \Delta T)/x'(T_p) = e^{-1/e} = 0.692$ (i.e., the specific mass loss rate at temperature $T_p - R T_p^2/E_a$ is 69% of the value at T_p for the first-order thermal decomposition of an infinitesimal mass of solid). A plot of equation 6 is shown in figure 3 for $\beta = 1$ K/s and $A = 9 \times 10^{15}$ s^{-1}, $E_a = 253$ kJ/mole determined for poly(hexamethyleneadipamide) (PA66) from MCC data (see section 8.1). The temperature interval between $x'_{max} = 20$ mg/g-s and $x' = 0.692 x'_{max} = 13.8$ mg/g-s measured along the abscissa of the graph is $\Delta T = (494\text{-}475)°C = 19°C = 19K$. This result is identical to the predicted value when using equation 13 with $T_p = 494°C = 767K$, $\Delta T = (8.314 \text{ J/mole-K})(767K)^2/(253 \text{ kJ/mole}) = 19K$.

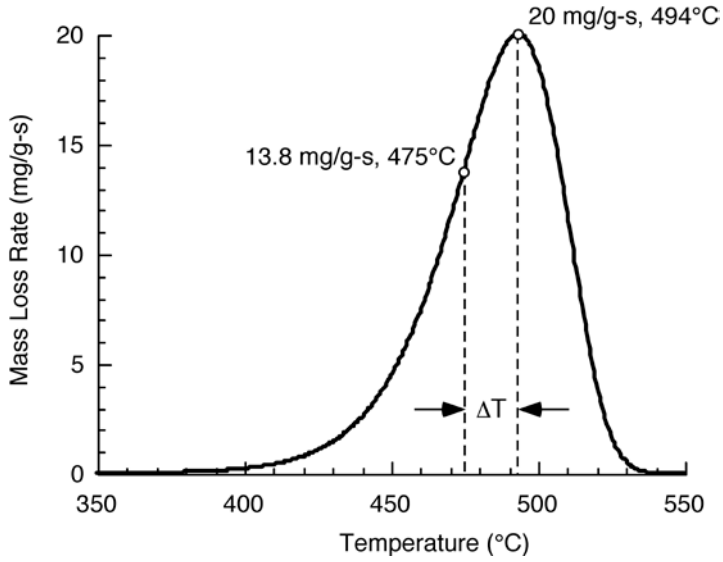

Figure 3. Plot of Specific Mass Loss Rate of PA66 (According to equation 6, showing the relationship between T_p and ΔT)

Substituting equation 13 into equation 7, with $k(T_p) = k_p = \beta E_a / R T_p^2 = \beta / \Delta T$, the pyrolysis temperature is related to the Arrhenius parameters and heating rate:

$$T_p = \frac{E_a}{R \ln\left[A \Delta T / \beta\right]} = \frac{E_a}{R \ln\left[A / k_p\right]} \tag{14}$$

Multiplying the specific mass loss rate (equation 6) by the heat of complete combustion of the fuel gases h_c (J/g-volatiles), gives the specific heat release rate history of the sample Q' (W/g-sample) as a function of temperature in the MCC for a material undergoing a first-order thermal decomposition reaction at constant heating rate, during which the pyrolysis gases are completely oxidized (combusted).

$$Q' = Q_\infty \, k(T) \exp\left[-Y(T)\right] \tag{15}$$

In equation 15, Q_∞ (J/g-sample) = $(1-\mu)h_c$ is the heat of complete combustion of the sample. It follows that the heat of combustion of fuel gases is:

$$h_c = \frac{Q_\infty}{1-\mu} \quad \text{(J/g-gas)} \tag{16}$$

Figure 4 compares experimental MCC data for PA66 at a heating rate of β = 1 K/s to a fit of the first order kinetic model (equation 15) using the indicated kinetic and combustion parameters (see table 5). Figure 4 shows that equation 15 describes the Q' history well for PA66 and illustrates the relationship between the various thermal combustion properties. The onset temperature for thermal decomposition (fuel generation), T_{onset}, is the temperature at which Q' reaches a few percent of $Q'_{\max}$ or the temperature at which the tangent to Q' intersects the temperature axis in the early part of the experiment. The maximum Q' for a first-order pyrolysis/combustion process is obtained by multiplying equation 9 by h_c.

$$Q'_{\max} = -\frac{h_c}{m_0} \left.\frac{dm}{dt}\right|_{T=T_p} = \frac{\beta Q_\infty}{e^\gamma R T_p^2 / E_a} = \frac{\beta Q_\infty}{\Delta T_p} \tag{17}$$

The half-width of the pyrolysis peak on the temperature axis is the denominator of equation 17:

$$\frac{e^\gamma R T_p^2}{E_a} = e^\gamma \Delta T \equiv \Delta T_p$$

It has been shown [5] that Q'_{max} is not strictly proportional to β because of the heating rate dependence of T_p (see equation 9), which can be accounted for by defining a reference heating rate, β_0 = 1 K/s, so that:

$$Q'_{max}(\beta) = Q'_{max}(\beta_0)\left[\frac{\beta}{\beta_0}\right]^{1-a} = \frac{\beta_0 Q_\infty}{eRT_{p,0}^2}\left[\frac{\beta}{\beta_0}\right]^{1-a} = \frac{\beta_0 Q_\infty}{\Delta T_{p,0}}\left[\frac{\beta}{\beta_0}\right]^{1-a} = \beta_0\,\eta_c\left[\frac{\beta}{\beta_0}\right]^{1-a} \quad (18)$$

In equation 18, $a = 2RT_{p,0}/E_a$ and $T_{p,0}$ is the temperature at Q'_{max} when $\beta = \beta_0$. Equation 18 defines a theoretical parameter η_c that is independent of test conditions (β), contains only material properties (Q_∞, $T_{p,0}$, and E_a), and has the units (J/g-K) and significance of a heat release capacity [5 and 15].

$$\eta_c = \frac{Q'_{max}}{\beta}\left[\frac{\beta}{\beta_0}\right]^{a} = \frac{Q_\infty}{e^\gamma RT_{p,0}^2 / E_a} = \frac{Q_\infty}{\Delta T_{p,0}} \quad (19)$$

Equation 19 is used to calculate η_c from Q'_{max} measured at any heating rate β. The heating rate dependence of Q'_{max}/β predicted by equation 19 (shown as solid lines in figure 5) is computed from the β_0 = 1 K/s data in figure 5 for high-density polyethylene (HDPE), high impact polystyrene (HIPS), polymethylmethacrylate (PMMA), polyoxymethylene (POM), and fluorinated ethylene propylene (FEP), tested in the MCC over a wide range of heating rates (shown as symbols in figure 5). The effect of heating rate on Q'_{max}/β is about ±10% over the range of heating rates in figure 5, but is only about ±4% over the range of heating rates β = 0.5 to 2 K/s typically used in MCC.

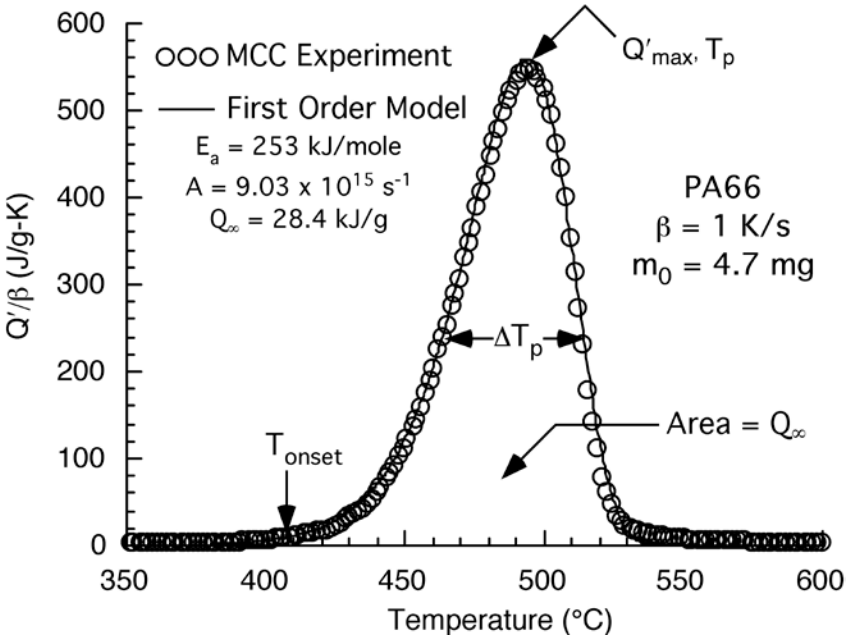

Figure 4. Comparison of MCC Experiment to First-Order Kinetic Model for PA66 at β = 1 K/s (Using the indicated parameters)

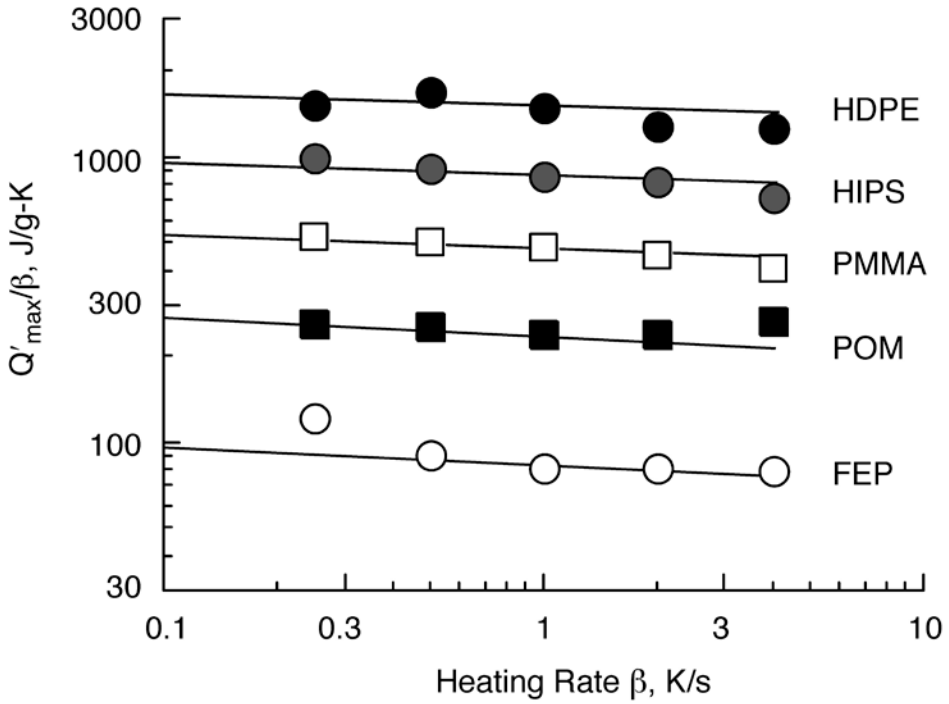

Figure 5. Plot of Q'_{max}/β vs. β in the MCC for HDPE, HIPS, PMMA, POM, and FEP (Points are experimental data. Solid lines are equation 19.)

2.3 COMBUSTION: THE HEAT GENERATION PROCESS.

In flaming combustion, the volatile fuel generated by pyrolysis at the burning surface reacts with the oxygen in the air to form a high-temperature diffusion flame that typically yields complete (CO_2, H_2O, HX) and incomplete (CO, HC) combustion products, where X is a halogen, HX is a halogen acid, and HC is an unburned solid or gaseous hydrocarbon. A simplified description of the gas-phase reaction for flaming combustion is [5 and 7]

$$\textit{Fuel Gases} + aO_2 \rightarrow \text{Complete and Incomplete Combustion Products}$$

The rate of fuel consumption by oxidation, therefore, follows *n*-th order reaction kinetics [7]:

$$-\frac{d[F]}{dt} = k_c[F][O_2]^a \tag{20}$$

In equation 20, the reaction order is $n = a + 1$, $[F]$ and $[O_2]$ are the molar concentrations of fuel and oxygen in the gas phase, respectively, in units of moles/m^3, and $k_c = A\exp[-E/RT]$ is the global temperature-dependent rate constant for combustion. The use of global kinetics (e.g., equation 20) to express the oxidation rate is a simplification that ignores intermediate species in diffusion flames, such as OH, HO_2, H, and O radicals that are susceptible to attack by such gas phase active flame retardants as halogens and PO_x species. Equation 20 shows that the rate of

fuel consumption by oxidation, $-d[F]/dt$, decreases when the oxygen concentration or the flame temperature is low, so that incomplete combustion is expected if the residence time in the combustion zone is short. However, if combustion occurs in a large excess of oxygen (e.g., premixed flame or MCC combustor), the instantaneous $[O_2]$ and initial $[O_2^0]$ concentrations of oxygen are effectively equal, and equation 20 becomes:

$$-\frac{d[F]}{dt} = \left\{k_c[O_2]^g\right\}[F] = k_{app}[F] \tag{21}$$

In equation 21, $k_{app} = k_c[O_2^0]^g = A[O_s^0]^g \exp[-E_a/RT]$ is an apparent rate constant for fuel combustion with the frequency factor A having units such that k_{app} has units of reciprocal time. Equation 21 is unimolecular (first order) with respect to the fuel species and can be solved for $[F]$ at time t when the fuel concentration at time zero is $[F]_0$.

$$\frac{[F]}{[F]_0} = \exp\left[-k_{app}\, t\right] = 1-\chi \tag{22}$$

Equation 22 contains the extent of reaction of the fuel gases with oxygen, $\chi = \chi(t,T)$. Rearranging equation 22 gives the time t_χ required to achieve the extent of reaction χ at constant temperature T for a gaseous fuel having oxidation kinetic parameters $A(s^{-1})$ and E_a (J/mole).

$$t_\chi = \frac{-\ln[1-\chi]}{A}\exp\left[E_a / RT\right] \tag{23}$$

Kinetic parameters for isothermal oxidation of methane (Methane1) and the pyrolysis products of polypropylene (PP) and polymethylmethacrylate (PMMA) in excess oxygen (fuel lean) conditions were obtained in our laboratory [16]. Kinetic parameters for oxidation of methane (Methane2) [17], PMMA1, PMMA2, polybutadiene (PB), polyisoprene (PIS) rubber, ethylene-propylene rubber (EPR), and a polycarbonate/acrylonitrile-butadiene-styrene (PC/ABS) blend were obtained from the literature [18]. Table 1 shows these kinetic parameters for oxidation of these gaseous fuels.

Reaction times t_χ for complete combustion (χ = 0.995) of methane and polymer pyrolysis products in excess oxygen, calculated using the kinetic parameters listed in table 1, are shown in figure 6 versus temperature. It is clear from figure 6 that thermal oxidation of hydrocarbons under fuel-lean conditions (excess oxygen) is essentially (99.5%) complete in less than 10 seconds at 900°C. Figure 7 shows that oxygen (and methane) are entirely consumed by combustion for a stoichiometric 1:2 molar ratio of methane to oxygen (i.e., $CH_4 + 2O_2 \rightarrow CO_2 + 2H_2O$) at a residence time of 8 seconds and at a combustor temperature above 800°C [5], in agreement with the data in figure 6.

Table 1. Kinetic Parameters for Thermal Oxidation of Gaseous Fuels

Fuel	E (kJ/mole)	A (s^{-1})	Temperature Range (K)	Ref.
Methane gas (Methane1)	241	10^{12}	1020-970	16
Methane gas (Methane2)	230	10^{10}	1000-2000	17
PMMA1	62	10^{4}	725-973	16
PMMA2	130	10^{7}	773-898	18
PP	94	10^{5}	607-656	16
PB	91	10^{5}	800-945	18
PIS	75	10^{4}	825-975	18
EPR	133	10^{8}	800-975	18
PC/ABS blend	188	10^{10}	800-975	18

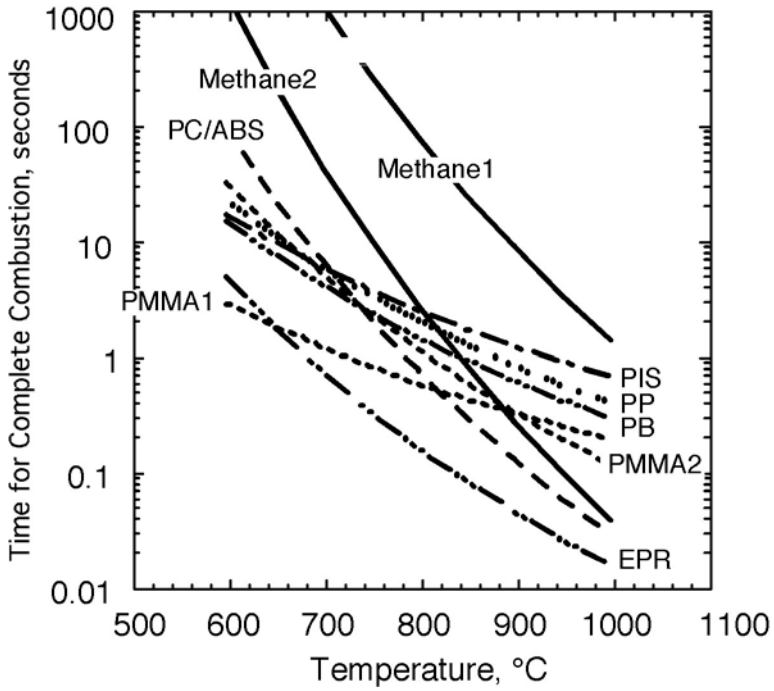

Figure 6. Time-Temperature Curves for 99.5% Combustion of Various Fuel Gases

If m_{O_2} and m_F are the mass of oxygen and fuel in the combustion stream, the stoichiometric oxygen/fuel mass ratio is $r_0 = [m_{O_2}/m_F]_{stoich}$ and the equivalence ratio for an arbitrary oxygen/fuel mass ratio $[m_{O_2}/m_F]$ is [7]:

$$\Phi = \frac{\left[m_{O_2} / m_F \right]_{stoich}}{\left[m_{O_2} / m_F \right]} = \frac{\left[m_F / m_{O_2} \right]}{\left[m_F / m_{O_2} \right]_{stoich}} = r_0 \frac{[m_F]}{[m_{O_2}]} \tag{24}$$

Using this definition of the equivalence ratio, $\Phi<1$ for fuel-lean (oxygen-rich) mixtures, $\Phi = 1$ for stoichiometric mixtures, and $\Phi>1$ for fuel rich mixtures.

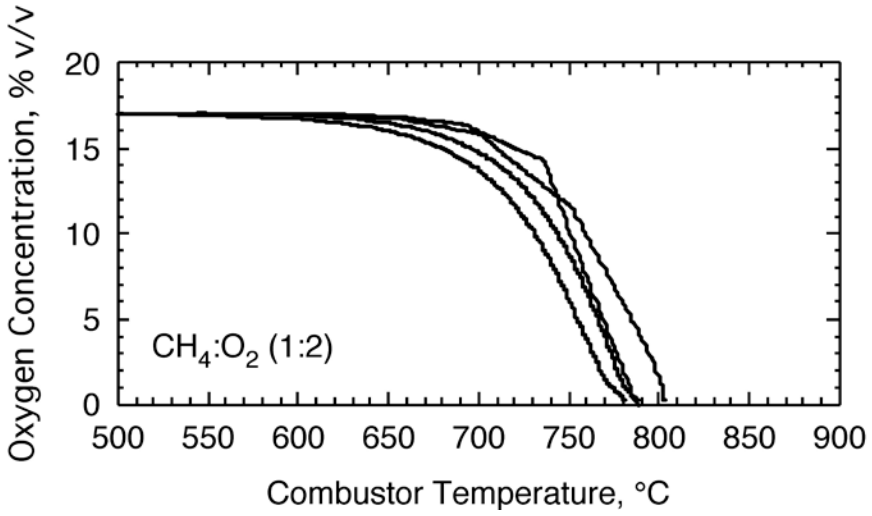

Figure 7. Oxygen Concentration vs. Combustor Temperature for a Stoichiometric Mixture of Methane and Oxygen at a Flow Rate of 100 cm^3/min in the MCC (Multiple experiments)

Under normal MCC operating conditions, $\Phi<1$ and there is sufficient time (9 seconds) and temperature (900°C) for complete thermal oxidation of the fuel gases to CO_2, H_2O, and possibly HX in nonflaming combustion. Figure 7 shows that thermal oxidation of methane is complete, even at the stoichiometric oxygen/fuel mass ratio (mole ratio 2:1). Thus, for $\Phi\leq1$, the only products are those of complete combustion and the amount of oxygen consumed is uniquely related to the fuel composition, $C_cH_hO_mN_nX_x$

$$C_cH_hO_mN_nX_x + (c + \frac{h - x - 2m}{4})\, O_2 \rightarrow cCO_2 + \frac{h - x}{2}\, H_2O + \frac{n}{2}N_2 + xHX \tag{25}$$

The stoichiometric oxygen/fuel mass ratio r_0 is readily calculated from equation 25 for fuels of known composition, and is in the range $r_0 = 2.0 \pm 1.5$ for the majority of organic compounds [19]. Thornton [20] was the first to notice that the net heat of complete combustion of organic gases and liquids h_c^0 (J/g-fuel) divided by the stoichiometric oxygen-to-fuel mass ratio r_0 (g-O_2/g-fuel) was essentially constant and independent of the type of fuel.

$$C = h_c^0/r_0 = 13.1 \pm 0.6 \text{ kJ/g-}O_2 \tag{26}$$

Thornton's observation that the heat of combustion of oxygen with typical organic liquids and gases is a constant value was extended to solids by Huggett [21] and became the basis for oxygen consumption calorimetry [22], whereby measurement of the mass of oxygen consumed from the combustion atmosphere is used to deduce the amount of heat released during the burning of materials and products [23]. Equation 26 is valid only for complete combustion (i.e., equation 25) as occurs in the MCC. In fire calorimeters, which measure the heat release rate-per-unit surface area in flaming combustion, the products of incomplete combustion must be measured and included in the calculation of q_c'' by oxygen consumption calorimetry [22].

3. MEASUREMENT PRINCIPLES.

3.1 OXYGEN CONSUMPTION FLOW CALORIMETRY.

Flow calorimetry is a method for determining the amount of heat produced or absorbed in a process (e.g., burning) that occurs in a fluid stream (e.g., air) as deduced from the properties and flow rate of the fluid stream before and after the event. The FAA uses this method to measure the HRR of aircraft cabin materials by measuring the sensible enthalpy rise (temperature increase) of an air stream passing by a burning sample at a constant flow rate [24 and 25]. Another flow-calorimetry method used for fire testing measures the flow rate and oxygen concentration of an air stream passing by a burning sample to deduce the heat produced using oxygen-consumption calorimetry [22], which is the most widely used method for measuring heat release by combustion in fire calorimeters [23]. The MCC also operates by oxygen-consumption flow calorimetry, except that in the MCC, the pyrolysis gases generated during the heating program are thermally oxidized to completion, rather than being partially oxidized as occurs in flaming combustion in fire calorimeters.

The rate at which heat is released by combustion is estimated by oxygen consumption from the equation [22],

$$q_c'(W) \equiv E\left[\dot{m}_{O_2}^{in} - \dot{m}_{O_2}^{out}\right] = E\left[\left(\rho_{O_2} F X_{O_2}\right)_{in} - \left(\rho_{O_2} F X_{O_2}\right)_{out}\right] \tag{27}$$

In equation 27, $\dot{m}_{O_2}^{in}$ and $\dot{m}_{O_2}^{out}$ are the mass flow rate of oxygen entering and exiting the combustor, respectively, E = 13.1±0.6 kJ/g-O_2 [21] is the average heat of combustion of oxygen with hydrocarbon fuels. The mass flow rates of oxygen are written in terms of the total volumetric flow rate, F, the oxygen mole (volume) fraction, X_{O_2}, and the oxygen density, ρ_{O_2} entering and exiting the combustor. In the ASTM D7309 method [6], the flow rate F_{in} and oxygen fraction $X_{O_2}^{in}$ entering the combustor are specified, and the flow rate F_{out} and oxygen fraction $X_{O_2}^{out}$ exiting the combustor are measured, all at room temperature (T_0 = 298K) and ambient pressure (P_0 = 1 Bar). In this case, ρ_{O_2} is the density of oxygen at 298K and 1 Bar, and the equation for oxygen consumption flow calorimetry as measured in ASTM D7309 is,

$$q_c' = E\rho_{O_2} F_{out}\left(X_{O_2}^{in} - X_{O_2}^{out}\right)\left\{1 + \frac{F_{in} - F_{out}}{F_{out}(X_{O_2}^{in} - X_{O_2}^{out})} X_{O_2}^{in}\right\} = q'\left\{1 + S_c X_{O_2}^{in}\right\} \tag{28}$$

The first term on the far right hand side of equation 28, q', is the heat release rate in Watts in the MCC computed from the flow rate and oxygen concentration of the dry gases exiting the combustor, while the bracketed term includes a stoichiometric coefficient, S_c that accounts for changes in the gas composition due to drying. If n_{O_2} and n_{N_2} are the (large) number of moles of oxygen and nitrogen entering the combustor compared to the n_F moles of fuel,

$$X_{O_2}^{in} = \frac{n_{O_2}}{n_{O_2} + n_{N_2} + n_F} \approx \frac{n_{O_2}}{n_{O_2} + n_{N_2}} = \frac{n_{O_2}}{\sum n_i^{in}} \tag{29}$$

The mole balance for stoichiometric combustion of fuel in the combustor that produces carbon dioxide and water as combustion products is: $n_F + \Delta n_{O_2} \rightarrow n_{CO_2} + n_{H_2O}$. In the MCC, water is removed from the combustion stream prior to measuring the final oxygen mole fraction in the presence of carbon dioxide, so the oxygen mole fraction exiting the combustor is,

$$X_{O_2}^{out} = \frac{n_{O_2} - \Delta n_{O_2}}{n_{O_2} - \Delta n_{O_2} + n_{N_2} + n_{CO_2}} = \frac{n_{O_2} - \Delta n_{O_2}}{\Sigma n_i^{out}} \tag{30}$$

Inserting equations 29 and 30 into the last term in equation 28, with $F_{in} = (RT_0/P_0)(d\sum n_i^{in}/dt)$, $F_{out} = (RT_0/P_0)(d\Sigma n_i^{out}/dt)$, and $(F_{out} - F_{in})/F_{in} << 1$, with R the gas constant,

$$S_c = \frac{F_{in} - F_{out}}{F_{out}(X_{O_2}^{in} - X_{O_2}^{out})} = \frac{\Delta n_{O_2} - n_{CO_2}}{\Delta n_{O_2} + n_{O_2}(F_{out} - F_{in})/F_{in}} \approx \frac{\Delta n_{O_2} - n_{CO_2}}{\Delta n_{O_2}} \tag{31}$$

For an initial sample mass m_0 and for $S_c X_{O_2}^{in} << 1$, the specific heat release rate measured in the MCC is:

$$Q' = \frac{q_c'/m_0}{1 + S_c X_{O_2}^{in}} = \frac{q_c'}{m_0}\left(1 - S_c X_{O_2}^{in} + (S_c X_{O_2}^{in})^2 - (S_c X_{O_2}^{in})^3 + \cdots\right) \approx Q_c'\left(1 - S_c X_{O_2}^{in}\right) \tag{32}$$

The apparent heat of combustion of the solid fuel is the time integral of equation 32,

$$Q_\infty = \int_0^\infty Q'(t)dt = Q_c\left(1 - S_c X_{O_2}^{in}\right) \tag{33}$$

The theoretical heat of combustion by oxygen consumption for n_F moles of fuel having molar mass M_F with M_{O_2} = 32 g/mole the molar mass of oxygen is,

$$Q_c = E\frac{m_{O_2}}{m_F} = E\frac{\Delta n_{O_2} M_{O_2}}{n_F M_F} \tag{34}$$

The term $S_c X_{O_2}^0$ on the right hand side of equations 32 and 33 accounts for the small difference in the composition of the combustion stream when water is removed. According to equation 31, the stoichiometric coefficient for a fuel having chemical composition $C_cH_hO_mN_nX_x$ is:

$$S_c = 1 - \frac{n_{CO_2}}{\Delta n_{O_2}} = \frac{h - x - 2m}{h - x - 2m + 4c} \tag{35}$$

The balanced stoichiometric combustion equations for four polymers that decompose largely or entirely as monomer leaving no pyrolysis residue are:

Polyethylene/PE: $C_2H_4 + 3O_2 \rightarrow 2CO_2 + 2H_2O$ (36)

Polystyrene/PS: $C_8H_8 + 10O_2 \rightarrow 8CO_2 + 4H_2O$ (37)

Polymethylmethacrylate/PMMA: $C_5H_8O_2 + 6O_2 \rightarrow 5CO_2 + 4H_2O$ (38)

Polyoxymethylene/POM: $CH_2O + O_2 \rightarrow CO_2 + H_2O$ (39)

Table 2 contains the theoretical heats of combustion Q_c for PE, PS, PMMA, and POM calculated by equation 34 using the repeat unit molar mass M_p and the stoichiometric coefficients, $S_c = 1 - n_{CO_2}/\Delta n_{O_2}$ obtained from the moles of oxygen consumed and carbon dioxide generated in equations 36-39. For example, S_c = 1 - (5 moles CO_2/6 moles O_2) = 1-(5/6) = 1/6 for PMMA. Figure 8 shows experimental data points for Q_∞ versus $X_{O_2}^{in}$ for PE, PS, PMMA, and POM (averages of triplicate measurements). The lines in figure 8 are calculated using equation 33 with the theoretical Q_c and S_c of table 2. Excellent agreement between the experimental and theoretical (stoichiometric) relationship between Q_∞ and $X_{O_2}^{in}$ is observed for PE, PS, PMMA, and POM, which represent the maximum possible range of S_c.

Table 2. Repeat Unit Molar Mass M_p, Heat of Combustion Q_∞^0 and Stoichiometric Coefficient, S_c for PE, PS, PMMA, and POM

POLYMER	M_p (g/mole)	Q_∞^0 (kJ/g)	S_c
PE	28	44.9	1/3
PS	104	40.3	1/5
PMMA	100	25.2	1/6
POM	30	14.0	0

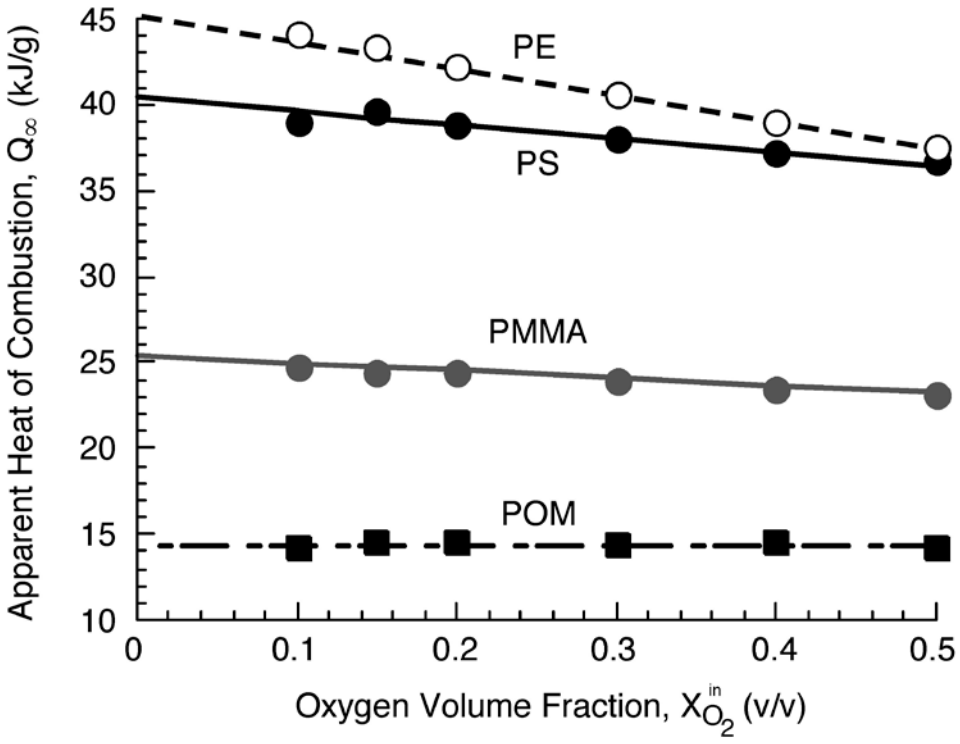

Figure 8. Apparent Heat of Combustion vs. Oxygen Fraction for PE, PS, PMMA, and POM (Points are Experimental Data. Lines are Theoretical Values.)

Equations 32 and 33 describe the effect of the chemical composition of the fuel on the heat release calculated in the MCC. If the chemical composition of the fuel is known, equations 32 and 33 can be used to correct the heat release data. If the chemical composition of the fuel is unknown, the magnitude of the effect can be estimated by measuring Q_∞ at different oxygen concentrations (e.g., $X_{O_2}^{in}$ = 0.2, 0.35 and 0.5) and fitting a regression line to the data to obtain Q_c as the intercept at $X_{O_2}^{in}$ = 0 and S_c as the ratio of the slope to the intercept. Under standard operating conditions, the deviation of the MCC heat release from the true value for typical polymers will be negligible. For example, under standard operating conditions, $X_{O_2}^{in}$ = 0.2, the relative deviation for typical S_c = 1/5 is of the order, $(Q_c\text{-}Q_\infty)/Q_c = S_c X_{O_2}^{in} = (1/5)(0.2) = 0.04$. This uncertainty of 4% in Q_c associated with stoichiometry is less than the reproducibility error of Q_∞ in the MCC (6%) and less than the coefficient of variation of E (5%).

For example, at $X_{O_2}^{0}$ = 0.2 the relative deviation for typical S_c = 1/5 is of the order,

$$\frac{Q_\infty^0 - Q_\infty}{Q_\infty^0} = (0.2)(1/5) = 0.04$$

This uncertainty of 4% in Q_∞^0 associated with stoichiometry is less than the reproducibility error of Q_∞ in the MCC (6%) and less than the coefficient of variation of E (5%).

Figure 9 is a schematic diagram showing the basic components of the MCC, including the independently heated and controlled pyrolysis and combustion sections, the purge and reactive gas inlets into these sections, respectively, and the flow-calorimetry section for the combustion gas stream, including the dryer, flow meter, and oxygen analyzer. Figure 10 is a detail of the integral pyrolyzer-combustor of the MCC. The single ceramic tube has an inner diameter of 1 cm and independently controlled heated lengths of 6.5 cm for the pyrolyzer and 21 cm for the combustor.

Previous MCC designs suffered from temporal distortion of the Q' history as a result of dilution of thermal decomposition products in the pyrolyzer by the incoming purge gas, condensation of the low-volatility pyrolysis products in the transfer line between the separate pyrolyzer and combustor, and axial mixing of the combustion products in the coiled combustor tube [4, 26, and 27]. These designs required heated transfer lines to ensure quantitative transport of pyrolysis products to the combustor and mathematical deconvolution (de-smearing) of the oxygen consumption history [3 and 4] to correct for mixing in the pyrolyzer and combustor to synchronize the recorded and actual Q' at temperature T. In the present design [5], the pyrolyzer and combustor are contiguous sections of a single ceramic tube and the temperature gradients overlap during sample heating so that the short (1 cm) section between the pyrolyzer and combustor is always at a temperature that is higher than the pyrolyzer (sample) temperature to prevent condensation of high-molecular-weight pyrolysis products on the walls of the tube.

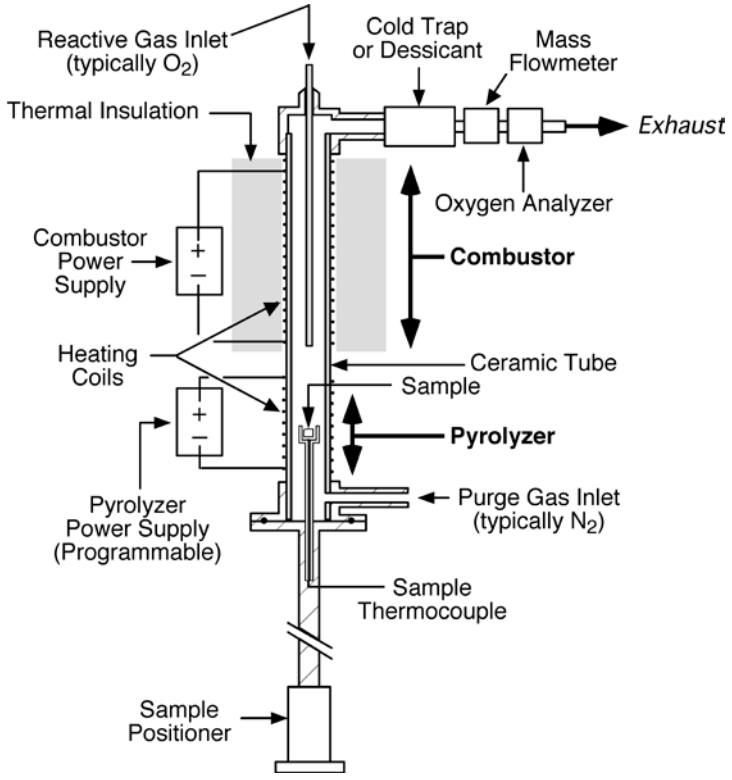

Figure 9. The MCC

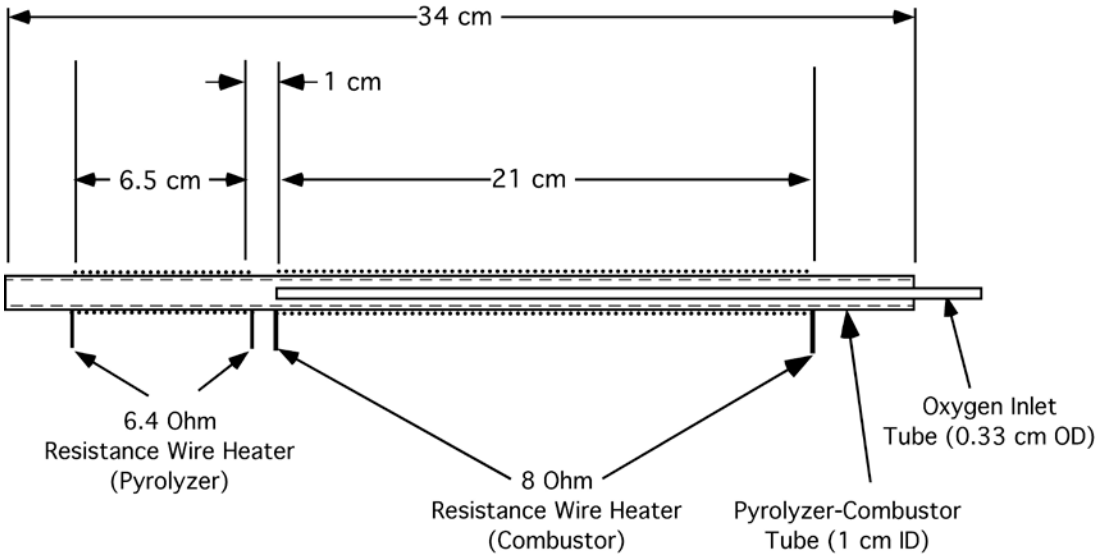

Figure 10. Pyrolyzer-Combustor in MCC Showing Heated Lengths and Heating Wire Resistance

3.1.1 Plug Flow Design.

In the current MCC design, the pyrolysis products and combustion gas stream move through the integral pyrolyzer-combustor in plug flow, which means that the flow is steady-state with no mixing in the axial (flow) direction and the temperature and properties of the gas stream are uniform in the transverse (radial) direction [7]. This design effectively eliminates the dead volumes and cold spots that had caused dilution and condensation of the pyrolysis products and axial mixing of the combustion products in previous designs [2 and 3].

The criteria for the dimensions of the integral pyrolyzer-combustor to ensure plug flow is that the residence time of the sample gases in the pyrolyzer (τ_p) and combustor (τ_c) are small compared to the time interval over which volatile fuel is generated (τ_f) and combusted.

To effect plug flow in the pyrolyzer of volume V_p, the residence time of the sample gases τ_p should be less than 10% of the time interval τ_f over which pyrolysis takes place during the test. According to figures 3 and 5, the majority of the fuel gases are generated over a temperature interval, $\Delta T_p = eR\,T_p^2/E_a \approx 60$K for typical polymer properties E_a = 200 kJ/mole and T_p = 750K [28 and 29], so for the typical heating rate β = 1 K/s, the characteristic fuel-generation time is $\tau_f \approx \Delta T_p/\beta$ = (60K)/(1 K/s) = 60 seconds = 1 minute. For a purge gas flow rate F_p = 80 cm^3/min through a pyrolyzer having volume V_p and heating rate β = 1 K/s:

$$\tau_p = \frac{V_p}{F_p} \le \frac{\Delta T_p}{\beta} \equiv (0.1)\left(\frac{60\text{K}}{1\text{K/s}}\right) = 6 \text{ seconds} \qquad (40)$$

This condition is satisfied for $V_p \le (F_p)(\tau_p)$ = (80 cm^3/min)(0.1 min) ≈ 8 cm^3, so the length of a cylindrical pyrolyzer with inner diameter d_0 = 1 cm must satisfy the requirement:

$$l_p \le \frac{4V_p}{\pi d_0^2} = \frac{(4)(8\text{cm}^3)}{\pi(0.93\text{cm})} = 10 \text{ cm} \qquad (41)$$

The heated length and transition zone (6.5 cm + 1 cm) in figure 10 satisfies this criterion for plug flow out of the pyrolyzer. Moreover, the distance/length between the start of the pyrolyzer and the inlet of the oxygen tube (combustor) satisfies the criterion for laminar flow entering the combustor, $l_p/d_0 \ge$ (10 cm)/(1 cm) $\approx$ 10 so the pyrolysis gases are at full concentration in N_2 and completely mixed when entering the combustor using the geometry of figure 10 with the typical operating parameters.

To ensure plug flow in the combustor so that the oxidized pyrolysis products exit in the order that they are introduced from the pyrolyzer, the residence time of the gases in the combustor should be less than 10% of the time interval over which the gases are introduced into the combustor from the pyrolyzer, i.e., $\tau_c/\tau_f \le 0.10$. The residence time of the fuel gas/nitrogen/oxygen mixture in the combustor is, $\tau_c = V_c/F$ for a combustor volume V_c and combustion stream flow rate F. The combustor volume must, therefore, satisfy

$$\frac{\tau_c}{\tau_f} = \frac{V_c / F}{1\text{min}} \le 0.10 \qquad (42)$$

Therefore, the maximum combustor volume V_c to avoid mixing of the combustion products with the incoming pyrolysis product/N_2 stream for F = 100 cm^3/min = 1.67 cm^3/s is $V_c \le (0.10)(1 \text{ min})(100 \text{ cm}^3/\text{min}) \approx 10 \text{ cm}^3$

Figure 10 shows that the length of the combustor tube having inner diameter, d_i = 1 cm, is approximately l = 21 cm, so the uniformly heated length is approximately $l_c = l - 4d_i$ = 17 cm. The outside diameter of the oxygen inlet tube in the center of the combustor is d_o = 0.33 cm, so the heated volume of the combustor is $V_c = \pi(d_i^2 - d_o^2)l_c/4 = (3.14)[(1 \text{ cm})^2 - (0.33 \text{ cm})^2](17 \text{ cm})/4 =$ 12 cm^3, which satisfies the general guidelines for plug flow. For the geometry of figure 10, the residence time of the N_2/O_2/fuel gas mixture in the combustor under standard test conditions is $\tau_c = V_c/F = (14.7 \text{ cm}^3)/(100 \text{ cm}^3/\text{min}) = 0.15 \text{ min} \approx 9$ seconds.

Consequently, thermal oxidation of the fuel in the combustor must be complete within 9 seconds. Figures 6 and 7 show that thermal oxidation of typical fuels is essentially complete in 8 seconds for a combustor temperature greater than 800°C.

3.1.2 Synchronizing *Q′* With Sample Temperature.

Figures 9 and 10 show that the oxygen analyzer and flow meter are separated from the pyrolyzer by the effective length of the combustor and dryer. This means that the oxygen signal corresponding to instantaneous combustion of the pyrolysis gases, as they are evolved by the sample, will be delayed by the transit time of the gases from the sample cup through the combustor and dryer to the downstream oxygen sensor. This delay time, which is slightly longer

than the residence time of the pyrolysis gases in the combustor, depends on the flow rate of the purge gas F_p, the volume of the pyrolyzer V_p, the total flow rate F, and the volumes of the combustor V_c and dryer V_s.

$$\tau_d = \frac{V_p}{F_p} + \frac{V_c}{F} + \frac{V_s}{F} \approx \frac{V_p + V_c + V_s}{F} = \frac{V_{eff}}{F} \tag{43}$$

The effective volume (V_{eff}) based on the volume of the pyrolyzer-combustor containing the 3 mm diameter oxygen inlet tube is $V_{eff} \approx 18$ cm^3, so the delay time should be $\tau_d \approx$ (18 cm^3)(60 sec/min)/(100 cm^3/min) = 11 seconds at the standard F = 100 cm^3/min total flow rate. This is within the range of measured values of 10 to 12 seconds for this design when the dryer is a tightly packed tube of desiccant (e.g., Drierite) so that V_s is small. Consequently, the Q' history at sample temperature T is related to the specific HRR history computed from the oxygen sensor reading at real time t, as $Q'(T) = Q'(t-\tau_d)$.

The effect of the time shift on the Q' versus temperature data is shown in figure 11 for polyethyleneterephthalate (PET) tested in the MCC at β = 1K/s. The dotted line in figure 11(A) is real-time data for $Q'(T)$ versus temperature computed from the product of the fractional mass loss rate $m'(T)$ of the sample at temperature T (determined by Derivative Thermogravimetric Analysis (DTGA)), and the heat of combustion of the sample gases h_c. The solid line in figure 11(A) is $Q'(T)$ computed from the downstream oxygen-consumption measurement in the MCC, showing the effect of the oxygen signal delay τ_d. Figure 11(B) shows how subtracting the measured τ_d = 10 seconds from the real-time data shifts the Q' data to lower temperatures so that $Q'(T)$ computed from the mass loss rate and $Q'(t)$ computed from oxygen-consumption rate are synchronized in magnitude and temperature. Equation 43 shows that the delay time changes if the total flow rate or the V_{eff} of the MCC changes, so it is important to keep these parameters constant or recalibrate the delay time if changes are made. Otherwise, the sample temperature will not be synchronized with the measured Q' history.

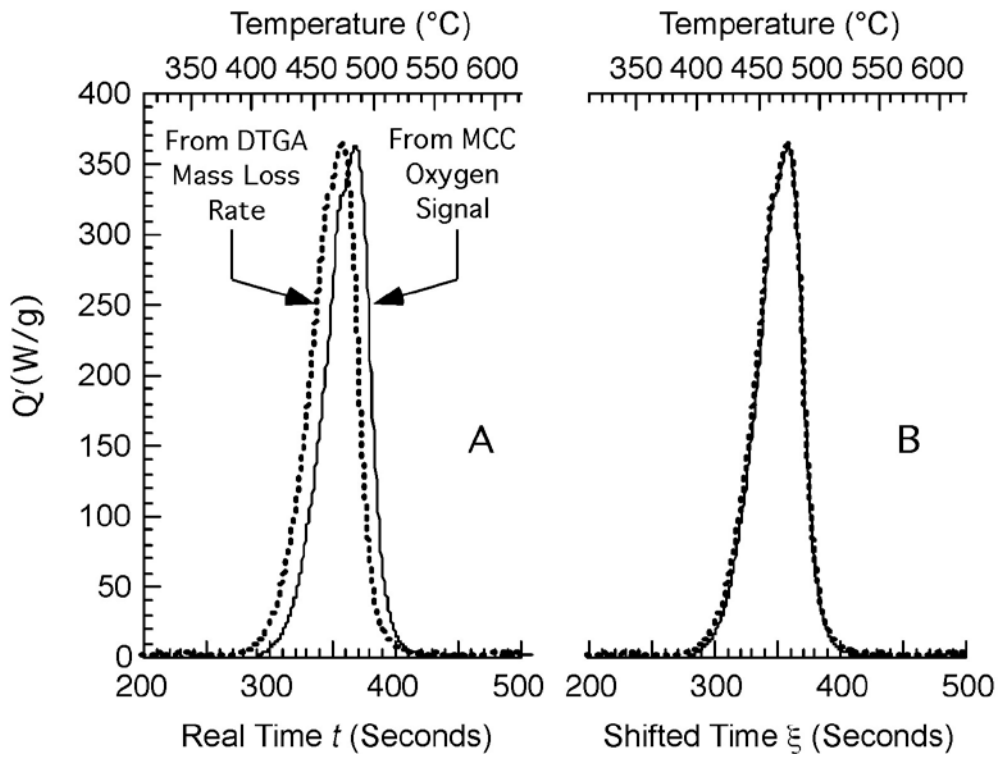

Figure 11. Real-Time (A) and Shifted-Time (B) Data for Q' vs. Temperature of PET in DTGA and MCC at β = 1 K/s

When the mass loss rate and oxygen depletion rate are synchronized with respect to sample temperature, as shown in figure 11(B), the Q' at sample temperature T per unit initial sample mass m_0 is calculated directly from corrected (instrument) time ($\xi = t - \tau_d$), the instantaneous volumetric flow rate of the dry ($N_2/O_2/CO_2$) combustion gas stream F (m^3-gas/second), the density of oxygen at standard temperature and pressure (ρ_{O_2} = 1.3 kg/m^3), the heat of combustion of oxygen with typical organic fuels (C = 13.1 ± 0.6 MJ/kg-O_2), and the change in the volume fraction of oxygen in the dried combustion gas stream ΔX_{O_2} = (RT_0/P_0) $\Delta[O_2]$ (m^3-O_2/m^3-gas), where T_0 and P_0 are the ambient temperature (T_0 = 298K) and pressure (P_0 = 1 atmosphere/10^5 P_a).

$$Q'(T) = Q'(t - \tau_d) = Q'(\xi) = \frac{\rho C F(\xi)}{m_0} \Delta X_{O_2}(\xi) \tag{44}$$

Equation 44 is used in the standard MCC method [6] to compute $Q'(T)$ at sample temperature T during the test from the time-shifted flow rate $F(\xi)$ and the difference between the initial/baseline oxygen fraction $X_{O_2}^0$ and the oxygen fraction at time ξ, $X_{O_2}(\xi)$.

3.1.3 Baseline Perturbations Due to Transient Heating.

In practice, the dry combustion stream flow rate $F(t)$ measured at the downstream flow meter in equation 44 is a function of time because the purge gas entering the pyrolyzer at room

temperature thermally expands into the combustor during the heating program, resulting in an increase in the flow rate measured downstream. If the purge gas is nitrogen (ASTM D7309, Method A), transient heating and expansion of the purge gas also changes the oxygen concentration in the combustor. To understand this effect, define F_{N_2} as the flow rate of nitrogen entering the pyrolyzer at room temperature and $F(\beta) = (dT/dt)(dV_{N_2}/dT) = \beta(dV_{N_2}/dT)$ as the change in flow rate due to volumetric thermal expansion of the nitrogen in the pyrolyzer during transient heating at heating rate β. If the pyrolyzer volume is V_p and the purge gas is ideal, $dV_{N_2}/dT = V_p/T$ with T in degrees Kelvin. If F_{O_2} is the constant flow rate of oxygen into the combustor, the time-dependent flow rate registered at the downstream flow meter is:

$$F(t) = F_{O_2} + F_{N_2} + F(\beta) = F_{O_2} + F_{N_2} + \beta V_p/T \tag{45}$$

The transient oxygen volume fraction (concentration) due to volumetric thermal expansion of the nitrogen purge gas into the combustor as recorded at the downstream oxygen analyzer in the absence of combustion reactions is:

$$X_{O_2} = \frac{F_{O_2}}{F(t)} = \frac{F_{O_2}}{F_{O_2} + F_{N_2} + \beta V_p / T} \tag{46}$$

Figure 12(a) compares flow-rate data for an MCC experiment in the absence of combustion (i.e., a baseline scan without a sample) at β = 1 K/s from 100°C to 900°C in the MCC with the flow rate calculated using the ideal gas expansion model (equation 45) for a pyrolyzer volume V_p = 7.8 cm^3 corresponding to the 10 cm heated length of the 1 cm diameter cylindrical section. Figure 12(b) compares the measured oxygen concentration to the ideal gas calculation (equation 46) for thermal expansion of the nitrogen purge gas. Qualitative agreement between the ideal gas expansion model and the measured flow rate and oxygen concentration is observed. Combining the data in figure 12 as per equation 31 produces the non-zero Q' baseline in figure 13 for a virtual sample mass, m_0 = 5 mg. The total baseline deviation due to transient heating of the purge gas is of the order of 10 W/g for a typical 5 mg sample having $Q'_{max} \approx 700$ W/g (e.g., baseline-corrected data in figures 4 and 11), so total baseline drift is approximately (10 W/g)/(700 W/g) = 0.014 ≈ 1% over the entire temperature range of a typical experiment.

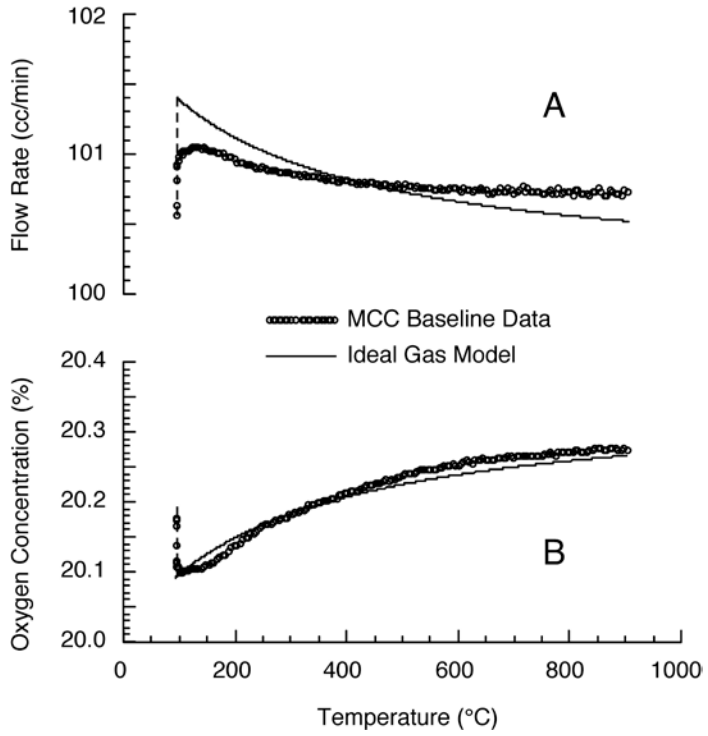

Figure 12. Comparison of Experimental Flow Rate (a) and Oxygen Concentration (b) vs. Temperature to Ideal Gas Model During Heating of an Empty Sample Pan at β = 1 K/s in MCC

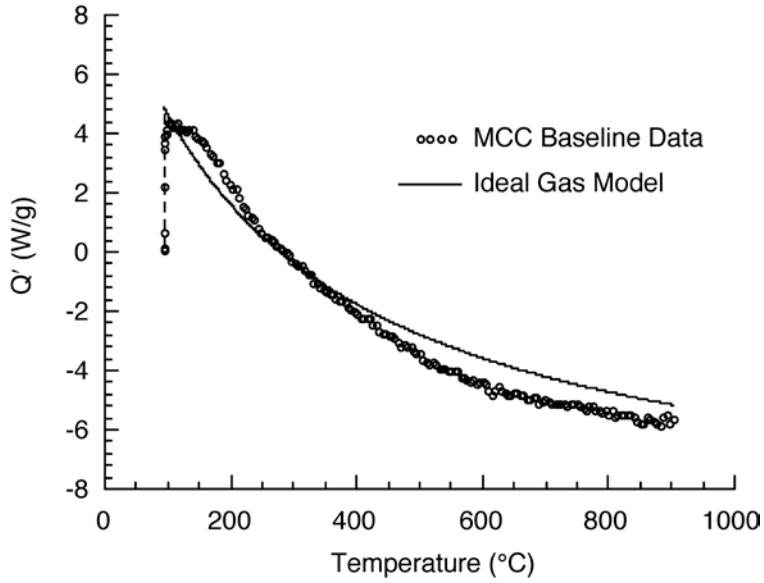

Figure 13. Comparison of Experimental MCC Baseline to Ideal Gas Model for a Virtual Sample Mass of 5 mg Heated at β = 1 K/s

3.2 HEATING RATE CONTROL.

A novel heating rate control methodology was developed specifically for the MCC to reliably reproduce the high heating rate ($\beta \approx 1$ K/s) at the surface of burning plastics [30]. Temperature histories, obtained by application of constant voltages to the MCC pyrolyzer with an empty sample container, are shown in figure 14. It is apparent that the equilibrium temperature is linearly related to the applied voltage and that the transient temperature rise can be described by an exponential function.

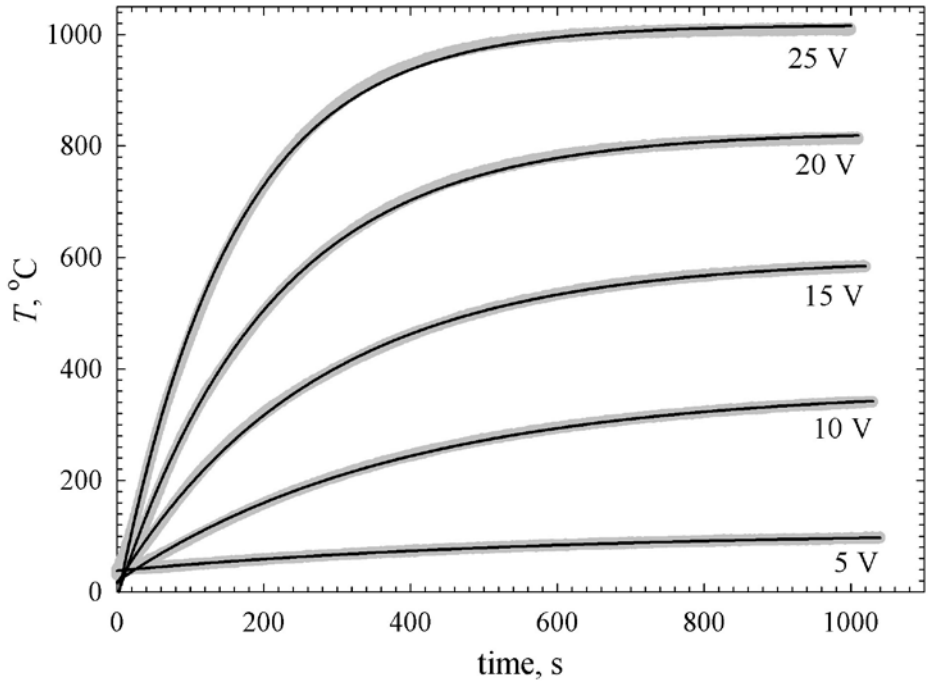

Figure 14. Constant Voltage Temperature Histories of MCC Pyrolyzer (Gray dots are experimental data. Black lines are least-squares fits of equation 47.)

$$T = B - Ae^{-kt} \tag{47}$$

where *B*, *A*, and *k* are adjustable parameters and *t* is time. The results of the least-square fitting of the experimental data with this function are presented in figure 14. Differentiation of equation 47 with respect to time and subsequent expression of the result in terms of temperature (using equation 47) yield a linear relation between the temperature and heating rate:

$$\frac{dT}{dt} = k\left\{Ae^{-kt}\right\} = k\left\{B - T\right\} = kB - kT \tag{48}$$

The *kB* product and *k* are two parameters that depend on the voltage applied to the furnace. The values of these parameters (obtained from the fitting of the constant-voltage temperature histories) are plotted with respect to the voltage, *U*, in figure 15.

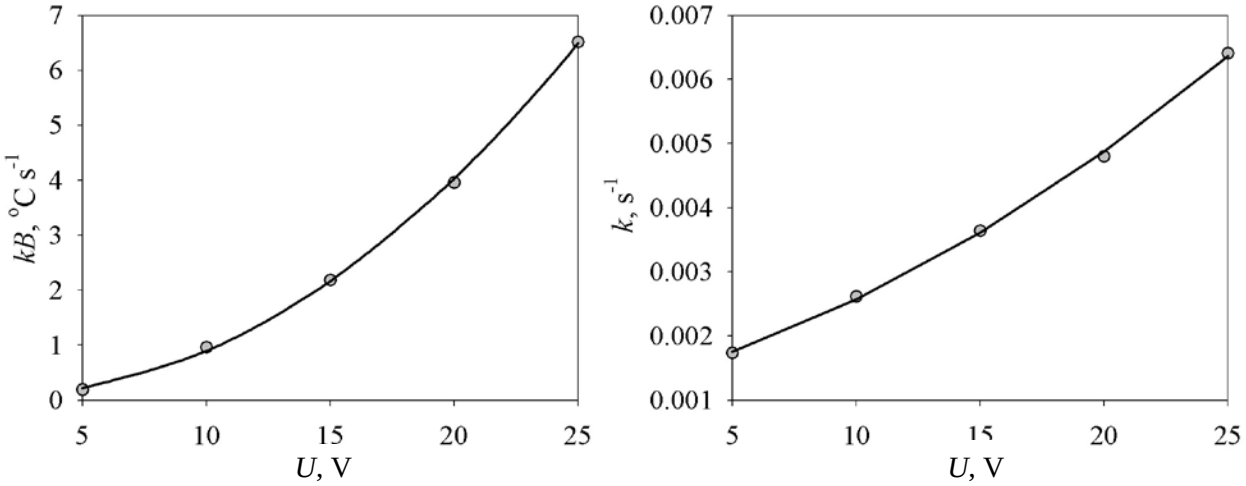

Figure 15. Dependence of Parameters of Equation 48 on Voltage (Circles are experimental data. Solid lines are the least-squares fit of equations 49 and 50.)

As demonstrated by the graphs in figure 15, these dependencies can be captured by second-order polynomials:

$$kB = b_0 + b_1 U + b_2 U^2 \tag{49}$$

$$k = k_0 + k_1 U + k_2 U^2 \tag{50}$$

Substitution of these polynomial expressions (equations 49 and 50) into equation 48 yields a quadratic equation:

$$\{b_2 - k_2 T\} U^2 + \{b_1 - k_1 T\} U + \left\{b_0 - k_0 T - \frac{dT}{dt}\right\} = 0 \tag{51}$$

The positive root of this equation is an expression for the applied voltage in terms of the temperature T and heating rate $dT/dt = \beta$:

$$U = U(T, \beta) = \frac{-\{b_1 - k_1 T\} + \sqrt{\{b_1 - k_1 T\}^2 - 4\{b_2 - k_2 T\}\{b_0 - k_0 T - \beta\}}}{2\{b_2 - k_2 T\}} \tag{52}$$

This expression, which is subsequently referred to as the control expression, provides the means to calculate the voltage that needs to be applied to the furnace to heat a sample, which is currently at temperature T, at the rate $\beta = dT/dt$. The six coefficients b_0, b_1, b_2, k_0, k_1, k_2 used by the control expression equation 52 are generated during the automated temperature calibration routine and stored in the instrument parameter file (see section 4).

Applicability of equation 52 to heating rate control is based on the assumption that changes in the calculated voltage are sufficiently slow to allow the temperature to follow constant-voltage heating curves. It is further assumed that the presence of a sample does not have a significant

effect on the heating process. The range of heating rates and temperatures covered by the control expression is determined by the range of voltages used in the generation of constant-voltage temperature histories and by the ability of the second-order polynomials (equations 49 and 50) to interpolate resulting dependencies of *kB* and *k* on voltage.

Heating rate deviations are minimized using a simple implementation of proportional-integral-differential PID control to correct the heating rate input to the control expression. In the beginning of the heating cycle, the control expression heating rate (dT/dt) was assigned the value of the set heating rate $(dT/dt)_{set}$. Subsequently, when the measured heating rate $(T-T_{old})/(t-t_{old})$ deviated further from the set point, the control expression heating rate was re-evaluated as follows:

$$\frac{dT}{dt} = \left(\frac{dT}{dt}\right)_{old} + \left\{\left(\frac{dT}{dt}\right)_{set} - \left(\frac{T - T_{old}}{t - t_{old}}\right)\right\}\left(\frac{t - t_{old}}{t_{control}}\right) \tag{53}$$

Here, *old* subscripts are used to refer to the values that correspond to the preceding cycle of the control algorithm and $t_{control}$ is a characteristic response time of the deviation from the set point. Setting this parameter to 12 seconds provided an adequate rate of response at a heating rate of 0.5°C/s and no further optimization of $t_{control}$ was required.

3.3 THERMAL EQUILIBRIUM OF THE SAMPLE DURING TRANSIENT HEATING.

The effect of heating rate and sample mass on the Q' history measured in the MCC on the temperature gradient inside a thin, solid sample of initial mass m_0 (mg) that is heated at a constant rate β (K/s) is solved by assuming the temperature distribution $T(z)$ in the z (thickness) direction with volumetric internal heat generation or absorption q''' is given by the energy equation for one-dimensional unsteady conduction [31]

$$\frac{d^2T}{dz^2} = \frac{1}{\alpha}\frac{dT}{dt} + \frac{q'''}{\kappa} \tag{54}$$

In equation 54, $\alpha = \kappa/\rho c$ is the thermal diffusivity of the solid sample in terms of the thermal conductivity κ, density ρ, and heat capacity c. For heat absorption by thermal decomposition, the volumetric heat exchange term on the right side of equation 54 is $q''' = \rho h_p A\exp[-E_a/RT] = \rho h_p k(T)$, with h_p the specific heat of pyrolysis in Joules per gram. The maximum rate of heat absorption due to pyrolysis for a constant rate of temperature rise, $dT/dt = \beta$, (see equation 7) is $q''' = \rho h_p k(T_p) = \rho h_p \beta E_a/R T_p^2 = \rho h_p \beta/\Delta T$, substituting this result into equation 54:

$$\frac{d^2T}{dz^2} = \frac{1}{\alpha}\frac{dT}{dt} + \frac{\rho h_p}{\kappa} A\exp\left[\frac{-E_a}{RT}\right] = \frac{\beta}{\alpha}\left[1 + \frac{h_p}{c\Delta T}\right] = \frac{\beta}{\alpha_{eff}} \approx \frac{\beta}{\alpha} \tag{55}$$

Equation 55 is a steady-state approximation that assumes a constant heating rate β (see section 5.5) so that all of the time dependence is included in the effective thermal diffusivity, $\alpha_{eff} = \alpha/(1+h_p/c\Delta T)$, which is also assumed to be constant and equal to the nominal value (i.e., $\alpha_{eff} = \alpha$). The sample is approximated as a slab of half-width L with surface temperature T_p at $z = \pm L$, centerline temperature T_0, having temperature gradient, $dT/dz = 0$ at $z = 0$, as shown in Figure 16.

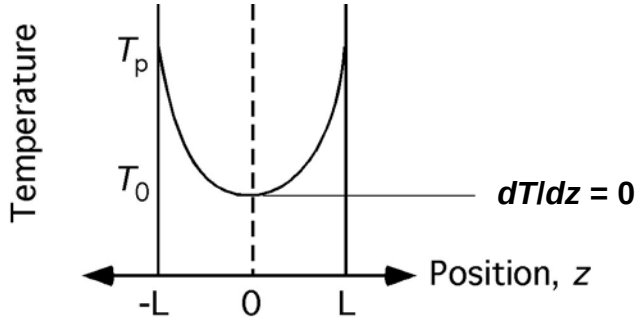

Figure 16. Geometry and Boundary Conditions of Heat Transfer Analysis

The generalized temperature distribution is obtained by integrating equation 55 twice.

$$T(z) = \frac{\beta}{2\alpha} z^2 + C_1 z + C_2 \tag{56}$$

The boundary conditions give $C_1 = 0$ and $C_2 = T_0$, so the temperature difference between the sample surface at temperature T_p and the center at temperature T_0 for a heating rate β is:

$$\Delta T = T_p - T_0 = \frac{\beta}{2\alpha} L^2 \tag{57}$$

The sample mass is $m_0 = \rho(2L)^3 = 8\rho L^3$, so the difference between the temperature at the surface and the center of the sample due to thermal inertia is:

$$\Delta T = \frac{\beta m_0^{2/3}}{8\alpha \rho^{2/3}} \tag{58}$$

The observed reaction (heat release) rate of the sample will be an average of the reaction rates at T_p and T_0 per equation 17 with $\Delta T = T_p - T_0$ per equation 57. Substituting equation 58 into equation 10 and computing the integral average of r for $E_a \Delta T / R T_p^2 << 1$:

$$\frac{Q'_{\max}(m_0,\beta)}{Q'_{\max}(0,\beta)} = \frac{1}{\Delta T}\int_0^{\Delta T} \exp\left[-\frac{E_a}{RT_p^2}\theta\right] d\theta \approx 1 - \frac{E_a}{RT_p^2}\frac{\Delta T}{2} = 1 - \frac{E_a}{RT_p^2}\frac{\beta m_0^{2/3}}{16\alpha\rho^{2/3}} \tag{59}$$

According to equation 59, the error in Q'_{max} is less than 5% when the sample mass m_0 and heating rate β satisfy the inequality: $E_a \beta m_0^{2/3}/(16\alpha R T_p^2 \rho^{2/3}) \leq 0.05$. For typical polymers [28 and 29]: T_p = 700K, α = 1.2 x 10^{-7} m^2/s, ρ = 1100 kg/m^3 = 1.1 x 10^9 mg/m^3, E_a = 200 kJ/mole, each with a range of about ±10%, so the criterion for less than 5% error in Q'_{max} due to temperature gradients within the sample is:

$$m_0(mg) \leq \left(\frac{2.0 \pm 0.4}{\beta(\mathrm{K/s})} \right)^{3/2} \tag{60}$$

Equation 60 is plotted in figure 17 to show the relationship between sample mass and heating rate for an error of less than 5% in Q'_{max} for a typical polymer that thermally decomposes via a first-order process. The grey band is the range of calculated values associated with the uncertainty in E_a, T_p, α, and ρ. Sample mass/heating rate combinations within this grey band represent the best tradeoff between signal-to-noise ratio and accuracy. Figure 17 shows that for the nominal heating rate β = 1 K/s, samples in the range of 2 to 4 mg should give errors of less than 5% for Q'_{max}, which is the repeatability of the test.

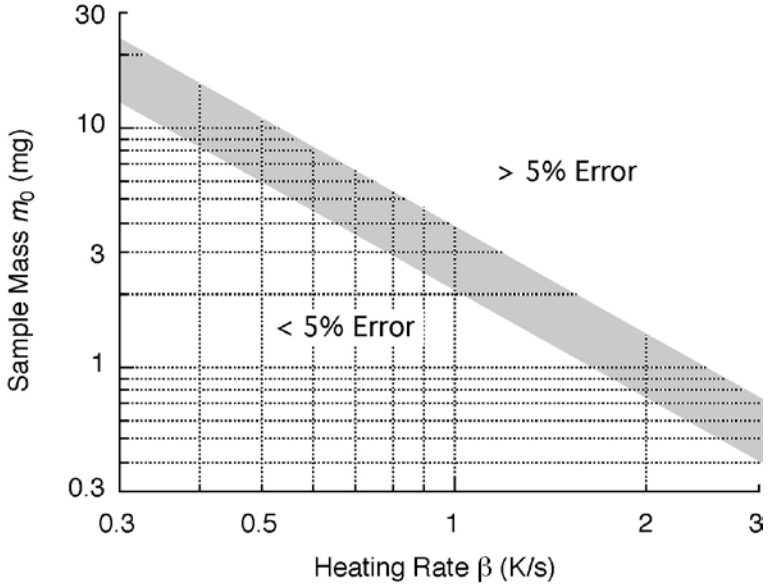

Figure 17. Relationship Between Sample Mass and Heating Rate for 5% Error in Q'_{max} of Typical Polymers (Gray band is optimum experimental range.)

3.4 THERMAL OXIDATION OF THE SAMPLE GASES IN THE COMBUSTOR.

Under normal operating conditions (Φ<1, 900°C, 10 seconds), the sample fuel gases should be completely oxidized in the combustor to H_2O, CO_2, and halogen acids. The relationship among the operating parameters of the MCC, the sample mass, and the heating rate required to completely oxidize the fuel gases in the combustor can be derived from previous results. The stoichiometric oxygen-to-fuel mass ratio at the maximum rate of thermal decomposition is obtained from equations 7, 13, 16, 26, and 44.

$$r_0 = \frac{h_c}{C} = \frac{m_{O_2}}{m_{fuel}} = \left[\frac{dm_{O_2}/dt}{dm_{fuel}/dt}\right]_{\max} = \frac{FX_{O_2}^0 \rho_{O_2}}{\beta m_0(1-\mu)/(eRT_p^2/E_a)} = \frac{FX_{O_2}^0 \rho_{O_2}}{\beta m_0(1-\mu)/\Delta T_p} \quad (61)$$

Rearranging equation 61 gives the product of the sample mass m_0 and the heating rate β at the stoichiometric oxygen-to-fuel mass ratio in the combustor at the baseline oxygen concentration. Under these conditions, oxygen is completely consumed to oxidize (combust) the fuel.

$$m_0\beta = FX_{O_2}^0 \rho_{O_2} C \frac{\Delta T_p}{(1-\mu)h_c} = \Omega \frac{\Delta T_p}{(1-\mu)h_c} \quad (62)$$

If ρ_{O_2} is the density of oxygen at room temperature (T_0), its density in the combustor at 900°C is $\rho_{O_2}(T_c) = \rho_{O_2}T_0/T_c$ = (1.3 x 10^{-3} g-O_2/cm^3-O_2)(300K/1173K) = 3.3 x 10^{-4} g-O_2/cm^3-O_2. Therefore, for the standard experiment (ASTM D 7309, Method A), the apparatus coefficient of equation 62 is Ω = (1.67 cm^3/s)(0.2 cm^3-O_2/cm^3)(3.3 x 10^{-4} g-O_2/cm^3-O_2)(13.1 kJ/g-O_2) = 1.5W, and the relation between sample size, heating rate, and heat of combustion of the fuel gases (to ensure complete oxidation in the combustor) is:

$$m_0 \le 1.5\,\mathrm{W}\frac{\Delta T_p}{\beta(1-\mu)h_c} \quad (63)$$

The equality in equation 63 gives the approximate sample mass that will consume all of the oxygen in the combustor. This is seen to be a function of the test parameters (Ω, β) and the sample properties (μ, ΔT_p and h_c) via equation 62. The range of sample mass for typical polymers is computed from the average polymer properties in table 5, ΔT_p = 53 ±18K, (1-μ)h_c = Q_∞ = 21 ±13 kJ/g, and standard (ASTM D7309, Method A) test conditions:

$$m_0 \le \frac{(1.5\mathrm{W})(53\mathrm{K})}{(1\mathrm{K/s})(21\mathrm{kJ/g})} = 4 \pm 3\mathrm{mg} \quad (64)$$

The lower bound on the sample mass (1 mg) is associated with polyolefins (e.g., HDPE, PP) because their fuel gases have the highest heat of combustion and r_0 of the common polymers [19 and 28] and they form no char on pyrolysis [28], so the entire sample mass is combusted. Larger samples of polyolefins can be tested if the baseline oxygen concentration in the combustor $X_{O_2}^0$ is increased or the heating rate in the test is decreased. This range of sample mass of typical polymers based on oxygen consumption under standard test conditions brackets the sample mass for thermal equilibrium (section 3.3). Therefore, the oxygen concentration in the combustor at $Q'_{\max}$ should be observed after the test to make sure that there is sufficient oxygen to completely oxidize the sample gases (see section 5.4).

4. CALIBRATING THE INSTRUMENT.

The measurement systems (data acquisition, flow controllers, flow meter, oxygen sensor) should be calibrated separately before the operating parameters for the sample temperature correction, heating rate control, and Q' delay are determined and the ten coefficients recorded in the operating parameters file. The first six coefficients of the operating parameters file are b_0, b_1, b_2, and k_0, k_1, and k_2 of equation 52 for the heating rate control algorithm. The next three coefficients are a_0, a_1, and a_2 of the polynomial temperature correction (see section 4.5). The last coefficient is the oxygen signal delay (time shift), τ_d. The parameter file is loaded and can be accessed when the MCC program is launched. The individual components of the MCC should be calibrated separately and checked periodically in the following order.

1. Data-acquisition system (board adjustment)
2. Flow controllers and flow meter (meter adjustment)
3. Oxygen analyzer (software adjustment)
4. Heating rate (six coefficients in parameter file)
5. Sample temperature (three coefficients in parameter file)
6. Q' Delay (one coefficient in parameter file)
7. System calibration check using reference material

Once calibrations 1 through 6 have been performed and the operating parameter file updated, a well-characterized reference material, such as polystyrene (PS) (see table 4), should be tested on a daily basis to confirm that all of the individual components and corrections (the systems) are operating properly; thus, the system calibration check (7) is performed.

4.1 THE DATA ACQUISITION AND CONTROL SYSTEM.

The data acquisition and control (DAC) board should be calibrated annually. If the DAC is out of calibration, the other components can be affected. Some of the other components are affected more than others because of the range of voltage output by that component. The O_2 sensor and thermocouple outputs are approximately several millivolts, whereas the flow controllers and meter are approximately 5 volts. The board is a National Instruments® product and has a calibration routine built in (figure 18). Figure 19 shows the Measurement & Automation Explorer (MAX) that can be used to adjust the board with an internal reference. Constants are adjusted using this calibration routine so the readings on the board match the reference. An external calibration can be performed if the board is removed and sent to a certified laboratory. The external calibration is referenced to traceable standards.

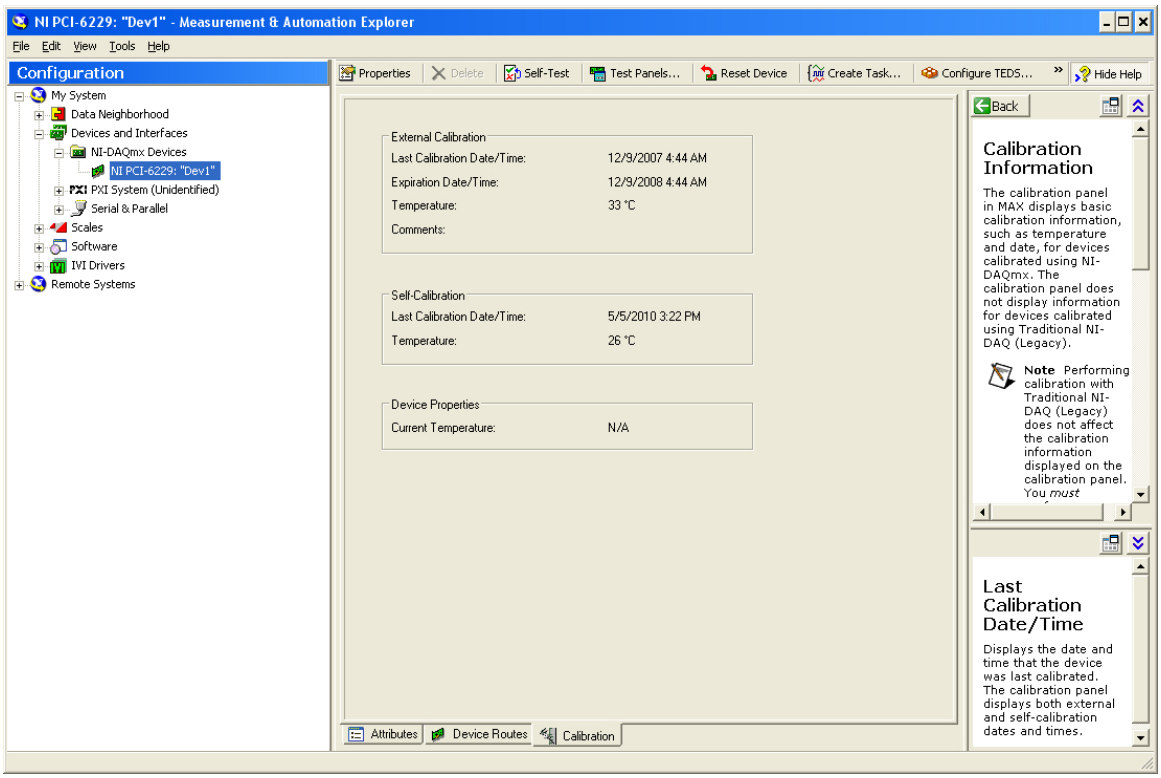

Figure 18. The MAX Screen for Testing and Calibrating DAC Board

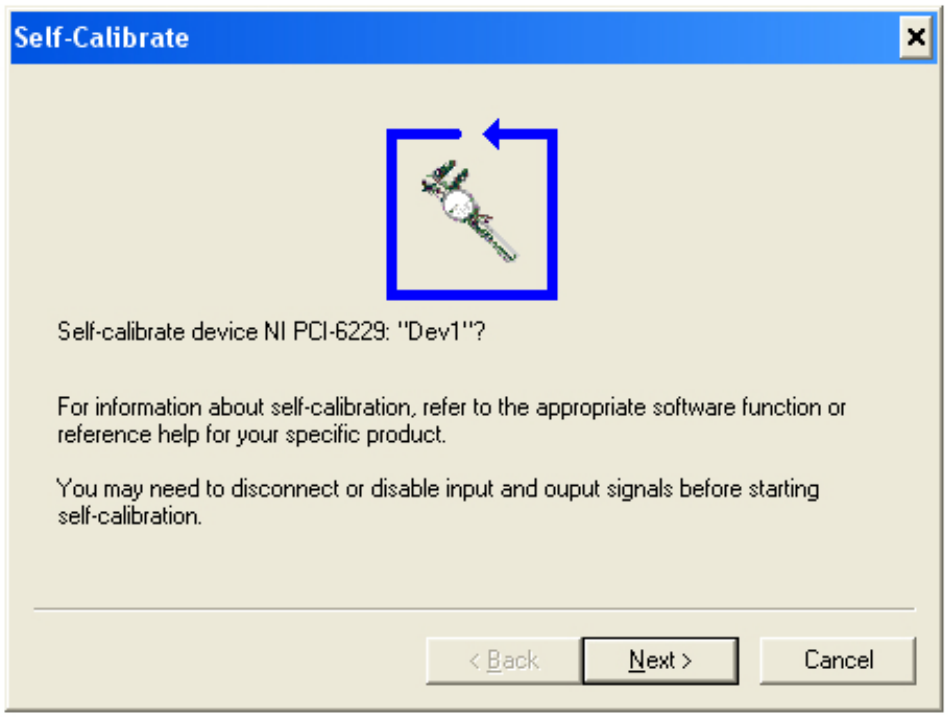

Figure 19. Self-Calibration Routine Referenced to Internal Standard

When calibrating the DAC all of the inputs and outputs need to be disabled. The easiest way to do this is to unplug the DAC cables from the computer and proceed with the automated calibration procedure. Make sure that the computer has been on for a while and that no DAC software is running other than MAX.

4.2 FLOW CONTROLLERS AND FLOW METER.

Flow controllers are calibrated at the factory and should be referenced to their respective gases at room temperature and 1 atmosphere pressure.

Flow meters should be calibrated biannually with a wet test meter or other gas flow calibrators. Make sure the power supply for the flow meter and controllers is outputting the correct voltage before making any adjustments. If the flow meters are found to be out of specification they should be calibrated by the original equipment manufacturer or by a certified laboratory. The flow meters can be adjusted by turning potentiometers on the meter until the zero and span output matches the flow calibrator.

Deviations in the flow rate are not necessarily due to the flow controllers/meter. There are other sources that can contribute to errors in the flow rate besides the flow meter calibration. To be sure that the flow controllers are not the problem, they should be tested using a wet test meter or a flow calibrator attached directly to the flow meters. Leaks in the system are also a possible source of low flows. Common leak spots are the scrubber tube connections and the sample post entry seal. Other leak points can be the O-ring seals on the furnace tube at the metal fittings. These seals sometimes deteriorate after years of thermal cycling.

4.3 OXYGEN ANALYZER.

The oxygen sensor used in the FAA MCC is a micro-fuel cell (Teledyne R17A, R21A, or R22A or similar). The oxygen sensor converts chemical energy to electrical energy. The electrical output from the rate of this reaction is linear and directly proportional to the oxygen concentration.

The oxygen sensor is reported to have a shelf life of 3 years in the original container and a continuous use life of about 1 year after installing it in the MCC. The analyzer has reached the end of its useful life if it does not calibrate properly and the response is slow. The oxygen sensor calibration should be checked after replacement (section 4.3).

The oxygen sensor is sensitive to moisture, so it is important to make sure that all moisture is removed from the combustion gas stream by the dryer. If moisture enters the oxygen sensor, the O_2 reading will be very inaccurate. The sensor reading will return to normal after the moisture is removed by purging with dry gas. The oxygen sensor is also sensitive to temperature. Keep the MCC and O_2 sensor out of direct sunlight and drafts to minimize temperature changes that cause long-term baseline drift. If long-term baseline drift is a concern, a fast response, low-cell volume, paramagnetic oxygen analyzer can be substituted with proper accounting for the time shift (see section 4.6 for a description of Q' Delay).

4.3.1 Calibration Description.

The calibration adjustment for the oxygen sensor can usually be made through the MAX software by adjusting one constant (the slope, *m*) in the equation of a line whose y-intercept X_{O_2} (Actual) is zero at $X_{O_2}^{meas}$ (Measured) = 0; that is, X_{O_2} (Actual) = $m\, X_{O_2}^{meas}$.

4.3.2 Calibration Procedure.

A single point calibration using prepared gas mixtures (e.g., 20% O_2 in N_2) or pure oxygen or air is sufficient for the oxygen sensor. In pure nitrogen, the oxygen sensor should output zero volts. If it reads above zero, it didn't purge long enough or it is malfunctioning. If it reads below zero, the DAC board is out of calibration and needs to be adjusted. Set the oxygen flow controller to its maximum output and the nitrogen flow controller to 0 cc/min. Allow the system to purge for 10-15 minutes with pure oxygen. Wait until the oxygen concentration $X_{O_2}^{meas}$ is steady and record the reading. Record the oxygen concentration.

4.3.3 Changing the Calibration.

Open the National Instruments® MAX. Expand the following folders within MAX to view the screen shown in figure 20.

My System
Scales
NI-DAQmx Scales
O_2 Cal

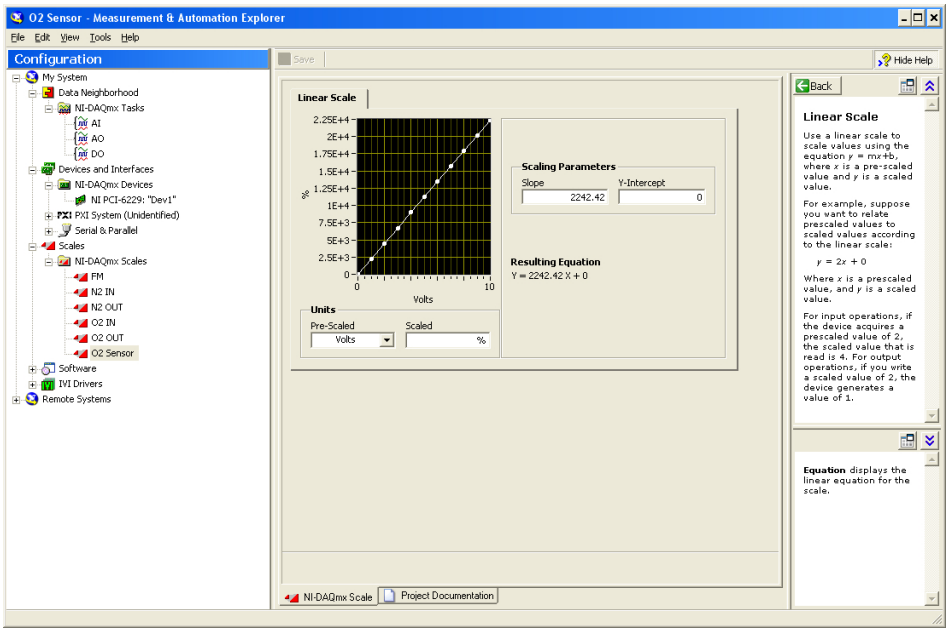

Figure 20. Screenshot of MAX Where Custom Scaling Parameters Are Entered

Open the O_2 Cal and use the following equation:

$$\frac{100 * OldSlope}{X_{O_2}^{meas}} = NewSlope$$

The OldSlope is the value in the Slope Box and the $X_{O_2}^{meas}$ is the recorded oxygen concentration from section 4.3.2. Change the value in the slope box to the *NewSlope* value. Make sure the Y-Intercept box is zero. Repeat the calibration procedure if you want to check your reading.

4.4 HEATING RATE.

4.4.1 Calibration Description.

Application of the control expression (section 3.2) to correct the heating rate virtually eliminates the need for calibration. Recalibration is required only when a new furnace tube or thermocouple post is installed. Recalibration may be required if the furnace is equipped with a mechanically unstable heating element. An advantage of the heating rate correction, however, is that, in addition to handling instabilities of the furnace, it may mitigate heating rate perturbations introduced by other sources (e.g., nitrogen flow, sample, etc.).

4.4.2 Calibration Procedure.

The heating-rate calibration is performed in the MCC Cal application. The system should be allowed to equilibrate under the normal operating conditions before any calibrations are attempted or initiated. An empty sample cup should be placed on the platform and loaded into the pyrolyzer. Once the temperature and flow rates are set and stabilized, the automated heating-rate calibration can be initiated. The software automatically runs the heater through different voltage set points and calculates the six coefficients of equation 51, needed to control the heating rate. This routine takes about 1 hour and, when it is finished, two files are generated. The first file is the temperature-rise data (see figures 14 and 15) that is used to derive the coefficients b_0, b_1, b_2, k_0, k_1, and k_2 for the control expression. These coefficients are written to the operating parameter file as the first six terms. The operator is prompted to name and save each of the files. The operator will be prompted to load the operating parameter file containing the six heating rate control coefficients when the MCC software is launched.

4.5 SAMPLE TEMPERATURE.

4.5.1 Calibration Description.

The default calibration for Nickel-Chromium (90/10)/Nickel-Aluminum-Manganese (95/2/3) K-type thermocouples is accurate to within a few degrees Centigrade for most of the useful temperature range. However, the thermocouple can be in error by as much as 20°C because of impurities in the alloys and because of the annealing that accompanies the thermal cycling of the thermocouple. Differences between the thermocouple reading and the sample temperature can

also be attributed to temperature gradients through the sample cup and thermal lag during transient heating.

The accuracy of the recorded temperature can be checked by measuring the differential temperature (DT) between the sample (measured) temperature T_{meas} and the program temperature, $T_{prog} = T_{start} + \beta t$ for reference materials with well-defined melting points, such as pure (99.999%) metals and salts [32]. A negative value of the differential temperature, DT = T_{meas} - T_{prog}, occurs at the melting temperature of the reference material when the thermal energy from the pyrolyzer is absorbed by melting crystals (a first-order phase transition) so the sample temperature lags the program temperature until melting is complete. Pure metals and salts that are suitable for temperature calibration include [32 and 33]:

Table 3. Melting Temperatures of Reference Materials

Reference Material	Chemical Symbol	Melting Temperature (°C)
Indium	In	157
Tin	Sn	232
Lead	Pb	327
Zinc	Zn	420
Lithium sulfate	$Li_2SO_4 \cdot H_2O$	578
Antimony	Sb	631
Aluminum	Al	660
Sodium chloride	NaCl	801
Silver	Ag	962
Gold	Au	1064

4.5.2 Calibration Procedure.

The sample temperature calibration should be conducted according to the standard practice for temperature calibration of differential scanning calorimeters and differential thermal analyzers [33] using new sample cups that are dedicated to a specific reference material. If metals are mixed or dirty pans are used, alloys and other reaction products can be formed, thereby changing the melting temperature of the metals. In practice, approximately 10 to 20 mg of each metal is placed in the center of a clean ceramic cup and then placed in the MCC under nitrogen purge (ASTM D7309, Method A). After waiting several minutes to purge the pyrolyzer with nitrogen to prevent oxidation of the metals at high temperature, the samples are heated at 1 K/s to 50K above the melting temperature of the reference material. After the test, the saved data file is recalled and analyzed using the curve-fit program. The sample temperature is plotted on the y-axis versus the same sample temperature on the x-axis and cropped from 50K below to 50K above the melting temperature interval. The cropping operation linearly interpolates between the sample temperature limits to approximate a linear temperature program over the melting interval,

which is subtracted from the measured sample temperature at each point in the melting interval to generate a temperature difference DT versus program temperature *T* plot as shown in figure 21. Figure 21 also shows the recommended [32 and 33] graphical method used to obtain the sample temperature at the onset of melting T_m of the reference material. Figure 22 shows the relationship between the sample temperature and the melting temperature for typical MCC devices.

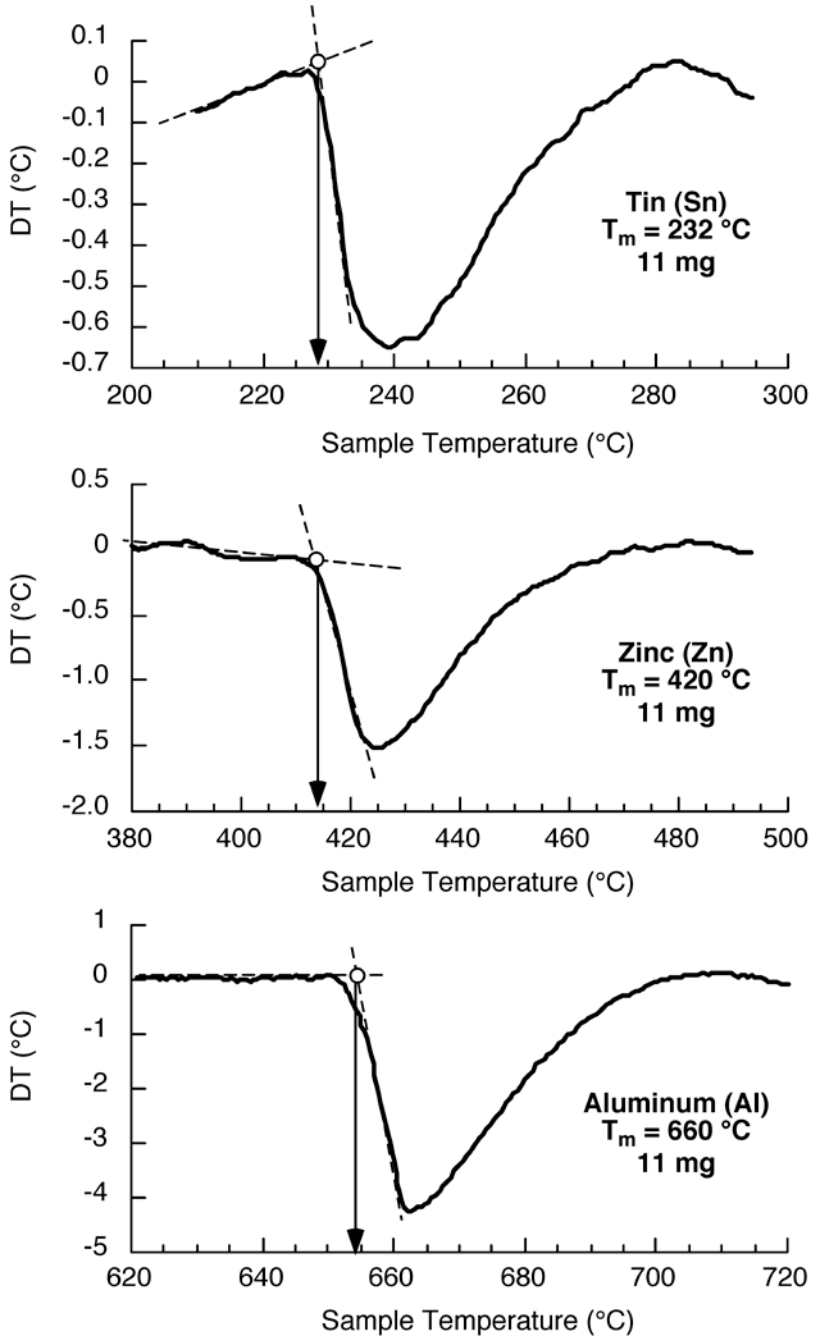

Figure 21. Graphical Method Used to Obtain Sample Temperature at Onset of Melting T_m for Reference Metals Tin (Sn), Zinc (Zn), and Aluminum (Al)

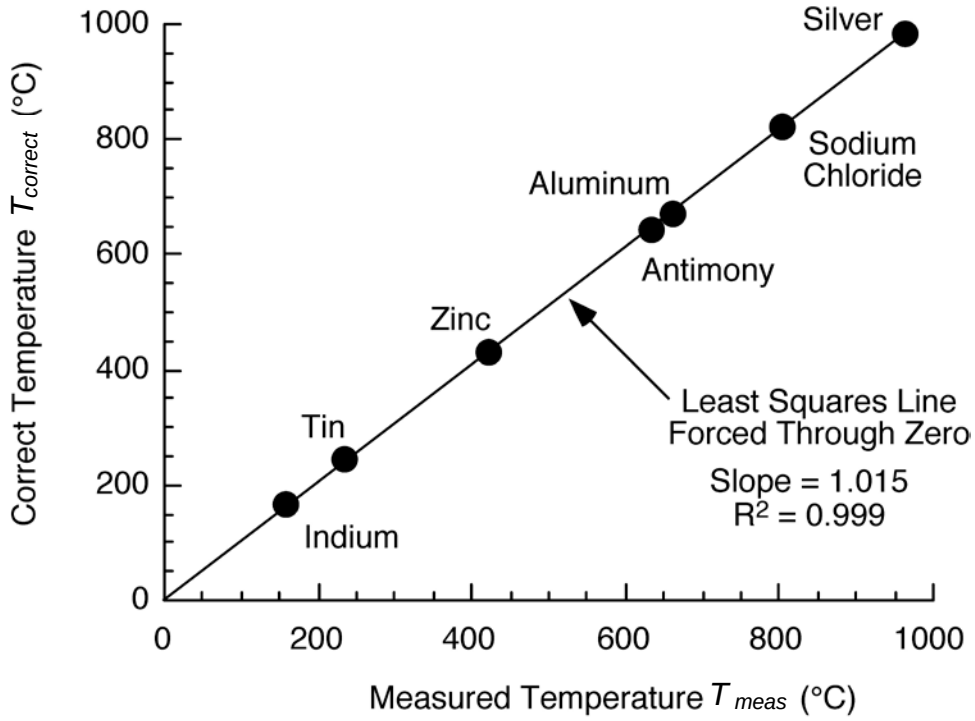

Figure 22. Calibration Curve for MCC Comparing the Reference Melting Temperature to the Temperature Measured at the Sample Location

The correct temperature $T_{correct}$ is assumed to be the melting temperature of the reference material and this temperature is plotted against the measured temperature at the sample location T_{meas} at the onset of melting, shown in figure 21. The $T_{correct}$ versus T_{meas} data are fit with a second-order polynomial equation using three coefficients, $T_{correct} = a_0 + a_1 T_{meas} + a_2 T_{meas}^2$. Typically, the measured temperature is lower than the correct temperature, but proportional to it, so a linear fit of the data forced through the origin is sufficient to obtain the correct temperature at the sample location. By way of example, the data in figure 22 were collected and are well described by the proportional relationship, $T_{correct} = 1.015 T_{meas}$, i.e., $a_0 = 0$; $a_1 = 1.015$; $a_2 = 0$. These temperature coefficients are added to the instrument parameter file as the seventh, eighth, and ninth terms. After the MCC is calibrated with the reference materials, PS (see section 4.7) can be used for day-to-day checking of the calibration.

4.5.3 Changing the Calibration.

The temperature calibration should be checked if different sample cups of a different design or material are used or if the sample thermocouple is replaced and these coefficients updated in the instrument parameter file. The temperature calibration ensures that the measured sample temperature is accurate, but it does not ensure that the sample temperature is synchronized with the sample Q' that is computed from the downstream (time delayed) oxygen sensor and flow rate signals. Section 4.6 addresses how to synchronize the sample temperature with its Q'.

4.6 THE Q' DELAY (TIME SHIFT).

4.6.1 Calibration Description.

The time shift calibration synchronizes the sample temperature and Q' signals in the MCC that are offset by the transit time of the combustion gases between the pyrolyzer and the oxygen sensor (see section 3.1.2). In the MCC, the corrected sample temperature is measured in real time, as are flow (pressure) disturbances that occur in the pyrolyzer. However, the evolved gases take time to travel through the combustor and tubing before they reach the oxygen sensor. The time shift accounts for this delay. The resulting Q' is calculated from the real time flow rate and shifted oxygen concentration measurements. When applied correctly, the time shift synchronizes the temperature, flow rate, oxygen concentration, and Q' (see figure 11).

4.6.2 Calibration Procedure.

When calibrating the time shift in the MCC, it is important to make sure the coefficient for the time shift is set to zero in the instrument parameter file before making any measurements. The time shift is the 10^{th} (last) coefficient in the instrument parameter file. The easiest method for determining the delay time is to load a sample into the MCC and wait for the flow stream to stabilize; then momentarily depress the sample platform and measure the time it takes for the oxygen spike in the flow stream to travel from the sample platform (pyrolyzer) to the oxygen sensor. This is the oxygen signal delay time, τ_d, which is typically on the order of 10 seconds.

4.6.3 Changing the Calibration.

After measuring the oxygen signal delay time in the MCC, change the value of τ_d in the instrument parameter file from zero to the measured value (in seconds) and launch the MCC software. The time delay is the 10^{th} (last) coefficient in the instrument parameter file. An accurate delay time is necessary to synchronize the temperature with the Q' so that accurate T_{onset} and T_p can be measured. Changes to the MCC that add or subtract volume from the flow stream will change the delay time, which results in a temperature offset with respect to $Q(t)$. In particular, changing the diameter of connecting tubing or incompletely filling the drying tube with desiccant changes τ_d.

4.7 STANDARD REFERENCE MATERIALS.

Once all of the components of the MCC have been individually calibrated, and in order to check the calibration of the MCC on a daily basis, it is advisable to test a well-characterized (standard) reference material. Table 5 lists several common polymers for which the thermal combustion properties heat release capacity η_c, heat of combustion of the sample Q_∞, char yield μ, and temperature T_p at $Q'_{\max}$ have been determined. The MCC will return accurate thermal combustion properties (e.g., table 5) if the flow controllers, oxygen analyzer, and heating rate are calibrated (Q_∞), the sample mass is appropriate (η_c), the oxygen signal delay is correct (T_p), and the weighing and handling procedure is accurate (μ).

Table 5 shows typical thermal combustion properties for pure polymers, but these values can vary significantly depending on the source of the material, so the properties in table 5 should be considered as approximate or generic values. By way of example, PMMA is used as the reference material for fire calorimeters [22] because it thermally degrades to methylmethacrylate monomer in quantitative yield at the surface of the burning specimen so the heat of combustion of the volatiles is a constant (h_c) value. However, PMMA can be made in a variety of ways, each one leading to very different molecular architectures. For example, acrylics contain other acrylate monomers (co-monomers) that are added to methylmethacrylate to modify mechanical or thermal properties of PMMA, especially the onset and maximum rate temperatures for thermal decomposition, T_{onset} and T_p, respectively. Figure 23 shows data for PMMA polymerized by a single mechanism and obtained from a single supplier to illustrate the impact of molar mass (molecular weight) on the MCC Q' history. The variability in the Q' histories is a result of the change in the decomposition mechanism of PMMA with molecular weight. Figure 23 also shows the variability of MCC Q' histories for generic PMMA (acrylic) from different suppliers. The inherent variability in the Q' history of PMMA from different suppliers suggests that if PMMA is to be used as an MCC reference material, samples should be drawn from the same, well-characterized (i.e., by calibrated DTGA) lot for all tests.

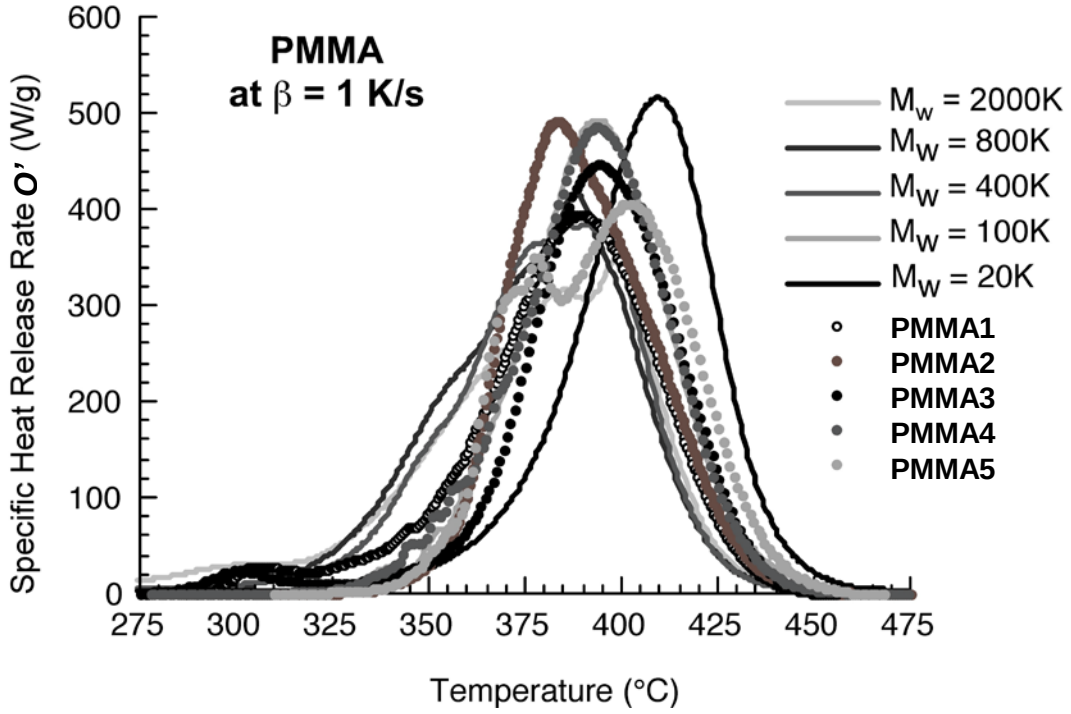

Figure 23. The MCC Data for Narrow Molecular Weight PMMA (Lines) and for General Purpose PMMA/Acrylic (Circles)

The only polymer tested to date that gives approximately the same thermal combustion properties regardless of source or supplier is atactic PS Chemical Abstracts Services Registry Number (CAS # 9003-53-6). PS thermally decomposes to styrene monomer in near-quantitative yield so the heat of combustion of the gases (h_c) is constant as with PMMA, but the thermal stability of the homopolymer chain is more uniform (T_p) from source to source because the decomposition

mechanism is simpler. Figure 24 shows Q' histories of PS in table 4 having a wide range of molar mass with a narrow molecular weight (M_w) distribution from different suppliers (Scientific Polymer Products Sp[2], Polymer Laboratories PL, and Polysciences, Inc., PSI) as well as general purpose, crystal clear (GP) PS from Dow Chemical, Styron, and Goodfellow. The thermal combustion properties listed in table 4 for each supplier are averages of N tests at $\beta = 1$ K/s using 3 mg samples. There is no significant difference between the thermal combustion properties of PS from different suppliers because all of the individual sample means (N = 10 to 25) are within 2 standard deviations of the population (N = 86) mean.

Table 4. Thermal Combustion Properties of PS From Different Suppliers, Number of Samples Tested (N), and Sample Mass (m_0) (Uncertainty is 1 Standard Deviation.)

Source of Polystyrene (CAS# 9003-53-6)	N	m_0, mg	η_c, J/g-K	Q_∞, kJ/g	T_p, °C	Char %
Polysciences Inc., Cat. No. 00575; M_w = 125-250K	10	3.6 ±0.7	1050 ±22	39.6 ±0.7	444 ±2	0
Scientific Polymer Products Cat. No. 687; M_w = 980K	10	3.7 ±0.4	1133 ±27	40.9 ±0.6	447 ±1	0
Polymer Laboratories, Inc. M_w = 8000K	10	3.7 ±0.2	1146 ±38	39.6 ±0.2	446 ±1	0 0
DOW 612 GP PS	10	3.9 ±0.5	1062 ±25	40.6 ±0.2	445 ±1	0
DOW 665 GP PS	10	3.2 ±0.6	1109 ±20	40.6 ±0.3	446 ±1	0
STYRON 666D GP PS	25	3.4 ±0.8	1026 ±47	39.8 ±0.5	444 ±2	
Goodfellow GP PS (granular)	12	2.5 ±0.5	1065 ±18	40.7 ±0.3	443 ±1	0
Average for All Polystyrenes	86	3.4 ±0.5	1084 ±45	40.2 ±0.6	445 ±1	0
Coefficient of Variation (%)			4%	2%	0.2%	—

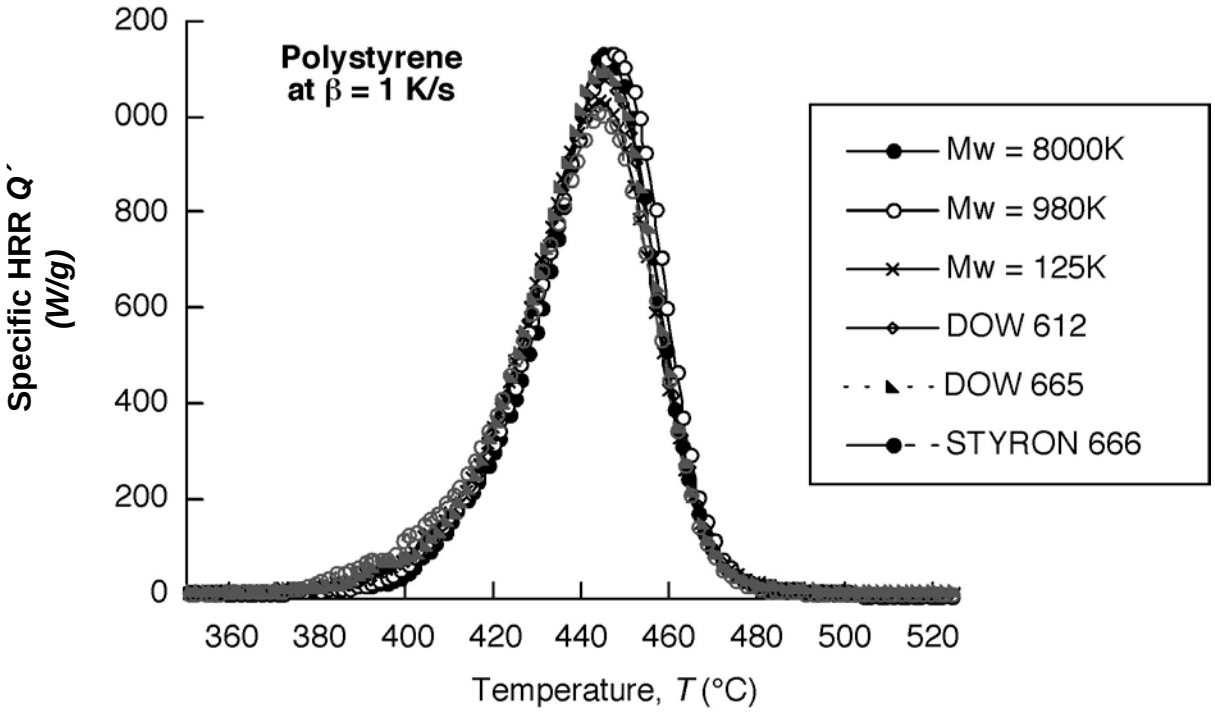

Figure 24. The *Q′* Histories of PS From Different Sources

5. SETTING THE TEST PARAMETERS.

The user-defined test parameters are input via the MCC DAC interface in figure 25, which include:

- Combustor temperature
- Pyrolyzer temperatures (initial and final)
- Gas flow rates
- Oxygen concentration in the combustor
- Heating rate
- Sample weight

5.1 COMBUSTOR TEMPERATURE.

The combustor temperature is entered as a test parameter in the lower left-hand corner of the MCC DAC Interface shown in figure 25 and monitored in the upper right-hand corner during operation. A combustor temperature of 900°C will ensure complete combustion of typical pyrolysis gases during the 10 seconds that they spend in the combustor with excess oxygen (see figures 6 and 7 in section 2.3). Check to make sure that the combustor has reached the set point temperature before starting the test.

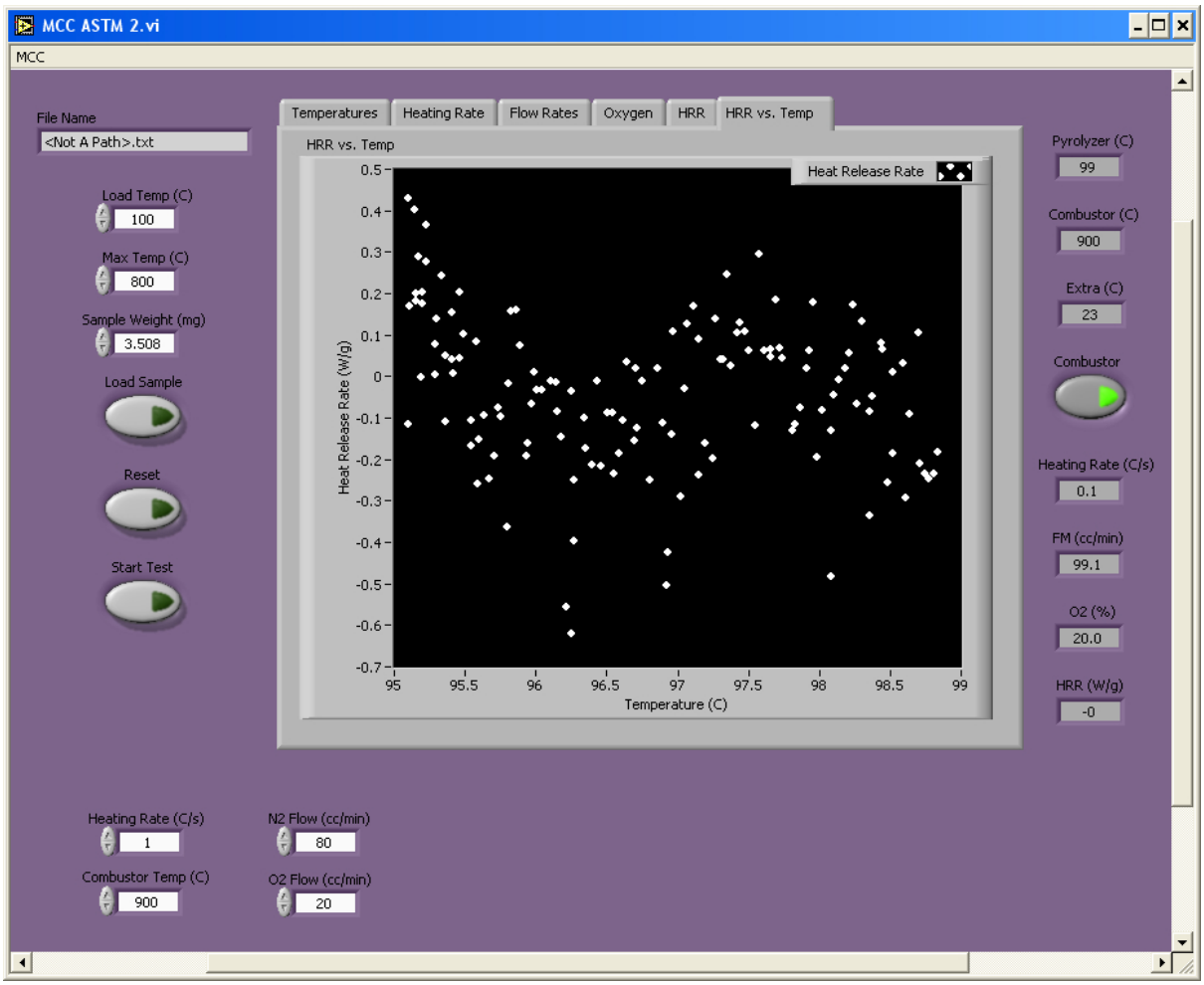

Figure 25. The Q' vs. Temperature Screen of the MCC DAC Interface at the Start of a Test Showing Fields for Entering Test Parameters

5.2 PYROLYZER TEMPERATURE.

The pyrolyzer temperature is monitored in the upper right-hand corner of the MCC DAC interface. The pyrolyzer is capable of controlled linear heating from 100°-1000°C, but a narrower temperature range may fully degrade the sample and expedite the analysis. Char-forming materials can have a low Q' that persists to relatively high temperatures due to char cracking, but which is usually difficult to detect above the baseline. In general, it is necessary to obtain at least 50°C of flat ($Q' = 0$) baseline before and after the pyrolysis temperature interval when $Q' \neq 0$, so that baseline correction can be performed to give accurate maximum (Q'_{max}) and integrated (Q_{∞}) values. Sufficient baseline before and after the pyrolysis interval is also important for some of the curve fitting routines.

5.2.1 Initial (Load) Temperature.

The starting temperature (Load Temp) is entered in the upper left-hand corner of the MCC DAC Interface in figure 25. The Load Temp is the maximum temperature of the pyrolysis furnace at the start of the test and the temperature at which the sample post will be lowered at the end of the test. If the Load Temp setting is too low, the sample will not be retracted from the pyrolyzer until the fan turns on and cools the pyrolyzer to the load temperature. The sample should be thermally stable at the Load Temp to avoid premature decomposition of the sample in the MCC before the test begins. In general, higher Load Temps result in shorter test duration and higher sample throughput. The Load Temp should be at least 100°C below the lowest temperature at which thermal decomposition of the sample begins (as determined, for example, by DTGA) to allow time/temperature for the baseline to establish (see section 3.1) and to make sure that the heating rate reaches the nominal (programmed) value before the sample begins decomposing and releasing heat.

5.2.2 Final (Maximum) Temperature.

The maximum test temperature (Max Temp) is entered in the upper left-hand corner of the MCC DAC Interface (figure 25). The Max Temp is the highest temperature reached by the pyrolyzer during the test. The Max Temp should be at least 100°C higher than the highest temperature at which heat is released during the heating program to assure that pyrolysis is complete and that baseline is re-established after the test. The final pyrolyzer temperature can be changed at any time during the test.

5.3 GAS FLOW RATES.

5.3.1 Purge Gas.

The purge gas flow rate is entered in the lower left-hand corner of the MCC DAC Interface. The purge gas enters the pyrolyzer to sweep the thermal decomposition products into the combustor during the test. The purge gas may be either an inert gas (nitrogen, noble gases) or a reactive gas (air, oxygen, or other non-corrosive gases) depending on the purpose of the test. The flow rate of the purge gas should be between F_P = 50 and 100 cm^3/min, but normally the purge gas is nitrogen or air and its flow rate is F_P = 80 cm^3/min.

For anaerobic pyrolysis, which is the operating mode of the MCC that simulates fire conditions (ASTM D7309, Method A), the purge gas is typically high-purity nitrogen. Anaerobic pyrolysis produces a solid carbonaceous residue (char) that is characteristic of fires (see section 2.2, figure 2).

For oxidative pyrolysis (ASTM D7309, Method B) the purge gas is typically high-purity dry compressed air or synthetic air blended in the MCC. Under oxidative pyrolysis conditions, the entire sample is oxidized, including the solid carbonaceous char residue if the pyrolyzer Max Temp is sufficiently high. The heat released by oxidative pyrolysis is the net heat of complete combustion (net calorific value), analogous to the gross calorific value measured in oxygen bomb calorimeters.

5.3.2 Reactive Gas.

The reactive gas flow rate is entered in the lower left-hand corner of the MCC DAC Interface. The reactive gas is introduced into the combustor to oxidize or chemically modify the fuel gases coming from the pyrolyzer. The reactive gas may be oxidizing or reducing, depending on the purpose of the test. To simulate fire conditions (ASTM D7309, Method A), the reactive gas is oxygen in sufficient quantity to completely oxidize all of the anaerobic pyrolysis products to carbon dioxide, water, and possibly acid gases (see section 2.3). To determine the net heat of complete combustion (ASTM D7309, Method B) with an oxygen bomb calorimeter experiment, the reactive (and purge) gas is typically high-purity dry air or oxygen-enriched dry air, depending on the material being tested. The flow rate of the reactive gas should be between F_R = 20 and 50 cm^3/min, but normally the reactive gas is oxygen or air and its flow rate is F_R = 20 cm^3/min.

5.3.3 Total Gas Flow Rate.

The total gas flow rate at the flow meter is monitored in the lower right-hand corner of the MCC DAC Interface of figure 25. The combined flow rate $F = F_R + F_P$ of the purge gas and the reactive gas should be between 50 and 200 cm^3/min, but normally it is F = 100 cm^3/min. Changing the total gas flow rate changes the Q' delay time τ_d, causing $Q'(t\text{-}\tau_d)$ to be out of synchronization with sample temperature (see section 3.1.2). Figure 26 shows the flow rate of nitrogen into the pyrolyzer, oxygen into the combustor, and the combined, final flow rate F versus sample temperature for a test of PS in the MCC using Method A. Note the small perturbation in F due to the change in the gas composition during the combustion process. This perturbation $F(t)$ is included in the Q' calculation (equation 44).

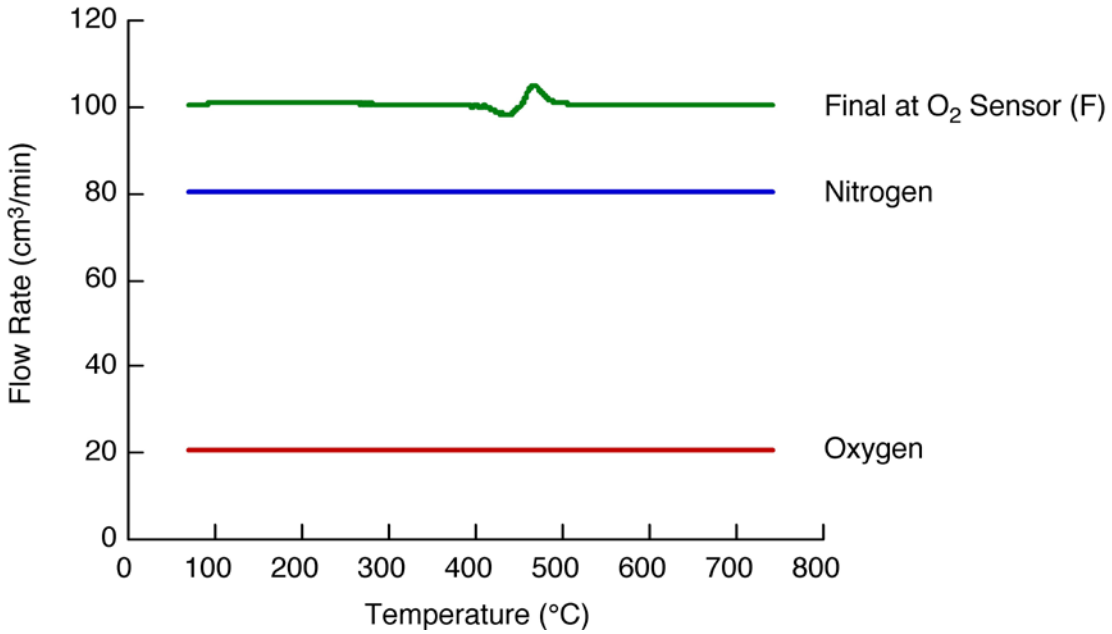

Figure 26. Oxygen and Nitrogen Flow Rates Into the MCC and the Total Flow Rate F out of the MCC Measured at the Oxygen Sensor

5.4 OXYGEN CONCENTRATION IN THE COMBUSTOR.

The volume fraction of oxygen in the combustor X_{O_2} for a reactive gas (oxygen or air) having flow rate F_R and oxygen volume fraction $X_{O_2}^R$ and a purge gas (nitrogen or air) having flow rate F_P and oxygen volume fraction $X_{O_2}^P$ is:

$$X_{O_2}^0 = \frac{F_R X_{O_2}^R + F_P X_{O_2}^P}{F_R + F_P} \tag{65}$$

For pure oxygen as the reactive gas $X_{O_2}^R$ = 1 at F_R = 20 cm^3/min, and pure nitrogen as the purge gas $X_{O_2}^P$ = 0 at F_P = 80 cm^3/min (ASTM D7309, Method A), the baseline oxygen concentration in the combustor is $X_{O_2}^0$ = [(1)(20)+(0)(80)]/(20+80) = 0.2 = 20%. If reagent-grade dry air is used as both the purge and reactive gas (ASTM D7309, Method B), $X_{O_2}^R$ = $X_{O_2}^P$ = 0.21, and for the nominal flow rates the baseline oxygen concentration in the combustor is, $X_{O_2}^0$ = [(20)(0.21)+(80)(0.21)]/(20+80) = 0.21 = 21%. Equation 65 should be used to determine the oxygen concentration in the combustor for other gases and flow rates and to check the linearity of the oxygen sensor response using the MCC to blend O_2 and N_2.

Figure 7 and related studies [34] suggest that typical fuels are completely oxidized at oxygen concentrations as low as a few percent in the combustor (i.e., $\Phi \leq 0.95$ for samples of a few milligrams). However, incomplete combustion products may form at low-oxygen concentrations and/or large sample mass that can pass through the flow meter and oxygen sensor, possibly damaging them. Figure 27 shows PS samples of appropriate (3.2 mg) and excessive (6.5 mg) mass on the resulting oxygen consumption and Q' histories. Figure 27 shows that if a sample consumes more than 95% of the oxygen in the combustor, the $Q'_{\max}$ is attenuated. In this case, a smaller sample should be used or the heating rate should be reduced (see section 5.5). Although not recommended for routine use, the oxygen concentration in the combustor can be increased at constant total flow rate F so that the delay time τ_d is unchanged. In general, the oxygen concentration in the combustor should be above 0.10 (10% by volume) at $Q'_{\max}$ to ensure that thermal oxidation of the fuel gases is complete.

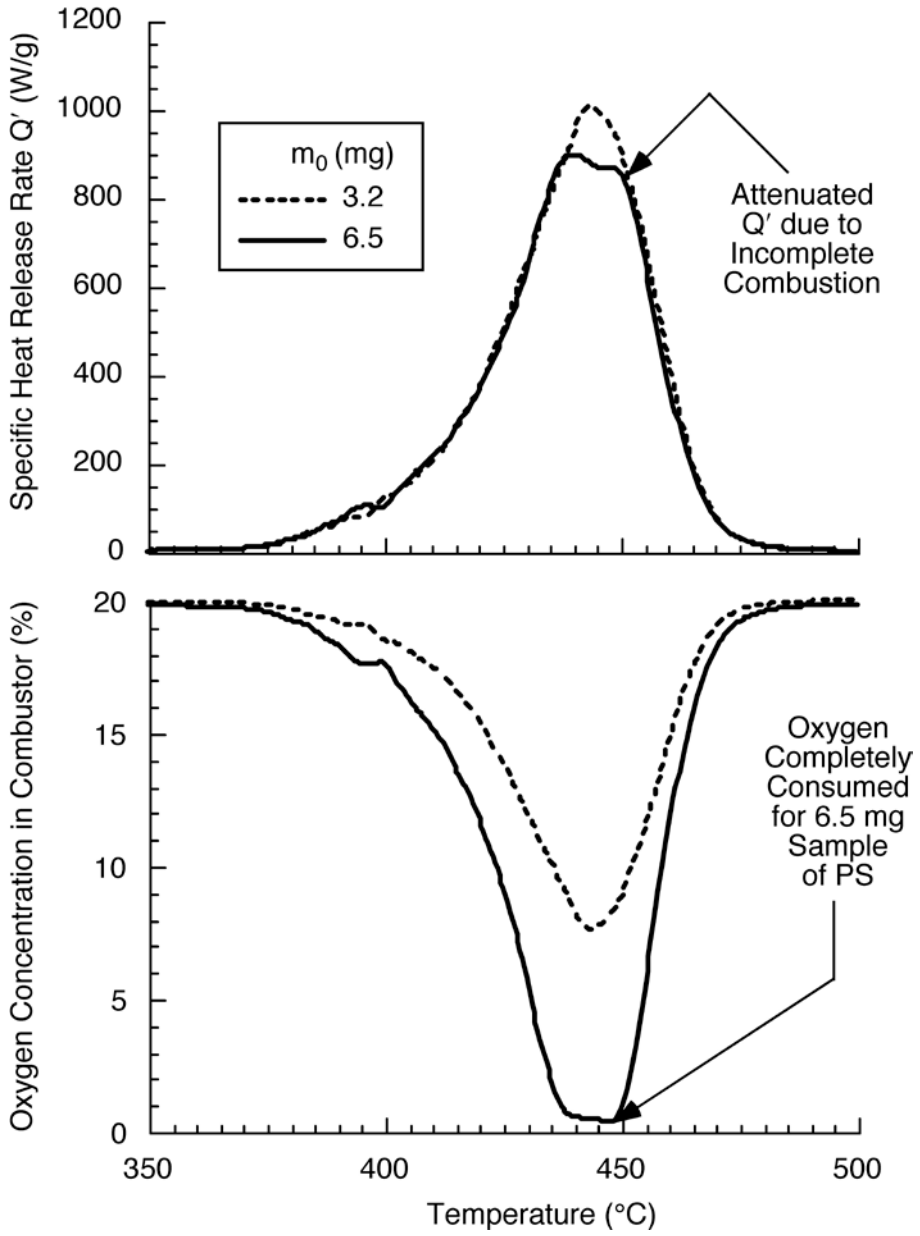

Figure 27. Oxygen Concentration in the Combustor vs. Sample Temperature for 3.2 and 6.5 mg PS Samples, Showing Incomplete Combustion of the Latter

5.5 HEATING RATE.

The heating rate can be set for controlled heating at any rate between $\beta = 0.2$ K/s and $\beta = 2$ K/s. The heating rate is constrained by the necessity to maintain thermal equilibrium of the sample (section 3.3) and chemical equilibrium of its fuel gases (section 3.4) during the test. In general, thermal equilibrium is achieved when the heating rate $\beta \leq (2.4 \text{ mg-K/s})/m_0^{2/3}$ (equation 60) where m_0 is the sample mass in milligrams. Complete combustion of the fuel gases (equation 64) has approximately the same sample mass requirement as that for thermal equilibrium under standard (ASTM D7309, Method A) test conditions using average polymer properties in table 5. If a

heating rate other than the nominal β = 1 K/s is used, η_c should be calculated from Q'_{max} using equation 19 with a = 0.055. Figure 28 shows the heating rate and sample temperature history for a 3-mg sample of PS at β = 1 K/s.

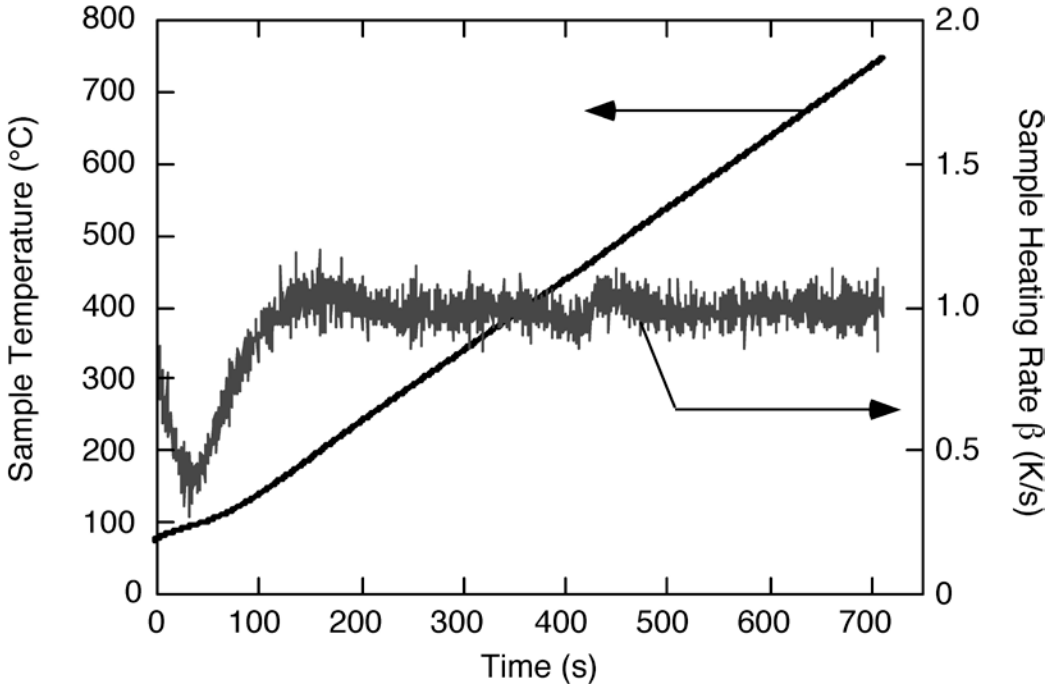

Figure 28. Sample Temperature and Heating Rate Histories for 3 mg of PS at β = 1 K/s

5.6 SAMPLE WEIGHT.

The sample weight is limited by thermal inertia (equation 60 in section 3.3) and oxygen consumption by the fuel gases during oxidation (equation 64 in section 3.4 and figure 27 in section 5.5). These rules are approximate, so a screening test of Q'_{max} versus sample mass (m_0), oxygen consumption (ΔX_{O_2}), and heating rate (β) is appropriate to optimize sample size. However, a reasonable starting point for a sample of an unknown composition would be a 4 to 5 mg sample heated at β = 1 K/s, using 20% oxygen in the combustor.

A balance with a range of at least 250 mg and an accuracy of 0.01 mg is required to measure the sample mass m_0 and the char mass m_c in the sample cup. A propagation of error study showed that weighing the sample was the largest single source of error. It is also important not to touch the sample with bare hands. Gloves can be worn or tweezers used to avoid contamination from oils, moisture, and dirt that may be present. Also, care should be taken to avoid breathing on the samples because the large surface area-to-volume ratio of milligram samples makes adsorbed moisture a significant fraction of the sample mass and a source of weighing error.

The sample must be weighed after the test to obtain the pyrolysis or combustion residue. Before weighing, the sample and sample cup must be allowed to cool and equilibrate with the

surroundings before a stable weight measurement can be obtained. This usually takes 10 to 15 minutes (1 sample cycle).

Sample holders are typically circular cups having a 6-mm (1/4-inch) outer diameter with a 3-mm-(1/8-inch) high wall of thickness of 0.5 mm (0.020-inch). Sample cups are made of a 99.8% alumina ceramic. These sample cups can be used repeatedly as long as they are cleaned thoroughly between tests. Sample cups can be cleaned by using a torch to burn off any residue or by heating in a muffle furnace at 1000°C for several hours in air to oxidize any carbonaceous residue (char). Sample holders are designed to fit on the sample platform in very close proximity to the thermocouple located at the end of the sample post.

There are no restrictions on the form of the samples to be tested, which may be films, pellets, plaques, granules, powders, fibers, or foams. Solid samples can be cut to size with a razor blade. Powder samples can be placed in a cup with a spatula, taking care not to get any on the outside of the sample cup. Film samples can be cut into strips, rolled into a cylinder, and placed into the cup. Fiber samples can be tied in knots and cut to fit in the cup or pulverized [35]. Laminated materials and sheets can be punched using a sheet metal punch. Oil and grease should be removed from tooling (punches, razor blades, pliers, etc.) used to cut the samples so as not to contaminate the sample by handling or by the tooling. Samples that are not homogeneous can be pulverized and homogenized to yield representative results [35]. If the sample cannot be homogenized, then the specimen should be sampled in several locations and the results of the individual tests averaged. When using this technique, a minimum of five replicate tests of a material are recommended instead of the usual three. Inhomogeneous samples include composites, systems with coarse fillers, mixtures, and laminated materials. A hole punch works well for composite panels that are less than 3 mm (1/8-inch) in thickness if the sample mass is appropriate. Laminated composite samples should be disassembled and the components analyzed separately. Heat of combustion and heat release capacity of each component are added according to their weight fraction to obtain the composite value (see section 8). Liquid samples that are vaporized below 100°C are difficult to weigh and test accurately.

6. ACQUIRING AND DISPLAYING DATA DURING TEST.

All of the measured signals can be displayed and monitored on the MCC DAC screen (figure 25) during the test. It is also important to monitor these signals prior to starting a test to make sure there are no problems with the equipment.

6.1 OXYGEN CONCENTRATION.

The baseline oxygen concentration $X_{O_2}^0$ in the combustor is determined by the flow rates of the purge (typically N_2) and reactive (typically O_2) gases and is monitored in the lower right-hand corner of the MCC DAC Interface (figure 25). Under standard (ASTM D7309, Method A) operating conditions $X_{O_2}^0$ should be about 20% O_2 by volume. After a sample is inserted, the oxygen concentration should be allowed to reach a steady state before the test is started. This will prevent abnormal baselines and baseline shifts during the test. While the test is running, the O_2 should be monitored as shown in figure 27 to make sure all of the O_2 is not consumed by the

decomposition. If all of the oxygen is consumed, then incomplete combustion products could be transferred to the flow meter and oxygen sensor, potentially causing damage. If samples exhibit high O_2 consumption, then the sample size should be reduced, the $X_{O_2}^0$ increased, or the heating rate reduced (see section 3.4). Conversely, if the sample consumes only a couple of percent of O_2 at Q'_{max}, then the sample size can be increased to improve the signal-to-noise ratio.

6.2 SAMPLE TEMPERATURE.

Sample temperature information is displayed graphically in two locations: the Temperature versus Time screen and the Q' versus temperature screen. The temperature versus time graph shows whether the sample temperature is increasing at the constant programmed rate β as indicated in figure 28. The combustor and pyrolyzer temperatures are also displayed in this window. On some equipment, there is an extra temperature indicator. This indicator is useful for diagnosing potential problems with the equipment. Because heating rate β is the control variable (see section 3.2) for the linear temperature history, a program temperature is not needed or recorded.

6.3 HEATING RATE.

The heating rate should reach the programmed β quickly and remain constant throughout the test, as shown in figure 28. If the heating rate does not stabilize and maintain the set rate, then the pyrolyzer must be recalibrated. Small changes in the heating rate can be observed when the sample is degrading because of the absorption or evolution of thermal energy. This perturbation appears around the decomposition temperature T_p = 445°C for PS in figure 28. The heating rate in the vicinity of the thermal decomposition event is plotted on an expanded scale for HIPS along with Q' in figure 29, where the perturbation occurs at T_p = 467°C for this polymer. These perturbations are small (5%) compared to the programmed heating rate. The reported heating rate for the test is an average over the pyrolysis interval and that heating rate is used to calculate η_c from Q'. If the heater does not maintain the programmed rate after recalibration, the electrical connections should be checked and tightened or the heater should be replaced.

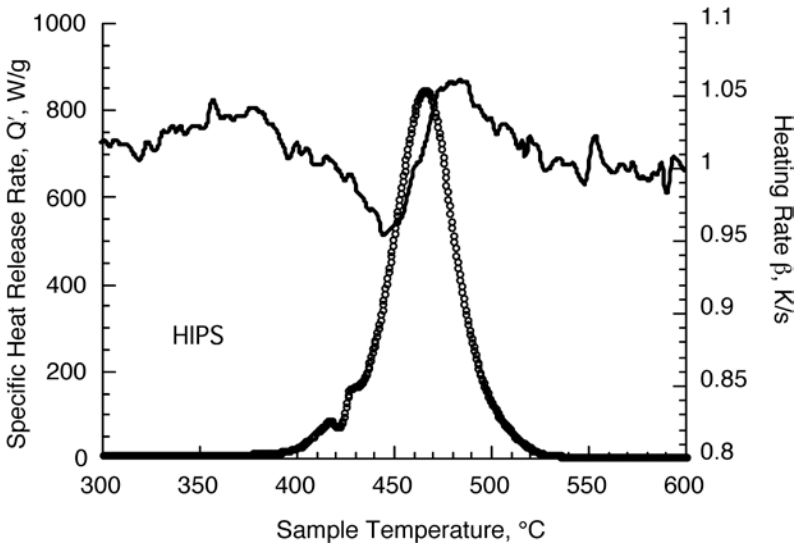

Figure 29. The Q' History and Heating Rate β During a Test of HIPS at the Programmed Rate $\beta = 1$ K/s

6.4 GAS FLOW RATES.

The gas flow rates screen shows the flow rates for all the mass flow controllers and final flow meter. The nitrogen and oxygen flow rates should be stable during a test as shown in figure 26, although the end flow fluctuates slightly at the beginning of the test, during the pyrolysis interval (section 3.1.3), and when the test specimen is decomposing. The end flow should be equal to the sum of the nitrogen and oxygen flows if the instrument is operating properly.

6.5 THE SPECIFIC HEAT RELEASE RATE.

The Q' history is plotted versus time and versus temperature on separate screens labeled HRR and HRR versus Temp, respectively. The HRR screen displays Q' in real time during the experiment with Q' calculated using equation 44. The transit time of the sample gases between the specimen cup and the oxygen sensor must be subtracted from the test time to synchronize the sample temperature with Q' and produce the data in the HRR versus Temp screen. Figure 30 is a composite plot of Q' versus Time (lower abscissa) and Sample Temperature (upper abscissa) for PS.

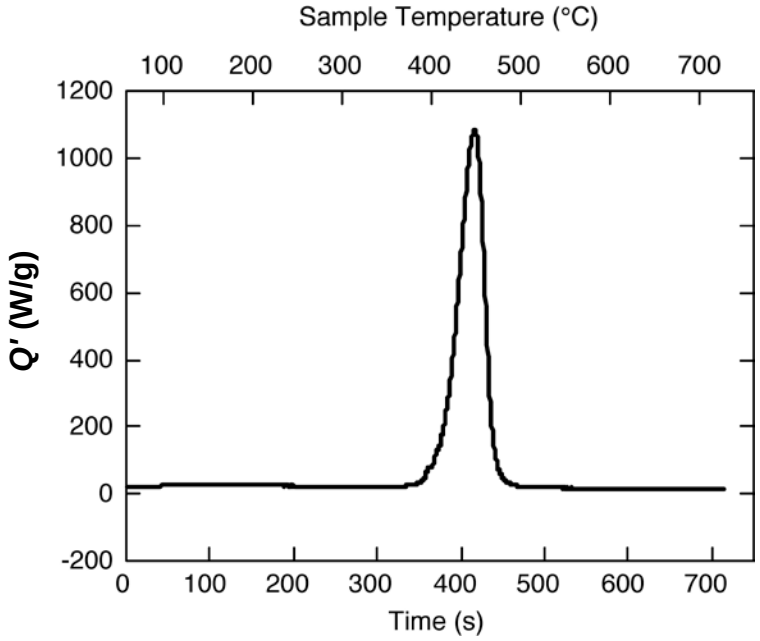

Figure 30. The Q' vs. Time and Temperature During a Test of PS

7. SAVING AND ANALYZING ACQUIRED DATA.

7.1 NAMING AND SAVING FILES.

The MCC DAC screen prompts the user for a file name when the sample is loaded into the pyrolysis furnace. Sample file names should be descriptive enough for the user's purpose. The .txt extension is automatically added to the file name it has been assigned.

7.2 ANALYZING DATA.

Data that have been acquired and saved using the MCC DAC Software can be analyzed using the MCC curve fitting program (Curve Fit). The Curve Fit application is accessed through the MCC Analysis Screen and is used to recall saved data and extract the sample properties that were measured during the test. After a data file is analyzed the data can be saved to another file. The save function in the Curve Fit program automatically adds a Fit.txt extension to the original test data so that it is not overwritten accidentally. Various analyses can be conducted with the MCC Curve Fit software, including correcting a sloping baseline, separating the Q' history into as many as five separate peaks, and obtaining thermal combustion properties of the sample or its components (peaks).

7.2.1 Baseline Correction.

The baseline for the MCC is slightly curved because of the thermal expansion of the purge gas during the heating program (see section 3.1.3). This curvature is exaggerated by small sample weights and auto-scaling of Q' for materials exhibiting low Q'_{max}. Most plastics that have a single-step decomposition degrade over a temperature interval of about 100°C, so the curvature

can be minimized by selecting the proper endpoints for cropping the data. Generally, it is good to have at least 50°C of baseline on each side of the peak(s). Once the data is cropped, a linear baseline correction is applied and values are tabulated. A peak finder locates peaks that are over 75% of the highest Q' measured during the test (if the data is noisy, the noise may be detected as peaks). A user-defined peak threshold value can also be used to accept/exclude peaks. The total heat released is calculated by a numerical integration of the baseline-corrected Q' versus time data (i.e., the Q' history). The heat release capacity η_c for a single component (single peak) material is computed by dividing Q'_{max} by the average heating rate over the cropped Q' history. For materials exhibiting multiple Q'_{max}, the individual peaks must be fit with symmetric or asymmetric distribution functions (see Peak Fitting) and the Q'_{max} of the individual peak fits summed to obtain η_c (see section 8.1.4).

7.2.2 Peak Fitting.

As many as five overlapping peaks can be separated using the curve fitting algorithms. Peaks must be separated to obtain η_c for samples that exhibit multiple Q'_{max}. The minimum number of peaks ($n \leq 5$) that provide an error of less than 5% should be used to obtain η_c. There are five different peak fits that can be used to fit the Q' data.

- Gaussian (G)—This bell-shaped curve is a normal (Gaussian) distribution of Q' versus temperature that is symmetrical about T_{max}, as shown in figure 31.

- Lorentzian (L)—This narrow curve with long tails is a Lorentzian distribution of Q' versus temperature peak that is symmetrical about T_{max}, as shown in figure 31.

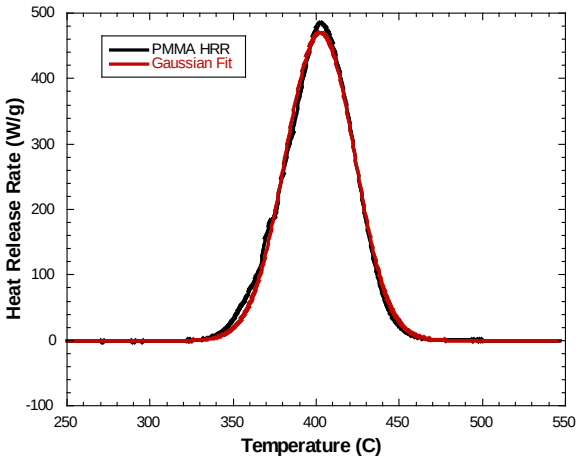

(a)

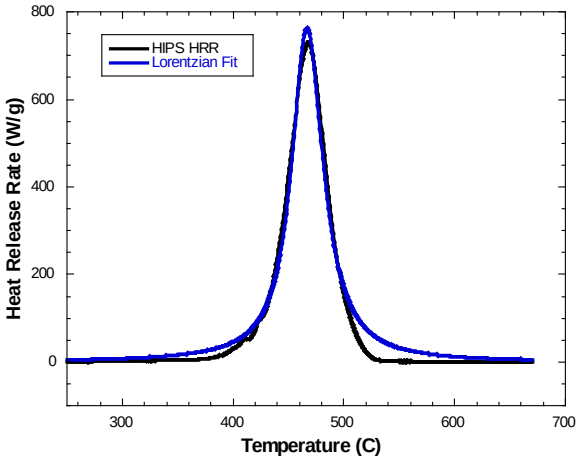

(b)

Figure 31. Gaussian fit of PMMA $Q'(T)$ History (a) and Lorentzian Fit of HIPS $Q'(T)$ History (b)

Asymmetric Gaussian (AG)—This based on a Gaussian function, but Q' is asymmetric about T_{max} with different peak half-widths, as shown in figure 32(a).

Asymmetric Lorentzian (AL)—This is based on a Lorentzian function, but Q' is asymmetric about T_{max} with different half-widths, as shown in figure 32(b).

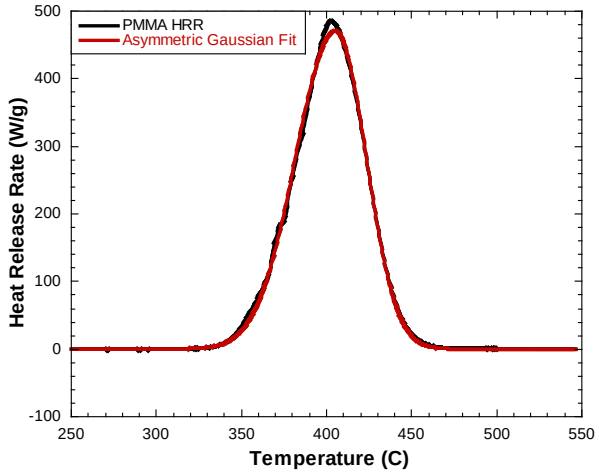

(a)

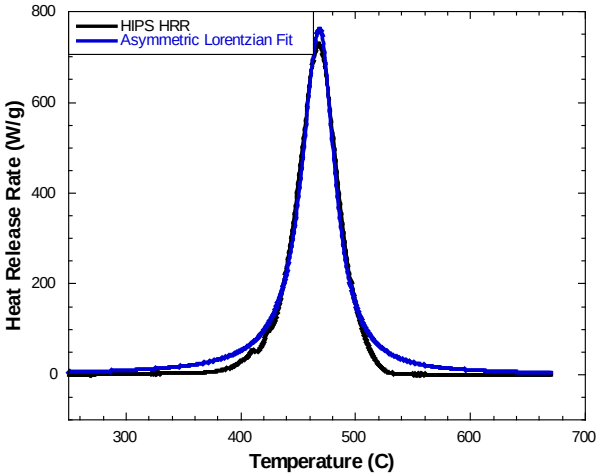

(b)

Figure 32. Asymmetric Gaussian Fit of PMMA $Q'(T)$ History (a) and Asymmetric Lorentzian Fit of HIPS $Q'(T)$ History (b)

Asymmetric Gaussian-Lorentzian (AGL) Hybrid—Combination of the Gaussian and Lorentzian curve shapes where the peaks have the same height and half-width, but the fraction of Gaussian and Lorentzian character is different for each side of the peak, as shown in figure 33 and for PMMA and HIPS, respectively.

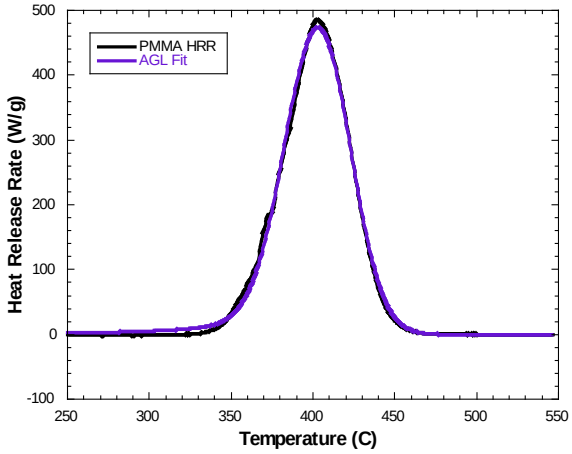

(a)

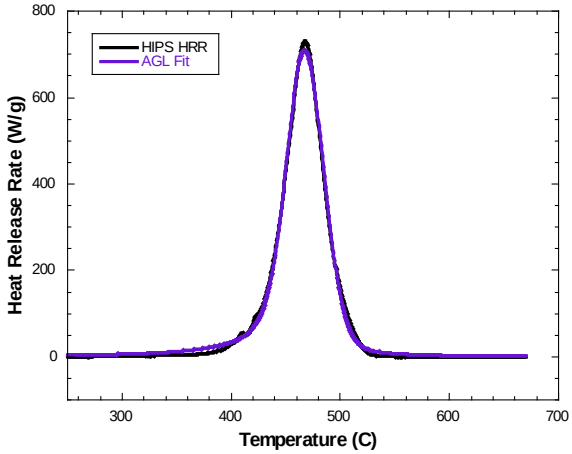

(b)

Figure 33. Asymmetric Gaussian-Lorentzian Hybrid Fit of PMMA $Q'(T)$ History (a) and Asymmetric Gaussian-Lorentzian Hybrid Fit of HIPS $Q'(T)$ History (b)

8. OBTAINING THERMAL COMBUSTION PROPERTIES.

8.1 ANAEROBIC PYROLYSIS (ASTM D7309, METHOD A).

1. Pyrolysis Residue (g/g): The pyrolysis residue is the mass fraction of sample remaining after anaerobic thermal decomposition as per ASTM D7309, Method A, obtained by weighing the sample before and after the test. To ensure that the pyrolysis residue represents an equilibrium value [36], the maximum test temperature should be set to 850°C or to a temperature that is at least 50°C above the temperature at which $Q' = 0$ at the end of the test.

2. Specific HRR, Q' (W/g): The maximum value of Q' during the test is the peak HRR Q'_{max}. Since Q'_{max} is roughly proportional to β (see equation 18), both must be reported together.

3. Heats of Combustion of Volatiles

- Heat of Combustion of Sample, Q_∞ (J/g-sample): The net heat of complete combustion of the volatiles liberated during controlled anaerobic thermal decomposition per unit initial sample mass using ASTM D7309, Method A is the specific heat release of the sample Q_∞. The specific heat release is the time integral of $Q'(t)$ over the entire temperature range of the experiment. The specific heat release is obtained under anaerobic pyrolysis conditions to reproduce the conditions at the surface of a burning sample where flaming combustion consumes all of the available oxygen.

- Heat of Combustion of Sample Gases, h_c (J/g-gas): The net heat of complete combustion of the sample gases per unit mass of volatiles, $h_c = Q_\infty/(1-\mu)$, is measured using ASTM D7309, Method A. This parameter is used to calculate the efficiency of flaming combustion χ from the effective heat of combustion (EHOC) measured in a fire calorimeter, $\chi = \text{EHOC}/h_c$ (see section 9.3).

4. Heat Release Capacity, η_c (J/g-K): The heat release capacity η_c is a derived quantity (equation 19) that represents the maximum capability (capacity) of a material to release combustion heat per degree of temperature rise during pyrolysis or burning. The units of η_c are Joules per gram degree Kelvin (J/g-K) and it has been shown to have a molecular basis [37 and 38]. The heat release capacity of a material with a starting mass m_0 that exhibits a single HRR peak $q'_{\max}$ (Watts) is $\eta_c = (q'_{\max}/m_0)/\beta = Q'_{\max}/\beta$ according to the first-order theory (equation 19). If the material exhibits multiple HRR peaks, the heat release capacity is calculated as if each peak represents a separate component, i = 1,2,3…n having mass m_i and heat release capacity $\eta_i = (q'_{\max,i}/m_i)/\beta$. In this case, the heat release capacity of the n-component mixture having $\Sigma m_i = m_0$ is simply the mass-fraction-weighted average of the heat release capacities of the components, which is the sum of the individual peak heights after deconvolution (peak fitting) to remove peak overlap:

$$\eta_c = w_1\eta_1 + w_2\eta_2 + \ldots w_n\eta_n = \left(\frac{m_1}{m_0}\right)\left(\frac{1}{\beta}\frac{q'_{\max,1}}{m_1}\right) + \left(\frac{m_2}{m_0}\right)\left(\frac{1}{\beta}\frac{q'_{\max,2}}{m_2}\right) + \ldots \left(\frac{m_n}{m_0}\right)\left(\frac{1}{\beta}\frac{q'_{\max,n}}{m_n}\right) \quad (66)$$

$$= \frac{1}{\beta}\left\{\left(\frac{q'_{\max,1}}{m_0}\right) + \left(\frac{q'_{\max,2}}{m_0}\right) + \ldots \left(\frac{q'_{\max,n}}{m_0}\right)\right\}$$

$$= \frac{1}{\beta}\left\{Q'_{\max,1} + Q'_{\max,2} + \ldots Q'_{\max,n}\right\} = \frac{1}{\beta}\sum_{i=1}^{n} Q'_{\max,i}$$

Because the multiple Q'_i peaks often overlap, they must first be separated and resolved using a peak-fitting procedure (section 7.2). The minimum number of peaks that provide an error of less than 5% in the composite curve maximum should be used to obtain η_c.

Figure 34 illustrates the process of obtaining the heat release capacity of a multi-component material by the peak fitting method. In this test, the heating rate was β = 1 K/s and the sample was a PC/ABS blend having 75% by weight PC and 25% by weight acrylonitrile-butadiene-styrene copolymer (ABS) for which the $Q'_{max,i}$ peaks are widely separated in temperature. The two main peaks are fit with an asymmetric Gaussian-Lorentzian hybrid function and the results are shown as a thick, solid line (ABS) and dashed line (PC). The composite curve obtained by adding the two fitted peaks together is shown as a narrow solid line passing through the majority of the experimental data (open circles). The error of the multiple peak-fit is calculated as the difference between Q'_{max} from the composite fit and Q'_{max} from the experimental data, normalized for the latter and expressed as a percentage.

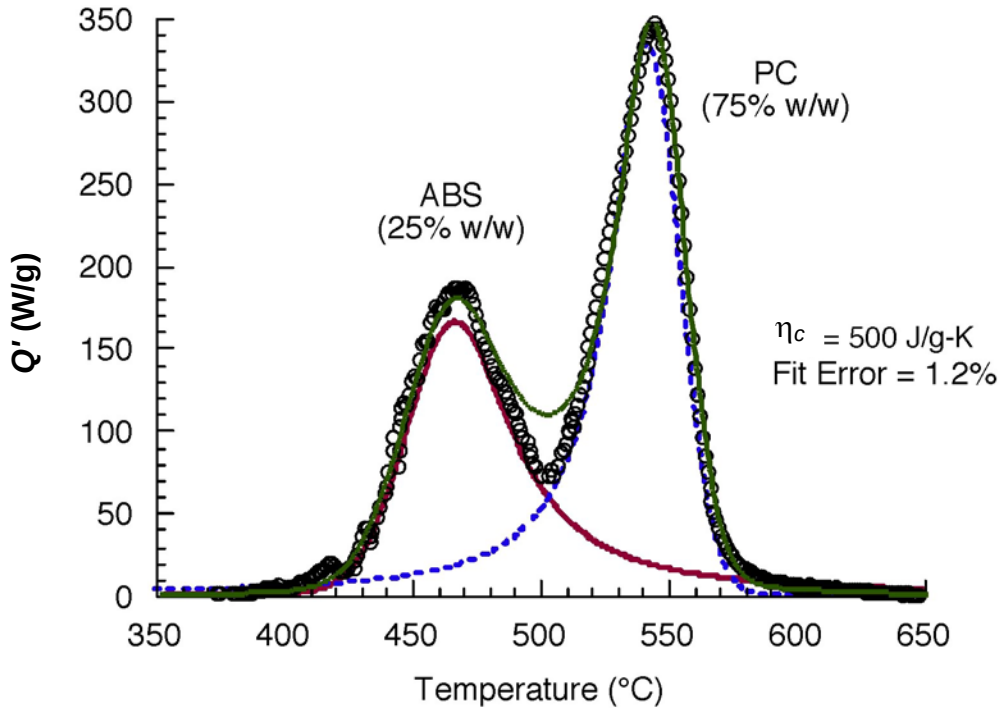

Figure 34. The MCC Data for PC/ABS Blend (75/25) at β = 1 K/s (Both peaks are fit with Asymmetric Gaussian-Lorentzian Hybrid function.)

From the curve fit, Q'_{max} (ABS) = 167 W/g and Q'_{max} (PC) = 333 W/g, so the heat release capacity of the PC/ABS blend is:

$$\eta_c(PC/ABS) = \frac{1}{\beta}\left(Q'_{max,ABS} + Q'_{max,PC}\right) = \frac{1}{1\,\mathrm{K/s}}\left(167\frac{W}{g} + 333\frac{W}{g}\right) = 500\frac{J}{g\,K} \qquad (67)$$

In this case, η_c is significantly higher than the result that would be obtained from the global maximum Q' in the test, i.e., $Q'_{max}/\beta \approx$ (350 W/g)/(1 K/s) = 350 J/g-K. The peak summation method used to obtain η_c follows from the requirement that the total heat of combustion of the sample is the sum of the heat of combustion of its components. To the extent that the Q' peaks

are approximately the same width on the temperature axes, summing the $Q'_{\max,i}$ is roughly equivalent to summing the peak areas ($Q_{\infty,i}$). This follows from equation 19, in which the pyrolysis temperature interval $\Delta T_{p,i}$ for each component i is constant $\Delta T_{p,i} \approx \Delta T_p$:

$$\eta_c = \sum_{i=1}^{n} \frac{Q'_{\max,i}}{\beta} = \sum_{i=1}^{n} \frac{Q_{\infty,i}}{\Delta T_{p,i}} \approx \frac{1}{\Delta T_p} \sum_{i=1}^{n} Q_{\infty,i} = \frac{Q_\infty}{\Delta T_p} \tag{68}$$

Physically, this corresponds to the surface of a burning sample when the temperature gradient extends into the sample and fuel is generated simultaneously at every depth at a rate determined by the local temperature and the kinetic parameters E_a and A, according to equation 1.

To confirm that η_c of a multi-component material, rather than the global maximum, $Q'_{\max}/\beta$, is the correct fire-hazard indicator, the ThermaKin numerical burning model [39 and 40] was used to simulate the areal heat release rate q''_c (W/m^2) of three virtual materials in flaming combustion. The computed MCC data for these two-component virtual materials (A, B, and C) are shown on the left-hand graph of figure 35. The right-hand graph in figure 35 shows the ThermaKin q''_c simulations for 6-mm slabs of the virtual materials in a standard fire calorimeter test [23] using the same kinetic parameters and heats of combustion of the A, B, and C materials that were used to compute the MCC data. $Q'_{\max}/\beta$ on the left-hand side of figure 35 varies by more than a factor of two for these materials (i.e., $Q'_{\max}/\beta$ = 230, 457, and 500 J/g-K for A, B, and C, respectively), yet all three have the same η_c by peak summation (500 J/g-K), the same Q_∞ (25 kJ/g), and the same maximum or peak heat release rate, q''_{peak} (430 kW/m^2) in the ThermaKin simulations. Although A and B ignite earlier because they decompose and release heat at a lower temperature, these data show that, in general, the heat release capacity $\eta_c = \Sigma\, Q'_{\max,i}/\beta$ is a better predictor of q''_{peak} (and probably fire hazards) than $Q'_{\max}/\beta$ for a multi-component mixture.

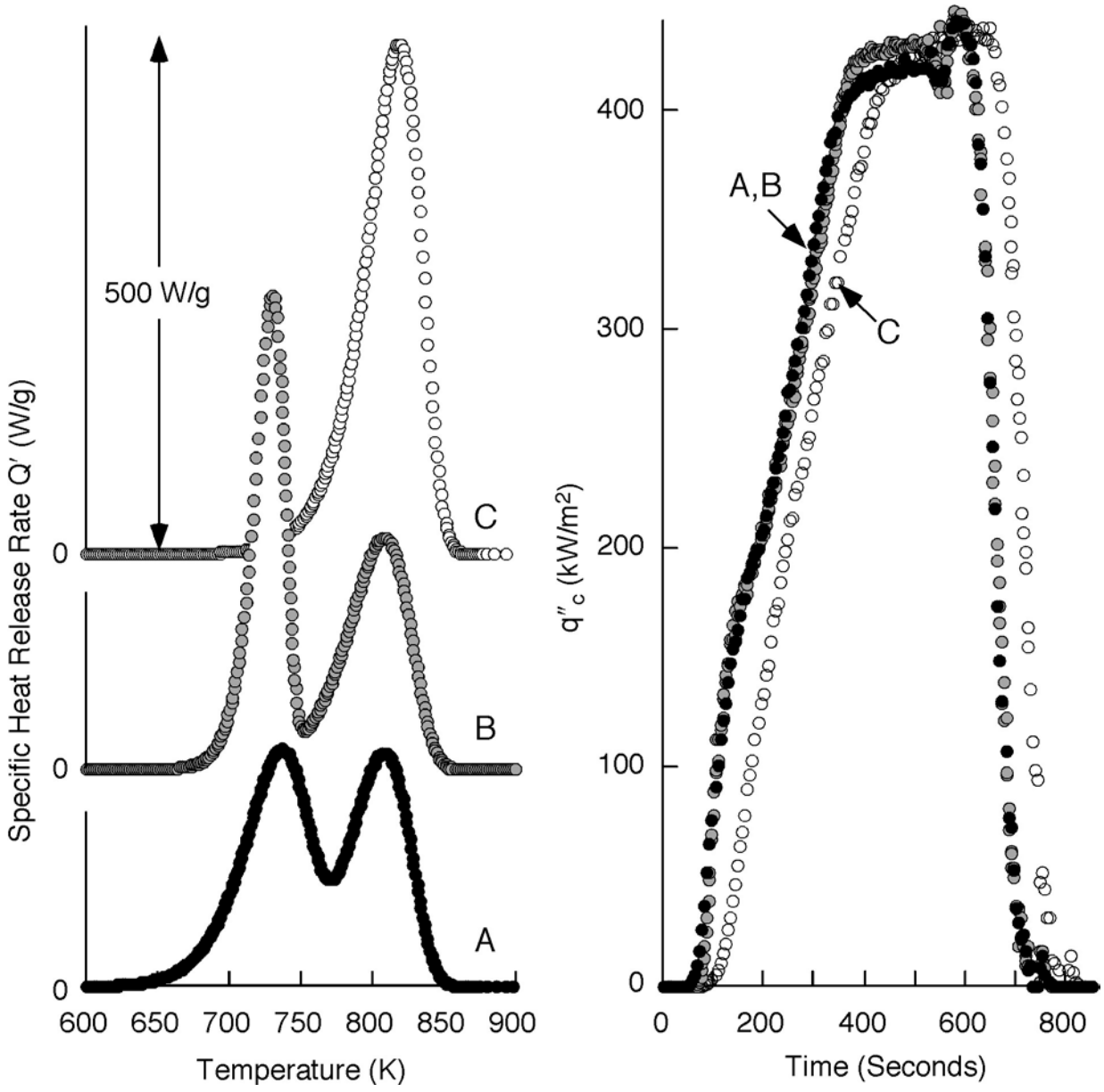

Figure 35. Simulated MCC (Left) and Fire Calorimetry (Right) Tests for a Material Exhibiting One (C) or Two (A, B) Q'_{max} in the MCC

5. Decomposition Temperatures: Following thermal analysis convention [11 and 41], the onset thermal decomposition temperature is variously defined as the temperature at which Q' reaches 1%, 3%, or 5% of Q'_{max} or as the temperature at the intersection of the tangent to $Q'(T)$ with the temperature axis (abscissa). The temperature at maximum pyrolysis rate T_p is the temperature at which Q' reaches the maximum value in the test, Q'_{max}.

6. Kinetic Parameters for Thermal Decomposition from a single test: The thermal decomposition kinetic parameters of the condensed phase (e.g., the global activation energy for pyrolysis E_a and the frequency/pre-exponential factor A) are important for

determining η_c from MCC data at heating rates other than β = 1 K/s (equations 18 and 19) and for fire modeling [13, 38, and 39]. These kinetic parameters are usually measured by DTGA [41 and 42] in which the instantaneous sample mass is recorded as a function of time at constant temperature (isothermal) or over a range of temperatures at a constant heating rate (non-isothermal). MCC data can also be used to obtain kinetic parameters. The MCC flammability properties that are used for the determination of kinetic parameters include the heat of complete combustion of fuel gases per unit of initial mass of sample Q_∞ (J/g-sample), the temperature at maximum pyrolysis rate T_p (K), and the specific heat release rate, Q' (W/g-sample).

- Instantaneous Rate Method: For a first-order (single-step) fuel-generation process at temperature T, $Q'(T) = Q'_T$ is proportional to the combustion heat remaining in the sample, which is the difference between the total heat of combustion Q_∞ and the heat evolved up to temperature T

$$Q'_T = k\left\{Q_\infty - Q_T(T)\right\} \tag{69}$$

For a non-isothermal temperature history, $T(\xi) = T_0 + \beta\xi$ where $\beta = dT/d\xi$ is a constant sample heating rate with respect to the shifted time ξ, the heat evolved up to temperature T is:

$$Q_T(T) = \frac{1}{\beta}\int_{T_0}^{T} Q'_T(\theta)d\theta \tag{70}$$

Defining a normalized HRR, $x'(T) = Q'_T/Q_\infty$, the kinetic rate constant at temperature T is:

$$k(T) = \frac{x'(T)}{1-\frac{1}{\beta}\int_{T_0}^{T} x'(\theta)d\theta} = A\exp\left[-\frac{E_a}{RT}\right] \tag{71}$$

The kinetic parameters E_a and A are thus determined from a single MCC experiment as the slope E_a/R and intercept $\ln A$ of a plot of the logarithm of the central term of equation 71 versus $1/T$.

$$\ln\left[\frac{x'(T)}{1-\frac{1}{\beta}\int_{T_0}^{T} x'(\theta)d\theta}\right] = \ln A - \frac{E_a}{R}\frac{1}{T} \tag{72}$$

Equations 71 and 72 apply to DTGA if $x'(T) = -m'(T)/(m_0-m_c)$, where $-m'(T)$ is the mass loss rate (mg/s) at temperature T and m_c is the pyrolysis residue at the end of the test.

- Peak Properties Method [42]: According to equations 7 and 17, the activation energy E_a for a first order, single-step thermal-decomposition process can be calculated from the peak properties $Q'_{\max}$ and T_p obtained for a small but finite sample mass tested at a constant heating rate β in an MCC experiment that is carried to completion so that Q_∞ is also determined:

$$E_a = \frac{Q'_{\max}}{Q_\infty}\frac{eRT_p^2}{\beta} - 2RT_p \tag{73}$$

The identity, $k_p = k(T_p) = A\exp[-E_a/RT_p] = e\,Q'_{\max}/Q_\infty$, follows from equation 15, and is used to calculate the frequency factor A from equation 73:

$$A = \frac{\beta E_a}{RT_p^2}e^{E_a/RT_p} = \frac{Q'_{\max}}{Q_\infty}\exp\left[1+\frac{E_a}{RT_p}-\frac{2RT_p}{E_a}\right] \tag{74}$$

Figure 4 showed the agreement between the first-order model (equation 15) and the experimental data for PA66 using the kinetic parameters in table 5 that were determined by the first-order peak property method (equations 73 and 74). Peak property methods of significantly greater complexity than the first-order method have been used to compute reaction kinetic parameters for arbitrary reaction orders from DTGA data [43 and 44].

7. Thermal Combustion Properties of Common Polymers: Table 5 contains thermal combustion properties and decomposition kinetic parameters for common polymers, several of which are used in aircraft. Also listed is the stoichiometric oxygen-to-fuel mass ratio of the polymer, r_0 [19 and 45]

Table 5. Thermal Combustion Properties of 17 Common Polymers

Polymer	r_0	η_c (J/g-K)	Q_∞ (kJ/g)	μ (%)	T_{onset} (°C)	T_p (°C)	A (s^{-1})	E_a (kJ/mole)
HDPE	3.43	1450	42.2	0	454	515	1.13×10^{30}	469
PP	3.82	1106	41.0	0	406	495	2.74×10^{22}	347
PS	3.07	1088	40.1	0	307	445	9.55×10^{20}	304
HIPS	3.10	873	38.4	2	391	467	5.80×10^{17}	269
ABS	2.76	585	36.1	1	373	465	7.33×10^{11}	187
PA66	2.41	565	28.4	1	404	493	6.80×10^{15}	251
PMMA	1.92	480	24.5	0	337	403	2.93×10^{13}	191
PC	2.27	578	20.5	23	489	554	3.38×10^{25}	422
PET	1.67	366	16.6	12	414	475	2.28×10^{17}	266
PPS	1.97	230	14.7	43	462	550	8.62×10^{12}	226
POM	1.07	200	14.0	0	305	422	2.55×10^{9}	144
PPSU	2.16	219	12.8	42	527	622	7.15×10^{15}	295
PEEK	2.28	345	12.0	53	582	626	3.34×10^{28}	510
PVC	1.41	157	11.1	19	260	478	1.67×10^{10}	168
PEI	2.29	197	9.6	55	517	575	2.52×10^{18}	319
PVDF	1.25	309	7.1	18	459	525	3.40×10^{38}	613
FEP	0.32	82	4.5	0	465	606	5.18×10^{16}	304

8.2 OXIDATIVE PYROLYSIS (ASTM D7309, METHOD B).

1. Combustion Residue ϕ (g/g): The combustion residue is the mass fraction of sample remaining after aerobic/oxidative thermal decomposition as per ASTM D7309 Method B, obtained by weighing the sample before and after the test. This residue is also referred to as ash since it is primarily inorganic/mineral in composition. Figure 36 shows data for oxidative pyrolysis of PC and poly ether ether ketone (PEEK) in the MCC using synthetic air (20/80 O_2/N_2) as the purge gas at $F = F_p = 100$ cm^3/min. Thermo-oxidative decomposition of PC and PEEK occurs at temperatures in the range of anaerobic pyrolysis (table 5), while cracking and oxidative pyrolysis of the char occurs at much higher temperatures. The separate processes of thermal oxidation of the polymer decomposition products in the combustor and the cracking and oxidation of the solid carbonaceous residue in the pyrolyzer are resolved using a 2-peak Asymmetric Gaussian fit of the Q' data in figure 36.

2. Net Calorific Value h_c^0 (J/g-sample): The net calorific value is the heat of complete combustion of the gases and combustion residue generated during thermo-oxidative decomposition of the sample using ASTM D7309 Method B. The net calorific value h_c^0 is the time integral of Q' over the entire temperature range of the experiment (i.e., the area

under the curves in figure 36). The net calorific value is equal to the value obtained by oxygen bomb calorimetry [46] after correcting the gross calorific value for the heat of condensation of water produced by combustion. Because the sample is thermo-oxidatively decomposed in an aerobic (oxygen-containing) environment, the carbonaceous residue that remains after anaerobic thermal decomposition is completely oxidized to carbon dioxide and water. Because of the possibility of ignition during thermo-oxidative decomposition in the MCC, this test method does not normally yield reproducible T_p or Q'_{max} for polymers with $Q_\infty > 20$ kJ/g. Figure 36 shows tests in which ignition did not occur, so it is possible to resolve thermo-oxidative decomposition and combustion of the gaseous and solid products into separate processes. The peak areas in figure 36 show that 68% of h_c^0 for PC is due to oxidation of the products generated during thermal decomposition of the polymer, while polymer decomposition accounts for only 26% of h_c^0 for PEEK, with char oxidation accounting for the balance of h_c^0 for both polymers.

3. Thermal Oxidation Properties of Common Polymers [6]

Thermal combustion properties ϕ and h_c^0 obtained by MCC on milligram samples are compared to the ash and h_c^0 obtained by oxygen bomb calorimetry on gram samples in table 6.

Table 6. Net Calorific Value of Polymers Determined by Oxygen Bomb Calorimetry and (MCC) ASTM D7309 Method B

	ASTM D7309 (B)		Oxygen Bomb		
POLYMER	ϕ (%)	h_c^0 (kJ/g)	Ash (%)	h_c^0 (kJ/g)	Relative Deviation in h_c^0(%)
HDPE	0	43.3	0	43.5	0.5
PS	0	39.8	0	39.4	-1.0
PEEK	0.47	30.2	0	30.7	1.7
PC	0.23	29.8	0	29.8	0
Phenolic Triazine	0.67	29.8	0	29.5	-1.0
Polyaramide fiber (Kevlar)	0.36	27.8	0	28.1	1.1
Polybutyleneterephthalate	0.02	26.7	0	26.3	-1.5
PMMA	0	24.9	0	25.0	0.4
PET	0.13	21.8	0	23.2	6.4
POM	0	15.9	0	16.0	0.6
			Average Relative Deviation		0.72

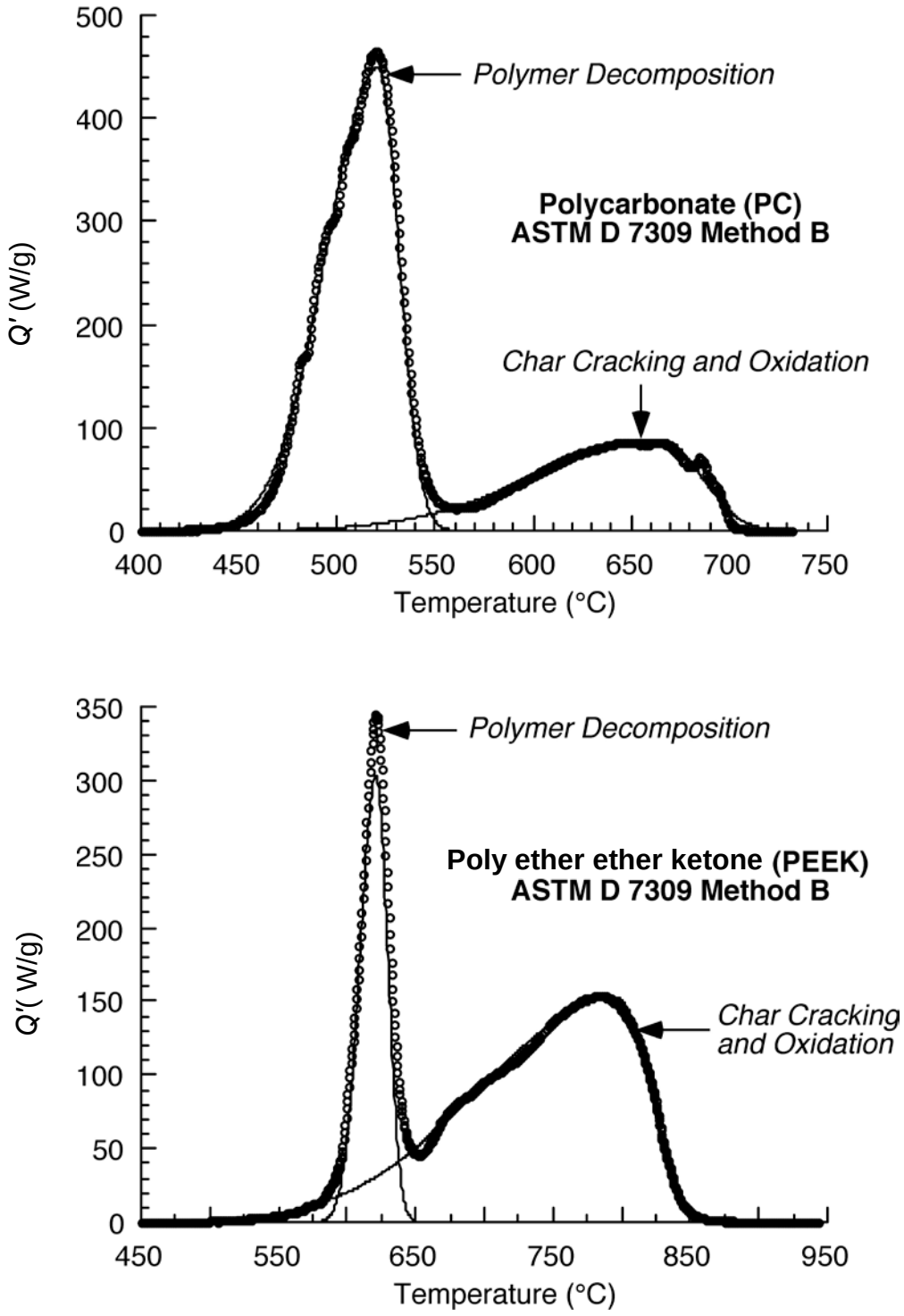

Figure 36. Thermoxidative Decomposition of PC and PEEK in the MCC (Circles are experimental data. Solid lines are AG fits of the indicated processes.)

9. THERMAL COMBUSTION PROPERTIES AND FLAMMABILITY.

It has been shown that the thermal combustion properties obtained from MCC are independent of test conditions, accurate, and highly reproducible [6]. In contrast, fire and flame tests (flammability) are highly dependent on test conditions, so standardized procedures are required to obtain reproducible results. Consequently, the results of fire and flame tests, which may be pass/fail outcomes or fire response parameters, are not material properties. Fire and flame test results are subject to extrinsic factors, such as thickness and edge effects, as well as physical and dimensional changes during burning, like swelling, melting, and dripping. Moreover, fire and flame test results are influenced by condensed/gas phase processes, such as barrier formation/flame inhibition that may be intrinsic to the material or caused by flame retardant additives under conditions of incomplete burning/combustion. The strong dependence of fire and flame test results on test conditions suggests, at best, a qualitative relationship to MCC thermal combustion properties. A simple, qualitative burning model that accommodates thermal combustion properties and fire test conditions is the steady heat release rate in flaming combustion per unit area q_c'' (W/m^2) derived from a surface energy balance [8 and 9]

$$q_c'' = \chi \frac{h_c}{h_g}\left(q_{ext}'' + q_{flame}'' - q_{loss}''\right) \tag{75}$$

The material fire properties in equation 75 are the heat of complete combustion of the volatiles h_c, the heat of decomposition per unit mass of volatiles [28 and 47] h_g, the heat loss from the surface due to convection and radiation, q_{loss}'', which depends on T_{onset} or T_p, and, under well-ventilated conditions, the combustion efficiency of the fuel gases in the flame χ. The test conditions that are incorporated into the burning model are the heat flux entering the surface from an external source (heater, Bunsen burner, fire), q_{ext}'', and the heat flux to the surface of the burning material from its attached flame q_{flame}'', which depends on the sample orientation with respect to gravity. The material fire properties in equation 75 can be expressed in terms of thermal combustion properties:

$$h_c = \frac{Q_\infty}{(1-\mu)} = \frac{\eta_c\,\Delta T_p}{(1-\mu)} \qquad\qquad h_g = \frac{H_g}{(1-\mu)} \equiv \frac{\eta_g\,\Delta T_p}{(1-\mu)} \tag{76}$$

The parameter η_g can be thought of as the heat absorption capacity of the solid (J/g-K) and, although it is not a thermal combustion property available from MCC, it is calculable (e.g., table 6) as $\eta_g \approx H_g/\Delta T_p$ using measured H_g [28 and 47] and the kinetic parameter $\Delta T_p = eR\,T_p^2/E_a$ (equation 19) from MCC, and these values are listed in table 7. Substituting thermal combustion properties for the fire properties in equation 75:

$$q_c'' = \chi \frac{\eta_c}{\eta_g}\left(q_{ext}'' + q_{flame}'' - q_{loss}''\right) = \chi \frac{Q_\infty}{H_g}\left(q_{ext}'' + q_{flame}'' - q_{loss}''\right) \tag{77}$$

The heat losses from the surface in equation 77 can be expressed in terms of the thermal decomposition temperatures T_{onset} and T_p, surface emissivity ε, average convective heat transfer coefficient $\bar{h}$, and the Boltzmann radiation constant σ:

$$q''_{loss} = \bar{h}\left(T_{onset} - T_0\right) + \varepsilon\sigma\left(T_{onset}^4 - T_0^4\right) \qquad \textit{Incipient ignition} \tag{78}$$

$$q''_{loss} = \varepsilon\sigma\left(T_p^4 - T_0^4\right) \approx \varepsilon\sigma T_p^4 \qquad \textit{Sustained ignition} \tag{79}$$

Equations 77 through 79 provide a physical basis for relating thermal combustion properties measured in MCC to q''_c measured in fire tests. One additional assumption, a minimum q''_c for sustained ignition, provides the physical basis for extinction in tests of flame resistance.

9.1 IGNITABILITY.

9.1.1 Ignition Temperature.

The concept of an ignition temperature T_{ign} is based on the assumption that a heated polymer will ignite when it reaches a particular temperature [8]. Not surprisingly, it has been found that T_{ign} approximately coincides with the temperature at which the polymer starts to thermally decompose to fuel gases T_{onset} at typical heating rates in a MCC or DTGA experiment [28]. In terms of the peak properties, equation 12(a) can be solved for T_{onset} by specifying a fractional mass loss rate at ignition (e.g., 5% of the maximum value at T_p). In this case, $x'(T_p\text{-}\Delta T)/\, x'(T_p) = 0.05$, for which $\lambda = 3$ and the ignition temperature can be expressed in terms of the peak properties:

$$T_{ign} \approx T_{onset} = T_p - \frac{4RT_p^2}{E_a} \tag{80}$$

9.1.2 Critical Heat Flux for Transient Ignition.

At incipient/transient ignition, $q''_{flame} = 0$, $q''_{ext} = q''_{loss}$, $T_{ign} \approx T_{onset}$, and the critical heat flux (CHF) for incipient piloted ignition is equation 78.

$$CHF = q''_{loss} = \bar{h}(T_{onset} - T_0) + \varepsilon\sigma(T_{onset}^4 - T_0^4)$$

9.1.3 Critical Heat Flux for Sustained Ignition.

After the flame is established on the burning surface and ignition is sustained, the heat losses due to convection cease, so $q''_{ext} + q''_{flame} = q''_{loss} = \varepsilon\sigma(T_b^4 - T_0^4) \approx \varepsilon\sigma T_p^4$ and the heat flux for sustained burning is equation 79.

$$CHF_b = q''_{loss} = \varepsilon\sigma T_p^4 \tag{81}$$

9.1.4 Critical Heat Release Rate (q''_{cr}).

A critical combustion energy density in the gas phase at the lower flammability limit of the pyrolysis gases (fuel) in air has been proposed as an ignition criterion [48]. For defined surface convective conditions, this criterion can be expressed as q''_{cr}. Assuming equations 77 and 78 apply with $q''_{flame} = 0$, ignition occurs when:

$$\chi \frac{\eta_c}{\eta_g} \left(q''_{ext} - CHF \right) \geq q''_{cr} \tag{82}$$

The q''_{cr} at incipient ignition occurs at unit efficiency, i.e., $\chi = 1$. In oxygen consumption fire calorimeters operated under standard conditions [23], incipient ignition occurs at a virtual q''_c, $q''_{cr} \approx 25$ kW/m^2 while, for self-sustained ignition, $\chi \leq 1$, $q''_{flame} > 0$, $CHF = CHF_b$, and $q''_{cr} \approx 66$ kW/m^2 [48].

9.2 EFFICIENCY OF FLAMING COMBUSTION.

It was shown (sections 2.3 and 3.4) that conversion of fuel gases to CO_2, H_2O, and HX in a diffusion flame or combustor are not complete if $\Phi > 1$ or if the residence time/temperature of the fuel/oxygen mixture in the flame sheet or combustor is insufficient. In diffusion flames, the products of incomplete combustion are primarily carbon monoxide (CO), soot, and unburned hydrocarbons, so the amount of oxygen consumed by incomplete combustion is necessarily less than the stoichiometric amount of oxygen. The completeness or efficiency of flaming combustion χ can thus be expressed as the ratio of the amount of oxygen consumed in the flame to the stoichiometric amount (e.g., as measured in the MCC). Assuming the fuel gases are the same in both the flame and the MCC, equations 22 and 26 give:

$$\chi = \frac{\begin{matrix} Effective\ Heat\ of\ Combustion \\ of\ Fuel\ Gases \end{matrix}}{\begin{matrix} Heat\ of\ Complete\ Combustion \\ of\ Fuel\ Gases \end{matrix}} = \frac{EHOC}{h_c} = \frac{EHOC}{Q_\infty / (1-\mu)} \tag{83}$$

Table 7 lists the combustion efficiency χ for over-ventilated ($\Phi<1$) burning of 3-mm thick specimens of the polymers in table 5 in a fire calorimeter [23] at external heat flux, $q''_{ext} = 50$ kW/m^2. Equation 83 was used to calculate χ from the EHOC measured in the fire calorimeter and $h_c = Q_\infty/(1-\mu)$ measured for the same polymers in the MCC. All values in table 7 are averages of three to five tests. Also shown in table 7 are the optical density of the smoke (specific extinction area (SEA) of smoke, m^2/kg-gas) and the weight fraction of carbon monoxide (CO) in the carbon oxides of the combustion gases, $CO_x = CO + CO_2$, measured in the fire calorimeter.

Table 7. Combustion Efficiency of 16 Polymers Burning in Over-Ventilated Conditions in a Fire Calorimeter at 50 kW/m^2 External Heat Flux

POLYMER	ρ (kg/m^3)	η_g (J/g-K)	EHOC (kJ/g)	$h_{c,gas}$ (kJ/g)	Combustion Efficiency, χ	SEA (m^2/kg)	CO/CO$_x$ (%, w/w)
POM	1420	47	14.6	14.0	1.04 ±0.02	14	0.1
PMMA	1175	31	25.0	24.5	1.02 ±0.03	130	0.4
HDPE	959	(85)	41.6	42.2	0.99 ±0.02	467	0.9
FEP	2150	19	4.34	4.5	0.96 ±0.14	27	6.4
PP	880	65	38.8	41.0	0.95 ±0.06	544	1.1
PEI	1270	33	20.1	21.3	0.94 ±0.03	348	2.8
PA66	1140	49	26.7	28.7	0.93 ±0.09	246	0.44
PET	1345	61	16.4	18.9	0.87 ±0.03	461	1.8
PPS	1300	50	21.9	25.8	0.85 ±0.04	471	7.2
PC	1200	47	21.4	26.6	0.80 ±0.03	907	3.1
ABS	1050	34	28.4	36.5	0.78 ±0.05	1195	3.0
PPSU	1320	53	16.8	22.1	0.76 ±0.08	660	2.9
HIPS	1045	37	28.9	39.2	0.74 ±0.05	1275	2.8
PVDF	1760	(171)	6.30	8.65	0.73 ±0.12	313	5.6
PEEK	1310	43	18.5	25.5	0.72 ±0.05	685	3.1
PVC	1415	16	7.80	13.7	0.57 ±0.08	760	7.3

Figure 37 is a plot of the data for SEA and CO/CO$_x$ versus χ for the polymers in table 7. A general trend of SEA and CO/CO$_x$ increasing as χ decreases is expected and observed. The implication for fire behavior comes from equation 77, which shows that, other factors being equal, lowering χ can reduce the q_c'' of a burning material below the critical value for sustained ignition, q_{cr}''. This is a common strategy for passing flame/ignition resistance tests using halogen-containing flame-retardant chemical additives.

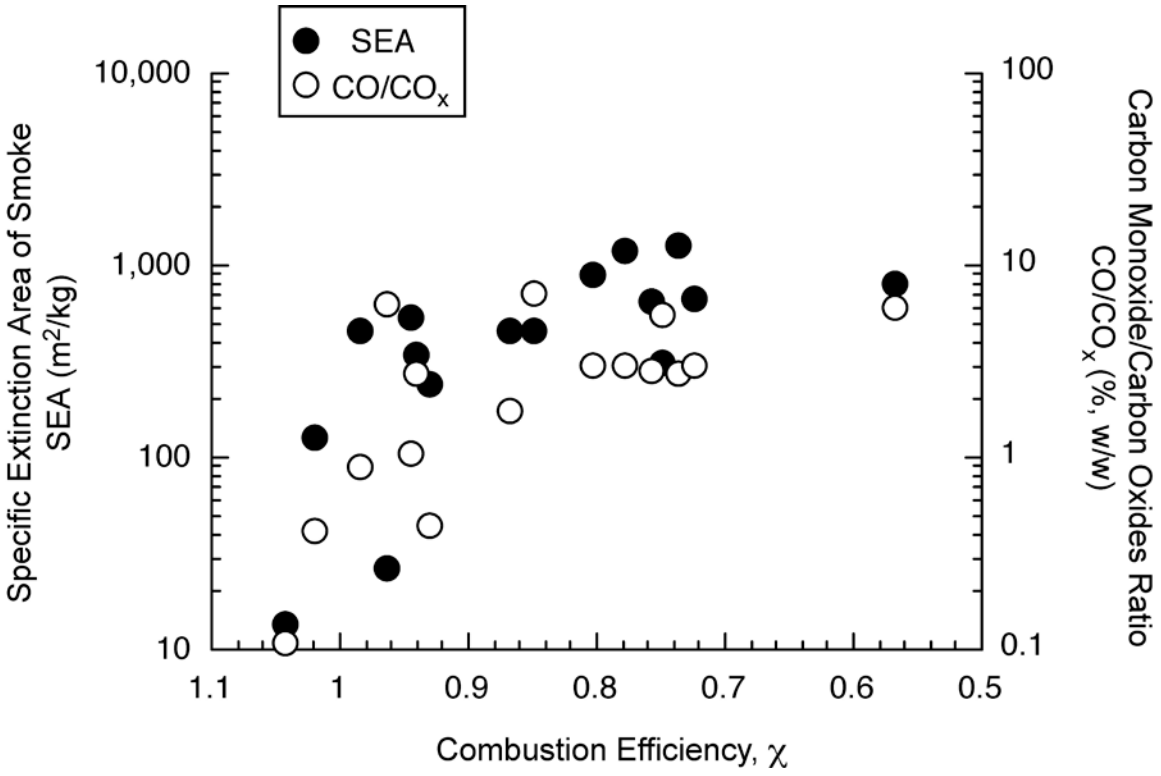

Figure 37. The SEA of Smoke and Carbon Monoxide Fraction (CO/CO_x) in the Combustion Gases vs. Flaming Combustion Efficiency χ (For the polymers of table 7 in an over-ventilated [Φ<1] fire calorimeter)

9.3 BURNING INTENSITY OR HEAT RELEASE RATE (q_c'').

The heat release rate in steady, one-dimensional burning is obtained from equations 77 and 79:

$$q_c'' = \chi \frac{\eta_c}{\eta_g}\left(q_{ext}'' + q_{flame}'' - \varepsilon\sigma T_p^4\right) \tag{84}$$

Figure 38 compares fire calorimeter data for the maximum areal heat release rate, q_{peak}'' of 3-mm-thick samples of the polymers in table 7 tested at q_{ext}''= 50 kW/m^2 to q_c'' calculated using equation 84. In the calculation, η_c and T_p were taken from table 5, χ was taken from table 7, η_g = 40 J/g-K was the average value in table 7, and a constant emissivity ε = 0.75 and a constant flame heat flux q_{flame}'' = 20 kW/m^2 [29 and 40] were assumed. Experimental q_{peak}'' are average values for $N\geq3$ tests and the error bars represent one standard deviation. Figure 38 shows the expected qualitative relationship (equation 84) between measured q_{peak}'' and that calculated using η_c, T_p, χ, and η_g with typical q_{flame}'' and constant ε.

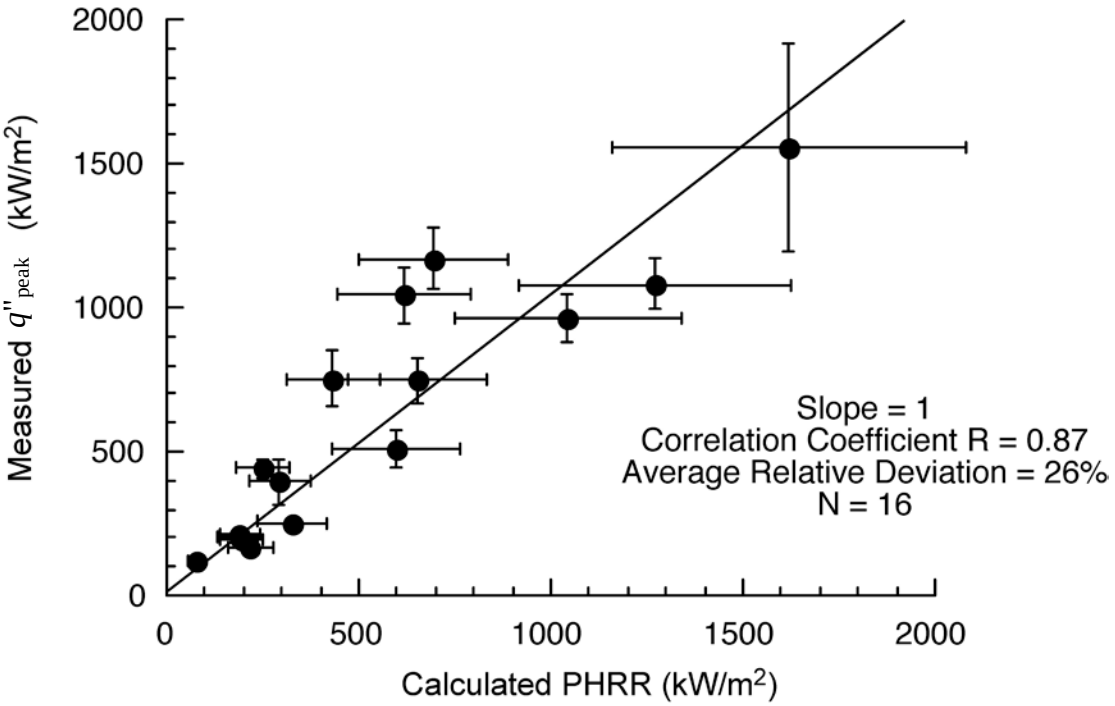

Figure 38. Measured and Calculated q''_{peak} in a Fire Calorimeter
(For the 16 polymers of table 7)

9.4 LIMITING OXYGEN INDEX [48].

The limiting oxygen index (LOI) of a polymer or plastic [49] is the minimum oxygen concentration in an oxygen/nitrogen atmosphere that will support candle-like/downward burning of a thin strip of the material. A qualitative relationship between the limiting oxygen index of a plastic and its thermal combustion properties follows from three assumptions/observations about burning behavior:

- The q''_c of a plastic in the LOI test is equation 77 with q''_{ext} = 0 after the igniter flame is removed [50].

- The flame heat flux is proportional to the oxygen concentration in the environment above a minimum value that will support combustion, i.e., $q''_{flame} = c\{ X_{O_2} - X_{O_2}^{\min} \}$ where $X_{O_2}^{\min} \approx 10\%$ [51] and c = 1.55 kW/m^2-%O_2 [52].

- Flame extinction occurs at q''_{cr} = 66 kW/m^2 [48].

On this basis, the condition for flame extinction in the LOI test can be formulated in terms of the thermal combustion properties and fire parameters of equation 77. After the methane igniter flame is removed, $q''_{ext} = 0$, $q''_{loss} = \varepsilon\sigma T_p^4$, and equation 84 becomes:

$$q_c'' = \chi \frac{\eta_c}{\eta_g}\left(c\left\{X_{O_2}^{ext} - X_{O_2}^{\min}\right\} - \varepsilon\sigma T_p^4\right) \le q_{cr}'' \tag{85}$$

At extinction $X_{O_2}^{ext}$ = LOI, and equation 85 becomes an equality with $q_c'' = q_{cr}''$

$$\text{LOI} = X_{O_2}^{\min} + \frac{\varepsilon\sigma}{c} T_p^4 + \frac{\eta_g q_{cr}'' / \chi c}{\eta_c} \tag{86}$$

Figure 39 shows measured LOI for 85 polymers and formulated polymers (plastics) versus the LOI calculated from equation 86 using $\varepsilon = 0.75$ [29], $\eta_g = 40$ J/g-K, and the measured T_p and η_c for these polymers. The combustion efficiency was calculated as per equation 83 for plastics with measured EHOC. Approximately half of the plastics did not have measured EHOC, so χ was used as an adjustable parameter in the range $\chi = 0.4$-0.8 for halogen-containing plastics and $\chi = 0.8$-1.0 for hydrocarbon and heteroatom polymers and plastics (see table 7). The results of these calculations are shown in figure 39, which also shows the least-squares line for the data forced through the origin having unit slope and correlation coefficient $R = 0.92$. Despite having treated η_g as a constant in equation 86, there is qualitative agreement ($R^2 = 0.85$) between the measured and calculated LOI in figure 39, suggesting a physical basis for extinction in the LOI test in terms of a $q_{cr}'' = 66$ kW/m^2, the thermal combustion properties of materials, and the influence of oxygen on the flame heat flux. Much better agreement between LOI and equation 86 was obtained for a narrower range of material properties by incorporating a term to account for heat transfer efficiency [34 and 53].

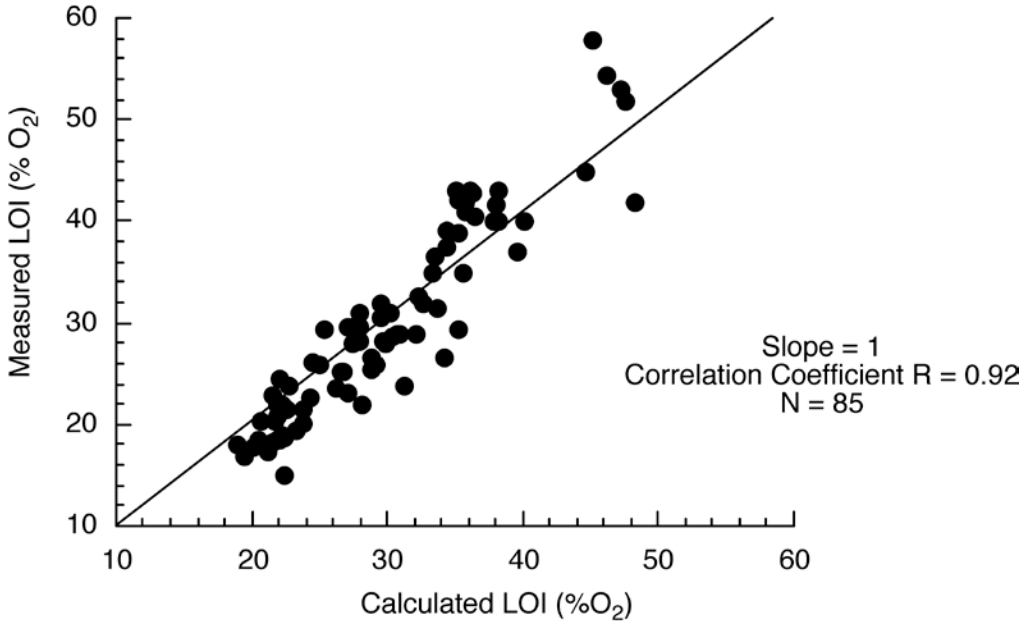

Figure 39. Measured vs. Calculated Limiting Oxygen Indices of Polymers, Plastics, and Textile Fabrics

9.5 FLAME RESISTANCE.

The criterion for flame extinction in Bunsen burner tests of ignition resistance [54 and 55] in terms of the thermal combustion properties is derived from equation 77 with the stipulation of a critical q_c'' for flame propagation, q_{cr}''. After the Bunsen burner is removed, $q_{ext}'' = 0$, $q_{loss}'' = \sigma T_p^4$, and equation 77 becomes:

$$q_c'' = \chi \frac{\eta_c}{\eta_g}\left(q_{flame}'' - \sigma T_p^4\right) \le q_{cr}'' \tag{87}$$

Flame extinction of a plastic specimen is expected after the Bunsen burner is removed if:

$$\eta_c \left(1 - \frac{\sigma T_p^4}{q_{flame}''}\right) \le \frac{\eta_g q_{cr}''}{\chi q_{flame}''} \tag{88a}$$

Or, multiplying through by ΔT_p:

$$Q_\infty \left(1 - \frac{\sigma T_p^4}{q_{flame}''}\right) \le \frac{H_g\, q_{cr}''}{\chi q_{flame}''} \tag{88b}$$

Equations 88a and 88b are criteria for flame extinction of a plastic in terms of its heat resistance ($\sigma T_p^4 / q_{flame}''$), its heat-release capacity (η_c), and its heat of combustion (Q_∞). The flame heat flux in standard tests of ignition resistance under ambient conditions (21% O_2) is largely determined by the size of the sample and its orientation in the test (e.g., horizontal, inclined, or vertical) because the direction of flame propagation with respect to gravity (upward or downward burning) determines the amount of convective pre-heating of the specimen by the attached flame. The flame heat flux is highest for upward burning of thin vertical specimens (e.g., UL 94V) because buoyancy increases convective and radiant preheating of the unburned material above the flame front. Other factors being equal, higher T_p and/or lower η_c or Q_∞ are required for flame extinction in upward vertical burning compared to flame extinction in horizontal, inclined angle or downward burning tests. Thus, both the thermal combustion properties and fire properties (χ, h_g, and q_{flame}'') determine whether or not flame extinction will occur within prescribed limits on the extent and duration of burning in standard tests of flame/ignition resistance.

Figure 40 shows flammability ratings plotted versus Q_∞, η_c, and μ for 114 polymers and plastics tested as 3-mm-thick prismatic bars in a flame spread test using a Bunsen burner ignition source [54 and 55] for which the thermal combustion properties were also measured by MCC. These tests classify plastic specimens according to their performance in upward vertical burning (V-0, V-1, and V-2) and horizontal burning (HB), and the severity of the tests are in the following order: V-0>V-1> V-2>HB. It is seen that very low values of Q_∞, η_c and high values of the char fraction μ are uniquely associated with the self-extinguishing/V-0 rating, while high values of Q_∞

and η_c are uniquely associated with the much-more-flammable HB classification. The transition from non-burning (V-0) to burning (HB) occurs over a broad range of thermal combustion properties with no sharp demarcation between the two states [56]. A statistical analysis of these data has been proposed [57] wherein the qualitative classifications are assigned a binary dependent variable, $Y_i = 1$ for a V-0 classification and $Y_i = 0$ for a V-1, V-2, or HB classification. The Y_i are ranked by the thermal combustion property, X_i, chosen as the independent explanatory variable (i.e., as shown in figure 40) and average values of Y_i and X_i are calculated for successive N-sample bins to obtain the frequency of a V-0 classification, $p_0 = \Sigma Y_i/N$ versus the bin-average thermal combustion property, $X_{avg} = \Sigma X_i/N$. Results of this bin-averaging procedure for the ranked data in figure 40 are shown in figure 41 as a plot of the frequency (probability) of obtaining a V-0 classification p_0 versus the average Q_∞, η_c, and μ for the bin. A clear trend in p_0 with Q_∞ and η_c is observed, which is less evident with μ, although char formation is generally thought to reduce the burning rate [58] and increase the limiting oxygen index [35].

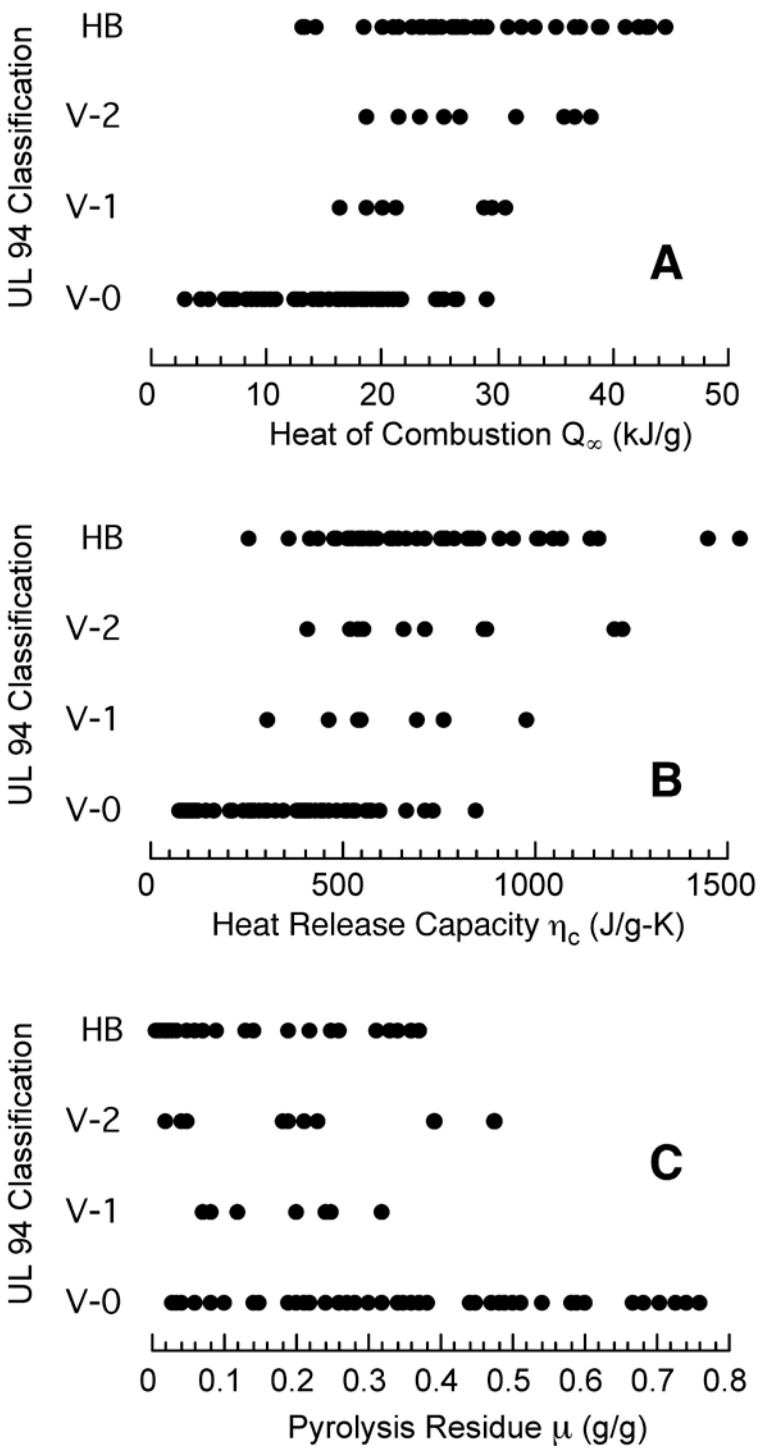

Figure 40. Flammability of 114 Plastics in the Underwriters Laboratories UL 94 Test vs. Thermal Combustion Properties From MCC

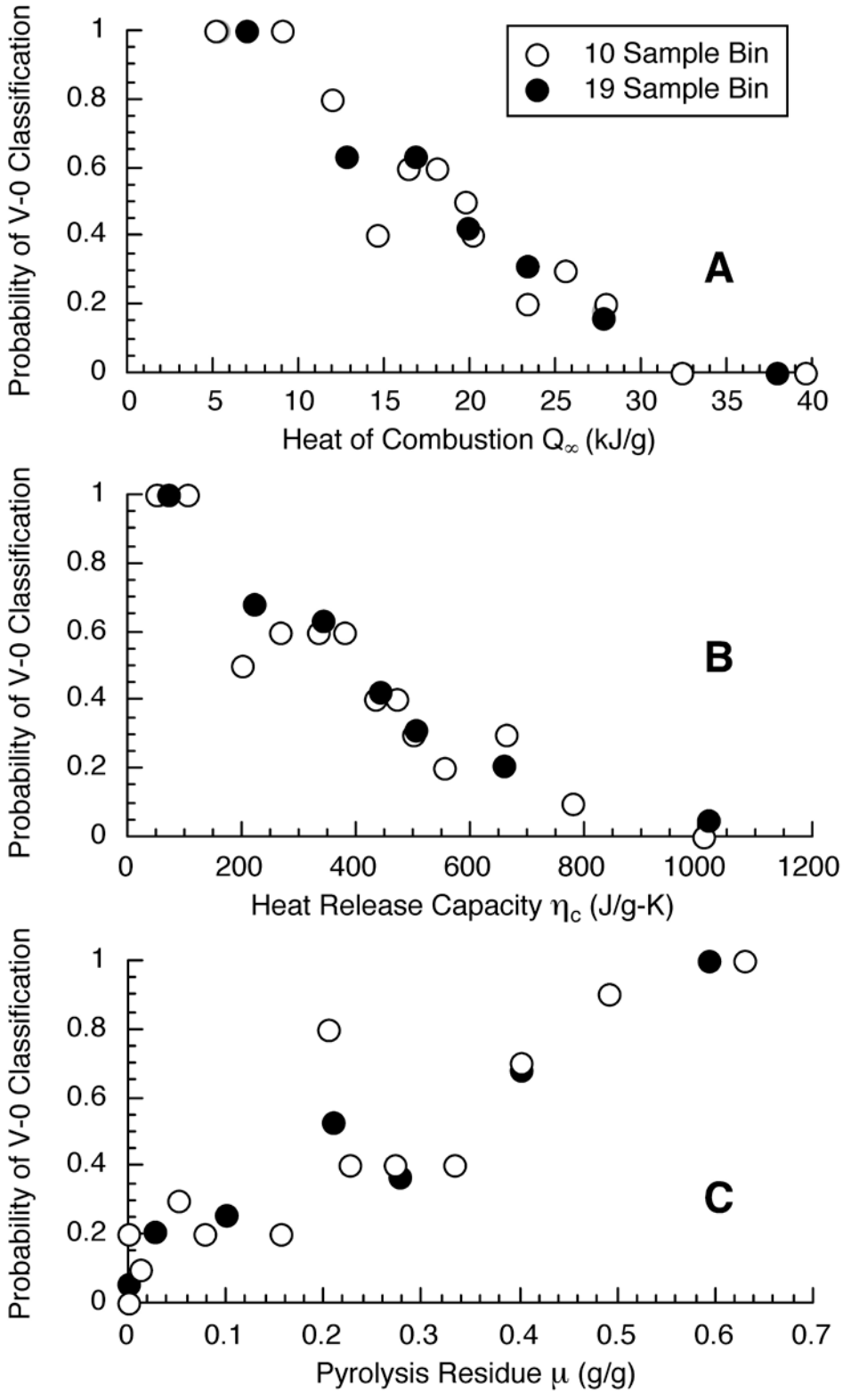

Figure 41. Probability of Obtaining a V-0 Classification in the UL 94 V Flammability Test vs. Thermal Combustion Properties Computed From the Data in Figure 39

10. REFERENCES.

1. Lyon, R.E. and Walters, R.N., "A Pyrolysis-Combustion Flow Calorimeter for the Study of Polymer Heat Release Rate," *9th Annual BCC Conference on Flame Retardancy*, Stamford, Connecticut, June 1-3, 1998.

2. US Patent 5,981,290, Microscale Combustion Calorimeter, November 9, 1999.

3. US Patent 6,464,391, Heat Release Rate Calorimeter for Milligram Samples, October 15, 2002.

4. Lyon, R.E. and Walters, R.N., "Pyrolysis Combustion Flow Calorimetry," *Journal of Analytical and Applied Pyrolysis*, Vol. 71, No. 1, 2004, pp. 27-46.

5. Lyon, R.E., Walters, R.N., and Stoliarov, S.I., "A Thermal Analysis Method for Measuring Polymer Flammability," *Journal of ASTM International*, Vol. 3, No. 4, 2006, pp. 1-18.

6. Standard Test Method for Determining Flammability Characteristics of Plastics and Other Solid Materials Using Microscale Combustion Calorimetry, ASTM D7309-13, American Society for Testing and Materials (International), West Conshohocken, Pennsylvania, April 1, 2013.

7. Turns, S.R., *An Introduction to Combustion*, 2nd ed., McGraw-Hill, New York, New York, 2000.

8. Drysdale, D.D., *An Introduction to Fire Dynamics*, 2nd ed., John Wiley and Sons, New York, New York, 1998.

9. Quintiere, J.G., *Fundamentals of Fire Phenomena*, John Wiley and Sons, New York, New York, 2006.

10. Lyon, R.E. and Janssens, M.L., *Polymer Flammability*, *Encyclopedia of Polymer Science & Engineering*, on-line ed., John Wiley & Sons, New York, NY, April 2005. http://onlinelibrary.wiley.com/book/10.1002/0471440264, Also published as Lyon, R.E. and Janssens, M.L., "Polymer Flammability," Final Report DOT/FAA/AR-05/14, May 2005.

11. Standard Method of Compositional Analysis by Thermogravimetry, ASTM E1131, American Society for Testing and Materials (International), West Conshohocken, Pennsylvania, 2008.

12. Lyon, R.E., "An Integral Method of Nonisothermal Kinetic Analysis," *Thermochimica Acta*, Vol. 297, No. 1-2, August 25, 1997, pp. 117-124.

13. Lyon, R.E., "Heat Release Kinetics," *Fire and Materials*, Vol. 24, No. 4, August 30, 2000, pp. 179-186.

14. Lyon, R.E., Safronava, N., and Stoliarov, S.I., "The Role of Thermal Decomposition Kinetics in the Burning Behavior of Polymers," INTERFLAM 2010, University of Nottingham, United Kingdom, July 5-7, 2010.

15. Lyon, R.E., Walters, R.N., and Stoliarov, S.I., "Thermal Analysis of Flammability," *Journal of Thermal Analysis and Calorimetry*, Vol. 89, No. 2, August 2007, pp. 441-448.

16. Lyon, R.E. and Walters, R.N., "A Microscale Combustion Calorimeter," DOT/FAA/AR-01/117, February 2002.

17. Heffington, W.M., Parks, G.E., Sulzmann, K.G.P., and Penner, S.S., "Studies of Methane Oxidation Kinetics," *Sixteenth Symposium (International) on Combustion*, The Combustion Institute, 1976, pp. 997-1010.

18. Reshetnikov, S.M. and Reshetnikov, I.S., "Oxidation Kinetic of Volatile Polymer Degradation Products," *Polymer Degradation and Stability*, Vol. 64, No. 3, June 1999, pp. 379-385.

19. Babrauskas, V., "Heat of Combustion and Potential Heat," *Heat Release in Fires*, V. Babrauskas, S. Grayson, eds., Elsevier Applied Science, 1992, pp. 207-223.

20. Thornton, W., "The Relation of Oxygen to the Heat of Combustion of Organic Compounds," *Philosophical Magazine* and *Journal of Science*, Vol. 33, No. 196, 1917.

21. Huggett, C., "Estimation of Rate of Heat Release by Means of Oxygen Consumption," *Fire and Materials*, Vol. 4, No. 2, June 1980, pp. 61-65.

22. Janssens, M.L. and Parker, W.J., "Oxygen Consumption Calorimetry," *Heat Release in Fires*, V. Babrauskas, S. Grayson, eds., Elsevier Applied Science, 1992, pp. 31-59.

23. Standard Test Method for Heat and Visible Smoke Release Rates for Materials and Products Using an Oxygen Consumption Calorimeter, ASTM E1354, American Society for Testing and Materials, West Conshohocken, Pennsylvania.

24. United States Code of Federal Regulations, Title 14: Aeronautics and Space, Vol. 1, Chap. I: Federal Aviation Administration, Parts 1-49, 2007.

25. Federal Aviation Administration, "Aircraft Material Fire Test Handbook," FAA Report DOT/FAA/CT-89/15, September 1990.

26. Walters, R.N. and Lyon, R.E., "A Microscale Heat Release Rate Device," *Society of Plastics Engineers Annual Technical Conference* (ANTEC 96), Indianapolis, Indiana, May 5-9, 1996.

27. Inguilizian, T.V., "Correlating Polymer Flammability Using Measured Pyrolysis Kinetics," Master of Science Thesis, University of Massachusetts, Amherst, January 1999.

28. Lyon, R.E., *Handbook of Building Materials for Fire Protection*, C. A. Harper (ed.), McGraw-Hill, New York, New York, 2004, Chap. 3, "Plastics and Rubber," 2004, pp. 3.1-3.51.

29. Stoliarov, S.I., Safronava, N., and Lyon, R.E., "The Effect of Variation in Polymer Properties on the Rate of Burning," *Fire and Materials*, Vol. 33, No. 6, October 2009, pp. 257-271.

30. Stoliarov, S.I., Walters, R.N., and Lyon, R.E., "A Method for Constant-Rate Heating of Milligram Sized Samples," *Journal of Thermal Analysis and Calorimetry*, Vol. 89, No. 2, 2007, pp. 367-371.

31. Siegel, R. and Howell, J.R., *Thermal Radiation Heat Transfer*, 4th ed., Taylor and Francis, New York, New York, 2002.

32. Gmelin, E. and Sarge, S.M., "Calibration of Differential Scanning Calorimeters," *Pure and Applied Chemistry*, Vol. 67, No. 11, 1995, pp. 1789-1800.

33. Standard Practice for Temperature Calibration of Differential Scanning Calorimeters and Differential Thermal Analyzers, ASTM E967, American Society for Testing and Materials (International), West Conshohocken, Pennsylvania, 2008.

34. Schartel, B., Pawlowski, K.H., and Lyon, R.E., "Pyrolysis-Combustion Flow Calorimeter: A Tool to Assess Flame Retarded PC/ABS Materials," *Thermochimica Acta*, Vol. 462, No. 1-2, October 2007, pp. 1-14.

35. Yang, C.Q., He, Q., Lyon, R.E., and Hu, Y., "Investigation of the Flammability of Different Textile Fabrics Using Microscale Combustion Calorimetry," *Polymer Degradation & Stability*, Vol. 95, No. 2, 2010, pp. 108-115.

36. Van Krevelen, D.W., *Properties of Polymers: Their Correlation With Chemical Structure, Their Numerical Estimation, and Prediction From Additive Group Contributions*, Third ed., Elsevier, Amsterdam, The Netherlands, 1997.

37. Walters, R.N. and Lyon, R.E., "Molar Group Contributions to Polymer Flammability," *Journal of Applied Polymer Science*, Vol. 87, No. 3, January 2003, pp. 548-563.

38. Lyon, R.E., Takemori, M.T., Safronava, N., Stoliarov, S.I., and Walters, R.N., "A Molecular Basis for Polymer Flammability," *Polymer*, Vol. 50, No. 12, 2009, pp. 2608-2617.

39. Stoliarov, S.I. and Lyon, R.E., "Thermo-Kinetic Model of Burning," DOT/FAA/AR-TN08/17, May 2008.

40. Stoliarov, S.I., Crowley, S., Lyon, R.E., and Linteris, G.T., "Prediction of the Burning Rates of Non-Charring Polymers," *Combustion and Flame*, Vol. 156, No. 5, May 2009, pp. 1068-1083.

41. Standard Method for Decomposition Kinetics by Thermogravimetry, ASTM E1641, American Society for Testing and Materials (International), West Conshohocken, Pennsylvania, 2007.

42. Safronava, N. and Lyon, R.E., "A Simple Method for Obtaining First-Order Kinetic Parameters From Thermal Analysis Data," *38th Meeting of the North American Thermal Analysis Society (NATAS)*, Philadelphia, Pennsylvania, August 15-18, 2010.

43. Kim, S., Jang, E.S., Shin, D.H., and Lee, K.H., "Using Peak Properties of a DTG Curve to Estimate the Kinetic Parameters of the Pyrolysis Reaction: Application to High Density Polyethylene," *Polymer Degradation and Stability*, Vol. 85, 2004, pp. 799-805.

44. Kim, Y.E., Kim, S.S., and Chung, S.H., "Application of Peak Property Method of Estimating Apparent Kinetic Parameters of Cellulose Pyrolysis Reaction," *Journal of Industrial Engineering Chemistry*, Vol. 12, No. 6, 2006, pp. 846-852.

45. Walters, R.N., Hackett, S.M., and Lyon, R.E., "Heats of Combustion of High Temperature Polymers," *Fire and Materials*, Vol. 24, No. 5, 2000, pp. 245-252.

46. Standard Test Method for Heat of Combustion of Liquid Hydrocarbon Fuels by Bomb Calorimeter (Precision Method), ASTM D4809, American Society for Testing and Materials (International), West Conshohocken, Pennsylvania, 2009.

47. Stoliarov, S.I. and Walters, R.N., "Determination of Heats of Gasification of Polymers Using Differential Scanning Calorimetry," *Polymer Degradation and Stability*, Vol. 93, No. 2, February 2008, pp. 422-427.

48. Lyon, R.E. and Quintiere, J.G., "Piloted Ignition of Combustible Solids," *Combustion & Flame*, Vol. 151, No. 4, December 2007, pp. 551-559.

49. Standard Method for Measuring the Minimum Oxygen Concentration to Support Candle-Like Combustion of Plastics (Oxygen Index), ASTM D2863, American Society for Testing and Materials, West Conshohocken, Pennsylvania, 2006.

50. Lyon, R.E., Fulmer, M.R., Crowley, S., and Walters, R.N., "The Limiting Oxygen Index Test (Revisited)," *21st Annual Conference on Recent Advances on Flame Retardancy of Polymeric Materials*, Stamford, Connecticut, May 24-26, 2010.

51. Zabetakis, M.G., "Flammability Characteristics of Combustible Gases and Vapors," Bulletin 627, U.S. Department of the Interior, Bureau of Mines, 1965.

52. Tewarson, A., Lee, J.L., and Pion, R.F., "The Influence of Oxygen Concentration on Fuel Parameters for Fire Modeling, Eighteenth Symposium (International) on Combustion," The Combustion Institute, Pittsburgh, Pennsylvania, 1981, pp. 563-570.

53. Yang, C.Q., He, Q., and Lyon, R.E., "Applications of Microscale Combustion Calorimetry to Flame Retardant Textile Research," *Proceedings of the 21st Annual Conference on Recent Advances on Flame Retardancy of Polymeric Materials*, BCC Research, Stamford, Connecticut, May 24-26, 2010.

54. Flammability of Plastic Materials, UL 94 Section 2 (Horizontal: HB) and Section 3 (Vertical: V-0/1/2), Underwriters Laboratories Inc., Northbrook, Illinois, 1991.

55. Standard Test Method for Measuring the Comparative Burning Characteristics of Solid Plastics in a Vertical Position, ASTM D 3801-06, American Society for Testing and Materials (International), West Conshohocken, Pennsylvania, 2006.

56. Quintiere, J.G., Downey, B.P., and Lyon, R.E., "An Investigation of the UL 94V Plastics Flammability Test," *Sixth Fire and Explosion Hazards Seminar*, University of Leeds, UK, April 12-14, 2010.

57. Lyon, R.E., Safronava, N., Walters, R.N., Crowley, S., and Stoliarov, S.I., "A Statistical Model for the Flammability of Plastics," *19th Annual BCC Research Conference on Recent Advances in Flame Retardancy of Polymeric Materials*, Stamford, Connecticut, 2008, June 9-11.

58. Stoliarov, S.I., Crowley, S., Walters, R.N., and Lyon, R.E., "Prediction of the Burning Rate of Charring Polymers," *Combustion and Flame*, Vol. 157, No. 11, November 2010, pp. 2024-2034.